UC San Diego

UC San Diego Electronic Theses and Dissertations

Title

Regulation of CD8+ T Lymphocyte Fate Specification by Proteasome Activity and Cellular Metabolism

Permalink

https://escholarship.org/uc/item/7gk4n4bv

Author

Widjaja, Christella Edlina

Publication Date

2017

Peer reviewed|Thesis/dissertation

eScholarship.org Powered by the California Digital Library
University of California

UNIVERSITY OF CALIFORNIA, SAN DIEGO

Regulation of $CD8^+$ T Lymphocyte Fate Specification by Proteasome Activity and Cellular Metabolism

A dissertation submitted in partial satisfaction of the

requirements for the degree Doctor of Philosophy

in

Biomedical Sciences

by

Christella Edlina Widjaja

Committee in charge:

Professor John Chang, Chair
Professor Jack Bui
Professor Ananda Goldrath
Professor Stephen Hedrick
Professor Gentry Patrick

2017

Copyright

Christella Edlina Widjaja, 2017

All rights reserved.

The Dissertation of Christella Edlina Widjaja is approved, and it is acceptable in quality and form for publication on microfilm and electronically:

Chair

University of California, San Diego

2017

TABLE OF CONTENTS

Signature Page iii

Table of Contents iv

List of Abbreviations vii

List of Figures ix

Acknowledgements xii

Vita xiv

Abstract of the Dissertation xv

Introduction 1

Chapter 1: $CD8^+$ T lymphocytes responding to infection exhibit molecular heterogeneity early during differentiation that correspond to distinct fates 6

1.1: Introduction 6

1.2: Results 6

1.2.1: Experimental setup and validation 6

1.2.2: $CD8^+$ T lymphocytes that have undergone their first cell division exhibit striking molecular heterogeneity 7

1.2.3: Supervised classifiers predict the identity of cells in intermediate stages of differentiation 9

1.3: Discussion 10

Chapter 2: Differentially-fated $CD8^+$ T cells exhibit distinct levels of proteasome activity 19

2.1: Introduction 19

2.2: Results 19

2.2.1 Differentially-fated $CD8^+$ T cells emerging from the first cell division have distinct rates of proteasome activity 19

2.2.2 Distinct rates of proteasome activity is a unique feature of differentially-fated $CD8^+$ T cells emerging from the first cell division 20

2.3: Discussion 21

Chapter 3: Proteasome activity influences $CD8^+$ T cell differentiation and function 27

3.1: Introduction 27

3.2: Results 27

3.2.1: A screen to identify effective pharmacological modulators of proteasome activity 27

3.2.2: Proteasome activity influences $CD8^+$ T cell differentiation and function in vitro 30

3.2.3: Proteasome activity influences $CD8^+$ T cell differentiation and memory formation in vivo 31

Chapter 4: Proteasome activity regulates $CD8^+$ T cell differentiation through effects on cellular metabolism 49

4.1: Introduction 49

4.2: Results 49

4.2.1: Transcriptomic and proteomic analyses identify that proteasome activity alters cellular metabolism 49

4.2.2: $CD8^+$ T cells with altered levels of proteasome activity utilizle different methods of cellular metabolism 51

4.2.3 Myc is a target of proteasome-mediated regulation of cellular metabolism 52

4.3: Discussion 55

Chapter 5: Conclusions 71

Appendix A: Materials and Methods 75

Appendix B: Supplementary Tables 90

References 93

LIST OF ABBREVIATIONS

2-DG	2-deoxy-D-glucose
2-NBDG	2-deoxy-2-[(7-nitro-2,1,3-benzoxadiazol-4-yl)amino]-D-glucose
ANOVA	Analysis of variance
cDNA	Complementary DNA
CFSE	Carboxyfluorescein succinimidyl ester
CFU	Colony forming unit
$Div1_{MEM}$	Division 1 Memory
$Div1_{TE}$	Division 1 Terminal Effector
ECAR	Extracellular Acidification Rate
GO	Gene Ontology
GSEA	Gene Set Enrichment Analysis
I.P.	Intraperitoneal
I.V.	Intravenous
LCMV-Arm	Lymphocytic choriomeningitis-Armstrong
Lm-OVA	Listeria monocytogenes-Ovalbumin
MFI	Mean fluorescence intensity
MSigDB	Molecular Signatures Database
NES	Normalized Enrichment Score
OCR	Oxygen Consumption Rate
PCA	Principal Component Analysis

PFU	Plaque forming unit
qPCR	Quantitative real-time PCR
RNA-seq	RNA sequencing
S.E.M.	Standard error of the mean
SILAC	Stable isotope labeling with amino acids in cell culture
SMART	Switch Mechanism at 5’ End of RNA Template
T_{CM}	T central memory
TCR	T cell receptor
T_{EM}	T effector memory
TPM	Transcripts per million
t-SNE	t-distributed stochastic neighbor embedding

LIST OF FIGURES

Figure 1.1 Experimental approach for transcriptional analysis of $CD8^+$ T lymphocytes responding to viral infection using single-cell RNA-seq 12

Figure 1.2. Quality control metrics in single cell RNA-seq. 13

Figure 1.3 Expression of $CD8^+$ T cell-associated genes across time points in a viral infection. 14

Figure 1.4 t-SNE analysis of single $CD8^+$ T cells reveals distinct subpopulations emerging from the first cell division. 15

Figure 1.5 Cells emerging from the first cell division express genes associated with effector or memory $CD8^+$ T cells. 16

Figure 1.6 Classifiers trained by Division 1 and fully differentiated effector and memory populations. 17

Figure 1.7 Early state and cell fate classifiers agree on the classification of intermediate-stage cells. 18

Figure 2.1 Structure of the pan-reactive proteasome probe MV003. 23

Figure 2.2 Differentially fated $CD8^+$ T cells exhibit distinct rates of proteasome activity. 24

Figure 2.3 Cells with distinct levels of proteasome activity differ in effector and memory $CD8^+$ T cell marker expression. 25

Figure 2.4 Proteasome activity of naïve, terminal effector cells, and memory cells are distinct from that of cells emerging from the first cell division. 26

Figure 3.1 Level of proteasome activity can be modulated pharmacologically. 34

Figure 3.2 Proteasome inhibiton or activation can influence $CD8^+$ T cell differentiation *in vitro*. 35

Figure 3.3 Proteasome inhibition or activation affects production of IFNγ. 36

Figure 3.4 Transient pre-treatment of $CD8^+$ T cells with cyclosporine does not block NFAT nuclear translocation. 37

Figure 3.5 Effects on proteasome activity and $CD8^+$ T cell differentiation are not a general feature of calcineurin inhibitors. 38

Figure 3.6 Validation of selected proteasome inhibitor and activator in modulation of proteasome activity. 39

Figure 3.7 Modulation of proteasome activity affects effector $CD8^+$ T cell differentiation. 40

Figure 3.8 Proteasome activity regulates effector $CD8^+$ T cell cytotoxic function. 41

Figure 3.9 Experimental approach in analysis of the effect of proteasome activity modulation on the $CD8^+$ T cell response to infection. 42

Figure 3.10 Proteasome inhibition does not affect percentage of effector $CD8^+$ T cells but decreases percentage of memory $CD8^+$ T cells. 43

Figure 3.11 $CD8^+$ T cells with decreased proteasome activity have a decreased percentage of memory precursor cells during contraction. 44

Figure 3.12 $CD8^+$ T cells with decreased proteasome activity have a reduced recall response to a secondary infection 45

Figure 3.13 Increasing proteasome activity does not affect percentage of effector or memory $CD8^+$ T cells. 46

Figure 3.14 $CD8^+$ T cells with increased proteasome activity have increased generation of central memory cells. 47

Figure 3.15 Memory $CD8^+$ T cells generated from proteasome activator-treated cells have an increased recall response. 48

Figure 4.1 Transcriptional profiling of $CD8^+$ T cells with decreased or increased proteasome activity reveals differential gene expression. 58

Figure 4.2 Pathway analysis reveals that modulation of proteasome activity affects many $CD8^+$ T cell functions including apoptosis, metabolic processes, and signal transduction. 59

Figure 4.3 Memory-associated genes have increased expression in proteasome activator-treated $CD8^+$ T cells. 60

Figure 4.4 Transcriptional profile of proteasome inhibitor-treated cells resemble effector $CD8^+$ T cells while proteasome activator-treated cells resemble memory $CD8^+$ T cells. 61

Figure 4.5 Mass spectrometry analysis reveals that proteasome activity modulation alters global proteome of $CD8^+$ T cells. 62

Figure 4.6 Functional characterization of differentially expressed proteins reveals that proteasome inhibition alters processes associated with cellular metabolism. 63

Figure 4.7 $CD8^+$ T cells with decreased proteasome activity have an increased rate of glycolysis and glucose uptake. 64

Figure 4.8 $CD8^+$ T cells with increased proteasome activity have an increased maximal respiratory capacity. 65

Figure 4.9 Proteasome inhibitor treatment of $CD8^+$ T cells results in increased expression of glycolysis genes. 66

Figure 4.10 Proteasome inhibitor treatment of $CD8^+$ T cells results in increased Myc expression. 67

Figure 4.11 Enhanced $CD8^+$ T cell effector function induced by proteasome inhibitor is dependent on Myc expression. 68

Figure 4.12 Pre-effector and pre-memory cells emerging from the first cell division express differential levels of Myc. 69

Figure 4.13 Myc degradation is dependent on level of proteasome activity. 70

ACKNOWLEDGEMENTS

I would like to acknowledge Dr. John T. Chang for his mentorship and guidance. John has supported me throughout my development as a scientist and has fostered a positive lab environment, which I am very grateful for.

I would also like to acknowledge the past and present members of the Chang Lab: Asoka Banno, Daniel Garcia, and Eric Van Baarsel for their work and helpful discourse on the proteasome project; Janilyn Arsenio and Pat Metz for their expertise in anything $CD8^+$ T cell related, Jane Klann, Brigid Boland, Soo Ngoi, and Justine Lopez for their helpful discussions, scientific expertise, and extended coffee breaks; Kelly Remedios and Kate Oakley for welcoming me into the lab space.

I would like to acknowledge the members of Dr. Gene Yeo's lab who helped us with all of our bioinformatic analysis throughout our many projects.

I would like to acknowledge my thesis committee: Dr. Jack Bui, Dr. Ananda Goldrath, Dr. Steve Hedrick, and Dr. Gentry Patrick. Your feedback and support have been very valuable to me.

I would like to acknowledge my partner Jiawei Huang for being my constant and my shelter throughout all the good times and the difficult times.

Chapter 1, in full, is an adapted version of the material in press at *Nature Immunology*. Kakaradov, Boyko; Arsenio, Janilyn; Widjaja, Christella E.; He, Zhaoren; Aigner, Stefan; Metz, Patrick J.; Yu, Bingfei; Wehrens, Ellen; Lopez, Justine; Kim, Stephanie H.; Zuniga, Elina I.; Goldrath, Ananda W.; Chang, John T.; Yeo, Gene W. 2016. Early transcriptional and epigenetic regulation of $CD8^+$ T cell

differentiation revealed by single-cell RNA-seq. *Nat Immunol*. In press. The dissertation author was the co-primary author of all material.

Chapters 2-4, in full, are an adapted version of the material that has been submitted for publication. Widjaja, Christella E.; Metz, Patrick J.; Phan, Anthony T.; Savas, Jeffrey N.; de Bruin, Gerjan; Leestemaker, Yves; Berkers, Celia R.; de Jong, Annemeike; Florea, Bogdan I.; Fisch, Kathleen; Lopez, Justine; Kim, Stephanie H.; Garcia, Daniel A.; Searles, Stephen; Bui, Jack D.; Yates III, John R.; Goldrath, Ananda W.; Overkleeft, Hermen S.; Ovaa, Huib; Chang, John T. 2016. Proteasome activity regulates $CD8^+$ T lymphocyte metabolism and fate specification. In revision. The dissertation was the primary author of all material.

VITA

2010	B.S., Molecular Biology, University of California, San Diego
2013-2016	National Institutes of Health T32 Predoctoral Trainee
2014	Graduate Teaching Assistant, University of California, San Diego
2017	Ph.D., Biomedical Sciences, University of California, San Diego

PUBLICATIONS

Widjaja, C.E., Metz, P.J., Phan, A.T., Savas, J.N., de Bruin, G.J., Leestemaker, Y., Berkers, C.R., de Jong, A., Florea, B.I., Fisch, K., Lopez, J., Kim, S.H., Garcia, D.A., Searles, S., Bui, J.D., Chang, A.N., Yates III, J.R., Goldrath, A.W., Overkleeft, H.S., Ovaa, H., Chang, J.T., Proteasome activity regulates CD8+ T lymphocyte metabolism and fate specification. In revision.

Kakaradov, B., Arsenio, J., **Widjaja, C.E.**, He, Z., Aigner, S., Metz, P.J., Yu, B., Wehrens, E., Lopez, J., Kim, S.H., Zuniga, E.I., Goldrath, A.W., Chang, J.T., Early transcriptional and epigenetic regulation of $CD8^+$ T cell differentiation revealed by single-cell RNA-seq. *Nat Immunol*, (2017).

Banno, A., Garcia, D. A., van Baarsel, E. D., Metz, P. J., Fisch, K., **Widjaja, C. E.**, Kim, S. H., Lopez, J., Chang, A. N., Geurink, P. P., Florea, B. I., Overkleeft, H. S., Ovaa, H., Bui, J. D., Yang, J. & Chang, J. T. Downregulation of 26S proteasome catalytic activity promotes epithelial-mesenchymal transition. *Oncotarget*, (2016).

Boland, B.S., **Widjaja, C.E**., Banno, A., Zhang, B., Kim, S.H., Stoven, S., Peterson, M.R., Jones, M.C., Su, H.I., Crowe, S.E., Bui, J.D., Ho, S.B., Okugawa, Y., Goel, A., Marietta, E.V., Khosroheidari, M., Jepsen, K., Aramburu, J., López-Rodríguez, C., Sandborn, W.J., Murray, J.A., Harismendy, O., Chang, J.T. Immunodeficiency and autoimmune enterocolopathy linked to NFAT5 haploinsufficiency. *J Immunol*, (2015).

ABSTRACT OF THE DISSERTATION

Regulation of CD8$^+$ T Lymphocyte Fate Specification by Proteasome Activity and Cellular Metabolism

by

Christella Edlina Widjaja

Doctor of Philosophy in Biomedical Sciences

University of California, San Diego, 2017

Professor John T. Chang, Chair

In an immune response, CD8$^+$ T lymphocytes can differentiate into effector cells that acutely clear the infection as well as memory cells that provide lasting immunity against the same pathogen. Previous studies have shown that differentiation of CD8$^+$ T cells in to effector and memory subsets occurs in a heterogeneous manner. Single-cell RNA-seq has revealed that transcriptional heterogeneity is present as early

as the first cell division. Using single-cell transcriptional profiling to create supervised classifiers revealed that the outcome of intermediate-stage cells could be predicted. In 'pre-effector' and 'pre-memory' cells resulting from the first $CD8^+$ T cell division *in vivo*, we observed distinctly low and high levels of proteasome activity, respectively. Pharmacological inhibition of proteasome activity early during differentiation resulted in acquisition of terminal effector cell characteristics, while enhancement of proteasome activity conferred attributes of memory lymphocytes. Transcriptomic and proteomic analyses revealed that modulation of proteasome activity in $CD8^+$ T cells affected cellular metabolism. These metabolic changes were mediated, in part, through differential expression of Myc, a transcription factor that controls glycolysis and metabolic reprogramming. Overall, these findings demonstrate that proteasome activity is an important regulator of $CD8^+$ T cell fate early during the differentiation process.

INTRODUCTION

The CD8$^+$ T cell response to infection

In response to microbial infection, naïve CD8$^+$ T lymphocytes undergo rapid clonal proliferation in response to their specific antigen and differentiate into terminal effector cells that mediate acute host defense and self-renewing memory cells that provide long-lived protection. Terminally differentiated, short-lived effector CD8$^+$ T cells are characterized by production of inflammatory cytokines, such as IFNγ and TNFα, as well as production of cytolytic granules that kill infected cells [1]. Circulating memory T cells can be subsetted into central memory (T_{CM}) cells and effector memory (T_{EM}) cells, which are distinguished by expression of L-selectin (CD62L) [2]. CD62L^{hi} T_{CM} are proficient at robustly re-expanding in response to a subsequent infection with the same pathogen while CD62L^{lo} T_{EM} can rapidly produce cytokines in the event of reinfection.

Regulation of CD8$^+$ T cell differentiation is dependent on diverse factors, including TCR signal strength, costimulatory molecules, cytokine signals, and the microenvironment [3-6]. These signals may drive the expression of important transcription factors that drive and maintain differentiation of CD8$^+$ T cells into effector and memory subsets. T-bet is a T-box transcription factor essential for expression of genes associated with terminal effector CD8$^+$ T cell differentiation and function [1]. Interferon regulatory factor 4 (IRF4) is another transcription factor recently identified to be critical for generation and maintenance of a protective effector CD8$^+$ T cell response [7]. In addition, IRF4 has been found to repress the expression of

Eomesodermin (Eomes), another T-box transcription factor that has been shown to play some redundant roles in effector differentiation early in the $CD8^+$ T cell response [8]. However, Eomes has also been shown to also sustain the expression of memory-associated molecules that promote longevity, including the anti-apoptotic transcription factor B cell lymphoma 2 (Bcl2) [9]. The balance of these transcription factors and many others can regulate $CD8^+$ cell fate decisions to differentiate into effector or memory cells.

Prior studies have shown that a single naïve $CD8^+$ T cell can give rise to both terminal effector and memory lymphocytes [10-12]. One mechanism by which terminal effector and memory cells can be derived from a single naïve cell is asymmetric cell division, an evolutionarily conserved process in which cellular components are unequally localized to opposing poles of a mitotic cell, thereby resulting in daughter cells that inherit different molecules and have tendencies to differentiate toward distinct fates [13]. $CD8^+$ T cells have been previously shown to undergo asymmetric cell division to generate daughter cells that are phenotypically effector-like and memory-like [14,15]. Single-cell gene expression profiling using a pre-selected panel of T cell-associated molecules showed that cells emerging from the first $CD8^+$ T cell division in response to a microbial infection are transcriptionally distinct [16].

One of the molecules found to undergo asymmetric localization during the first cell division is T-bet. T-bet asymmetry during mitosis has been shown to be mediated by localized degradation due to asymmetric segregation of the proteasome machinery in dividing $CD8^+$ T cells [17]. This observation raised the possibility that the degree of proteasome activity experienced by $CD8^+$ T cells emerging from the first division in

response to microbial infection may play a role in regulating the eventual fate of these cells.

The role of proteasome-mediated degradation in cell differentiation

The 26S proteasome is a multi-subunit protein complex that performs the majority of cellular protein degradation in a highly regulated manner. It is comprised of a 20S core particle (CP), a barrel-shaped degradation machinery that consist of four rings of seven subunits, where the inner rings contain catalytic sites that degrade peptides, and the 19S regulatory particle (RP), which contains a base of two non-ATPase and six ATPase subunits and an eight-subunit lid. The 20S CP when unbound to a regulator is closed and inactive [18]. The 19S RP attaches directly to the outer rings of the 20S CP and regulates substrate unfolding and entry [19]. Lymphocytes can also express specialized inducible immunoproteasome subnits, which are well characterized in their role in antigen processing and the generation of a diverse T cell repertoire [20,21]. Proteins are marked for degradation by the reversible post-translational process of ubiquitination, which is carried out by E1 ubiquitin activating enzymes, E2 ubiquitin-conjugating enzymes, and E3 ubiqutin ligases. Ubiquitin binding to the proteasome initiates the degradation of the marked peptide [22]. However, ubiquitination does not guarantee substrate degradation [23]. Thus, ubiquitination and deubiquitination of proteins, as well as regulation of proteasome activity itself, can control protein degradation.

Regulation of endogenous proteasome activity has been previously shown to control cell fate decisions of human embryonic stem cells and cancer stem cells [24,25].

Moreover, recent studies in lymphocytes have shown that proteasome activity can also influence their differentiation and function. Inhibition of proteasome activity using the small molecule proteasome inhibitor bortezomib in human T cells spared the $CD4^+$ T helper 2 (Th2)-promoting transcription factor GATA3 from degradation and promoted the expression of the inhibitory coreceptor cytotoxic T-lymphocyte antigen-4 (CTLA4), resulting in an impairment of the Th1 response [26]. Selective inhibition or deletion of the immunoproteasome subunit low-molecular mass polypeptide-7 (LMP7, encoded by the gene *Psmb8*) in $CD4^+$ T cells has been shown to promote differentiation into regulatory T cells (Tregs) at the expense of Th17 differentiation, reducing the severity of inflammation in mouse models of autoimmune disease [27-29]. While many studies have shown that proteasome inhibition can result in reduction of the inflammatory response, pan-immunosubunit deficient $CD4^+$ T cells were observed to have enhanced inflammatory function in an adoptive transfer model of colitis [30]. Overall, these studies suggest that inhibition of one or more proteasome subunits may be an effective way to modulate immune cell differentiation and function. The role of proteasome activity in regulation of $CD8^+$ T cell differentiation and immune function are not yet known. Taking into account the observation of asymmetric proteasome activity within mitotic $CD8^+$ T cells, we hypothesize that proteasome activity may be an important regulator of $CD8^+$ T lymphocyte fate specification.

In this dissertation, we demonstrated that $CD8^+$ T lymphocytes responding to infection exhibit significant molecular heterogeneity early during differentiation, and that these putative 'pre-effector' and 'pre-memory' cells that emerge from the first $CD8^+$ T cell division *in vivo* exhibit low and high rates of proteasome activity,

respectively. To experimentally determine whether proteasome activity plays a role in the regulation of $CD8^+$ T cell effector and memory fate specification, we utilized a small molecule proteasome inhibitor and a panel of novel small molecule proteasome activators in both *in vitro* and *in vivo* systems. We employed transcriptomic and proteomic analyses to elucidate the mechanism by which proteasome activity could be affecting $CD8^+$ T cell differentiation. Lastly, we showed that proteasome activity affects $CD8^+$ T cell differentiation via regulation of cellular metabolism. Together, these results suggest a critical role of proteasome activity in the multifaceted control of $CD8^+$ T cell differentiation and raise the possibility that modulation of proteasome activity may be a useful therapeutic strategy to enhance the generation of memory lymphocytes.

CHAPTER 1: CD8$^+$ T LYMPHOCYTES RESPONDING TO INFECTION EXHIBIT MOLECULAR HETEROGENEITY EARLY DURING DIFFERENTIATION

1.1: Introduction

Transcriptional profiling has identified many genes that regulate CD8$^+$ T cell fate specification in an immune response [31,32]. However, potential heterogeneity among individual cells are obscured in bulk population studies. Application of single-cell transcriptional profiling using a selected panel of CD8$^+$ T lymphocyte-associated genes has shown that the CD8$^+$ T cell response to microbial infection results in significant heterogeneity [16]. To take an unbiased approach in characterizing molecular heterogeneity in the CD8$^+$ T cell response, we employ single-cell RNA-seq, which enables us to analyze transcriptome-wide changes in individual CD8$^+$ T cells.

1.2: Results

1.2.1: Experimental setup and validation

To study gene expression changes in single CD8$^+$ T cells responding to a microbial infection *in vivo*, we adoptively transferred P14 CD8$^+$ T lymphocytes, which have transgenic expression of T cell antigen receptors that recognize an immunodominant epitope of LCMV, into congenic recipient mice which were infected i.p. 24 hours later with LCMV-Arm. For spleens to be harvested at days 2 or 4, an overtransfer of cell number was performed in order to detect an adequate number of cells at an early timepoint [14]. At 2, 4, or 7 days post infection, activated P14 CD8$^+$ T

cells, marked by surface expression of CD44hi, were isolated from the spleens of infected mice using magnetic enrichment followed by flow cytometry. At 42 days post infection, T_{CM} ($CD44^{hi}CD62L^{hi}$) and T_{EM} ($CD44^{hi}CD62L^{lo}$) cells were isolated. Naïve P14 $CD8^+$ T cells ($CD44^{lo}CD62L^{hi}$) were isolated from uninfected mice. The Fluidigm C1 Single-Cell Auto Prep System was used to perform SMART-based PCR amplification of full-length polyadenylated transcripts, followed by preparation and sequencing of single-cell cDNA libraries (**Fig. 1.1**) [33]. 10 to 20 million reads per cell were obtained with 60-90% uniquely mapped reads. After quantifying the expression for the entire dataset, PCA estimated a high information content by the Eigen spectrum of its highly structured covariance matrix. At least two technical replicates for each cell population was performed on separate sequencing plates to ensure reproducibility and absence of batch effects (**Fig. 1.2**). Taking into account these quality control measures, we included 256 single-cell libraries divided into 224 sequencing samples and 64 duplicates for further analysis.

1.2.2: $CD8^+$ T lymphocytes that have undergone their first cell division exhibit striking molecular heterogeneity

Single-cell whole transcriptome analysis detected over 6000 genes with a mean expression value of at least 1 TPM per cell. We assessed the expression of a subset of genes with known roles in $CD8^+$ T cell differentiation over the course of infection. The expression of specific terminal effector-associated genes, *Batf* and *Gzmb*, are absent in naïve cells and increasingly higher as the cells approach a terminal effector timepoint of 7 days post-infection (**Fig. 1.3**). Conversely, memory-associated genes

such as *Il7r* and *Sell* are initially high in naïve cells, but they decrease in expression and are robustly re-expressed in memory cells (**Fig. 1.3**). These findings demonstrate that the expression of known $CD8^+$ T cell effector-associated and memory-associated genes can be detected at the single-cell level using our methods.

Strikingly, we also found there was heterogeneous expression of many genes associated with both effector and memory $CD8^+$ T cells present at the first cell division (in *Batf, Gzmb, Il7r,* and *Sell*) or at 4 days post-infection (in *Batf*). This indicates that individual cells may have different levels of expression of these molecules, thus predisposing them to divergent cell fates. Therefore, single-cell whole transcriptome analysis can reveal heterogeneity that was previously obscured by transcriptional averaging in a bulk population analysis.

To characterize patterns of gene expression in single $CD8^+$ T cells across all the time points, we performed unsupervised t-SNE analysis, which assigns each single cell a location in a two-dimensional map to organize the cells into clusters of similarity (**Fig. 1.4**). We found that naïve cells (gray) formed its own cluster, suggesting a homogeneous population. $CD8^+$ T cells that had undergone their first cell division (Division 1, red) formed two distinct clusters. Day 4 (orange), Day 7 (yellow), T_{CM} (purple), and T_{EM} (green) cells formed their own clusters as well. T_{CM} cells clustered closer to naïve cells than T_{EM} cells did.

A striking feature of our t-SNE analysis is that Division 1 cells that were sorted without the use of phenotyping markers were separated into two distinct clusters. Differential gene expression analysis confirmed that these cells, which we have hypothesized to be $Div1_{TE}$ and $Div1_{MEM}$ cells, were molecularly distinct (**Fig. 1.4**).

930 genes distinguished these subpopulations, with 903 genes more highly expressed in $Div1_{TE}$ cells and 27 genes more highly expressed in $Div1_{MEM}$ cells. Some of the genes highly expressed in $Div1_{TE}$ cells include *Batf, Gzmb, Tbx21,* and *Hk2*, transcription factors known to promote effector function, effector differentiation, and metabolic reprogramming. Unexpectedly, many genes associated with memory $CD8^+$ T cell differentiation, such as *Eomes, Foxo1, Tcf7,* and *Il7r,* are also highly expressed in single $Div1_{TE}$ cells. $Div1_{MEM}$ cells, on the other hand, have increased expression of *Il10rb, Il7r, Klf2,*and *S1pr1*, molecules previously associated with memory lymphocytes (**Fig. 1.5**). All together, these data demonstrate that $CD8^+$ T lymphocytes emerging from the first cell division exhibit transcriptional heterogeneity, with a majority of transcriptional upregulation in Div1TE cells, including many genes previously associated with memory differentiation.

1.2.3: Supervised classifiers predict the identity of cells in intermediate stages of differentiation

Since we have observed that $CD8^+$ T lymphocytes emerging from the first cell division were transcriptionally distinct, we hypothesized that these two subpopulations are precursors to fully differentiated effector and memory $CD8^+$ T cells and that the transcriptional profiles of these cells could be used to predict the identity of subsequent, intermediate stages of differentiation. To test this hypothesis, we trained two distinct supervised classifiers: the early state classifier, which was trained on the two first division populations, and the cell fate classifier, which was trained using the terminal effector, T_{CM}, and T_{EM} populations (**Fig. 1.6**).

The early state binary classifier distinguished between $Div1_{TE}$ and $Div1_{MEM}$ cells with a misclassification error rate of 0%, while the cell fate classifier distinguished between terminal effector and the memory populations with an error rate of 1.5%. We utilized both early state and cell fate classifiers to independently predict the identity of $CD8^+$ T cells at day 4 post-infection, which are cells in an intermediate stage of differentiation. We found that the two classifiers utilized non-overlapping gene sets to predict whether the day 4 intermediate cells more closely resembled effector or memory $CD8^+$ T cells (**Fig. 1.7**). Most of the 34 Day 4 intermediate cells were sorted by both classifiers as an intermediate effector-like cells with a lower memory score (lower left quadrant) while a few of the cells were sorted by both classifiers as an intermediate memory-like cell (upper right quadrant). These findings suggest that the transcriptional programs of the Division 1 subpopulations are predictive of their future cell fates and that unique sets of genes may regulate effector and memory differentiation at early and late stages of differentiation.

1.3: Discussion

Single-cell RNA-seq has enabled us to characterize $CD8^+$ T cell heterogeneity in response to microbial infection in an unbiased manner. Most strikingly, unsupervised clustering of $CD8^+$ T cells emerging from the first cell division that were sorted without the use of phenotyping markers resulted in the identification of potential precursors of effector and memory $CD8^+$ T cells ($Div1_{TE}$ and $Div1_{MEM}$). Application of the transcriptional profile of these cell populations predicted the identity of intermediate-stage cells, which were also predicted using the transcriptional

profile of fully differentiated terminal effector anad memory cells, raising the possibility that the Division 1 populations are indeed precursors to effector and memory $CD8^+$ T cells and that independent sets of genes regulate early and late stages of differentiation.

Our data also shows that $Div1_{TE}$ cells are highly transcriptionally active compared to $Div1_{MEM}$ cells. Genes that were highly upregulated in $Div1_{TE}$ cells include those involved in effector function, proliferation, and metabolism. Many genes that are associated with memory $CD8^+$ T cell differentiation and function are also increased in $Div1_{TE}$ cells, raising the possibility that post-translational means of gene regulation might occur in order to promote $CD8^+$ T cell differentiation into memory cells.

Chapter 1, in full, is an adapted version of the material in press at *Nature Immunology*. Kakaradov, Boyko; Arsenio, Janilyn; Widjaja, Christella E.; He, Zhaoren; Aigner, Stefan; Metz, Patrick J.; Yu, Bingfei; Wehrens, Ellen; Lopez, Justine; Kim, Stephanie H.; Zuniga, Elina I.; Goldrath, Ananda W.; Chang, John T.; Yeo, Gene W. 2016. Early transcriptional and epigenetic regulation of $CD8^+$ T cell differentiation revealed by single-cell RNA-seq. *Nat Immunol*. In press. The dissertation author was the co-primary author of all material.

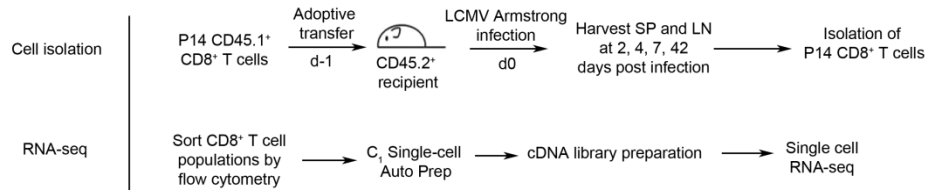


Figure 1.1 Experimental approach for transcriptional analysis of CD8$^+$ T lymphocytes responding to viral infection using single-cell RNA-seq. P14 CD8$^+$ T cells are adoptively transferred to congenically marked recipients then infected with LCMV-Arm. Spleens are harvested at various timepoints. Upon harvest, P14 CD8$^+$ T cells are enriched and sorted using flow cytometry. Single cells are isolated using the C_1 Auto Prep, followed by cDNA library preparation and single-cell RNA-seq.

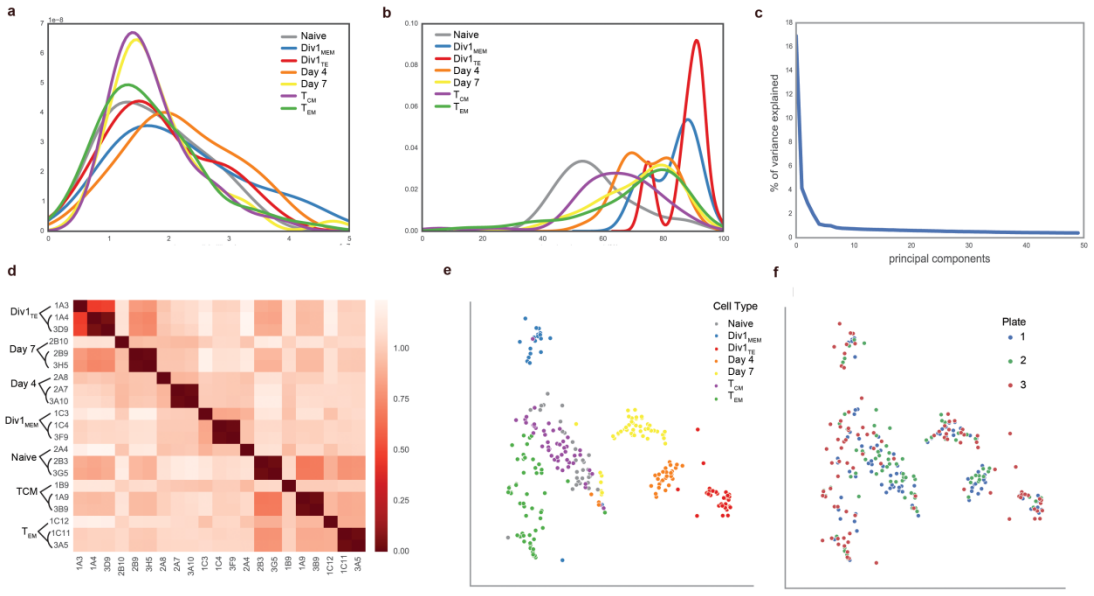


Figure 1.2. Quality control metrics in single cell RNA-seq. (A) Distribution of sequencing output in million of reads per cell for each cell population. **(B)** Distribution of alignment quality expressed as % of reads uniquely mapped. (**C**) Eigen spectrum of covariance for single-cell expression data matrix, sorted by % of variance explained for each principal component, justifying use of top 10 PCs for t-SNE. (**D**) Clustergram of pairwise distances between representative triples of decoy plus duplicate samples from each cell population. (E) t-SNE plot, colored by cell population, of each cell's raw expression counts, expressed in TPM, prior to log transformation. (**F**) Same t-SNE plot but colored by sequencing batch.

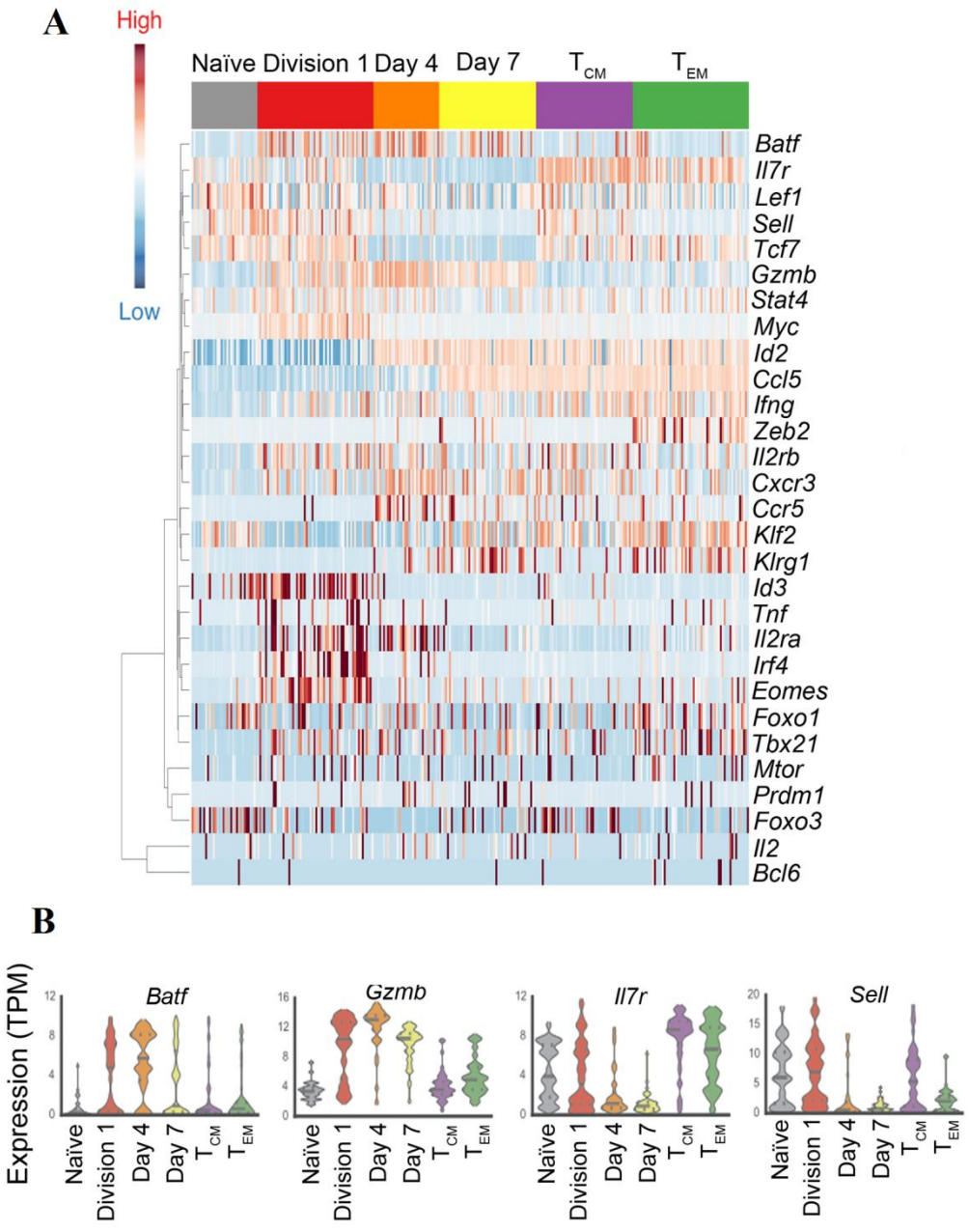


Figure 1.3 Expression of CD8$^+$ T cell-associated genes across time points in a viral infection. (A) Single-cell expression of CD8$^+$ T cell-associated genes in naïve cells (gray), Division 1 cells (red), Day 4 (orange), Day 7 (yellow), T_{CM} (purple), and T_{EM} (green). **(B)** Expression of select genes associated with CD8$^+$ T cell differentiation.

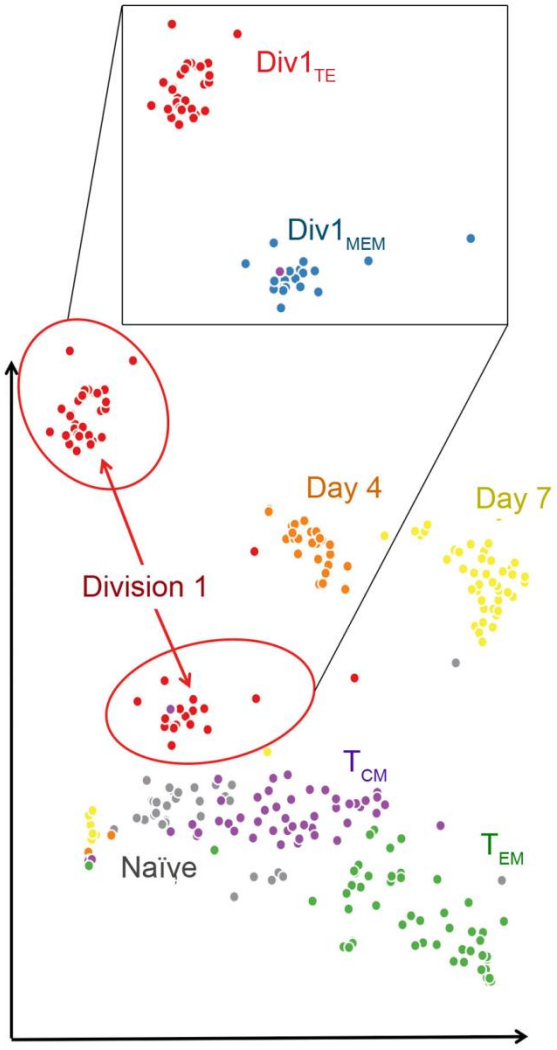


Figure 1.4 t-SNE analysis of single CD8$^+$ T cells reveals distinct subpopulations emerging from the first cell division. (A) t-SNE analysis of 6000 expressed genes from single CD8$^+$ T cells across various timepoints: naïve (gray), Division 1 (red), Day 4 (orange), Day 7 (yellow), T_{CM} (purple), and T_{EM} (green). Each dot represents a single cell. Inset shows the separation of Division 1 cells into $Div1_{TE}$ and $Div1_{MEM}$.

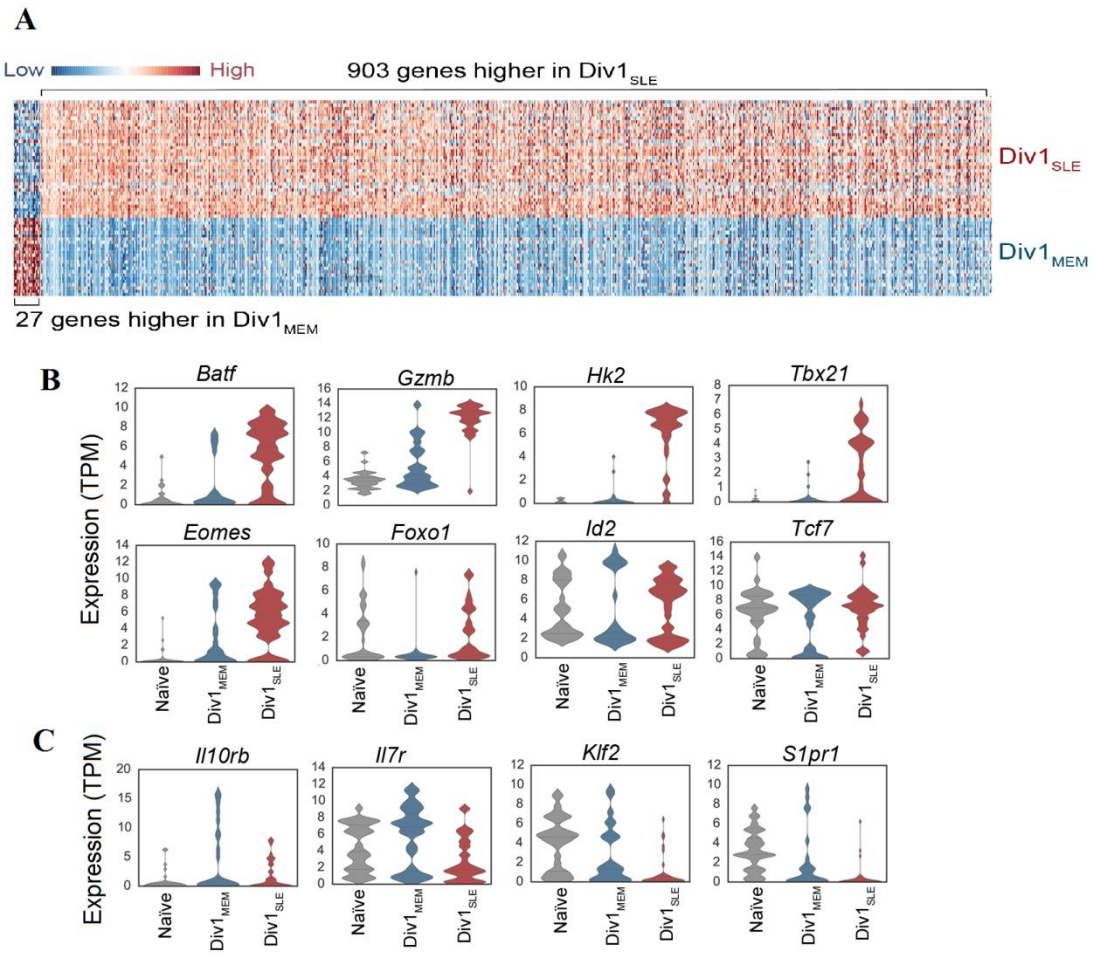


Figure 1.5 Cells emerging from the first cell division express genes associated with effector or memory CD8$^+$ T cells. (A) Heatmap of differential expression of genes in Div1$_{TE}$ and Div1$_{MEM}$ cells. **(B)** Expression of select genes that have increased expression in Div1$_{TE}$. **(C)** Expression of select genes associated that have increased expression in Div1$_{MEM}$.

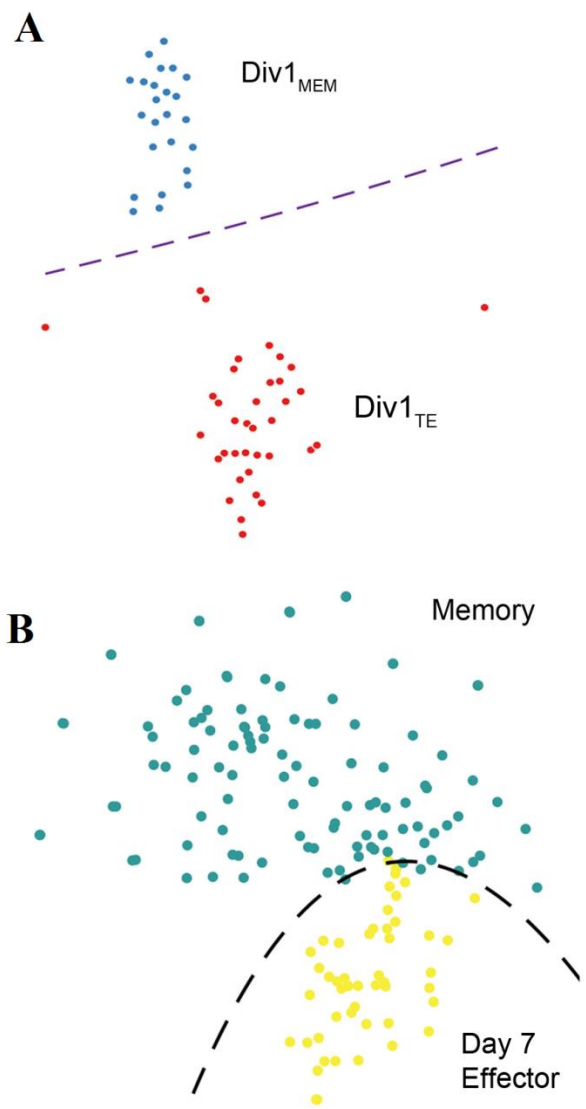


Figure 1.6 Classifiers trained by Division 1 and fully differentiated effector and memory populations. (A) Schematic representation of the early state classifier (purple dashed line) trained on Division 1 lymphocyte populations ($Div1_{MEM}$, blue, n = 24; Div1TE, red, n = 36). **(B)** Schematic representation of the cell fate classifier (black dashed line) trained on Day 7 effector (yellow, n = 48) and total memory cells, which combines T_{CM} and T_{EM} (teal, n = 96).

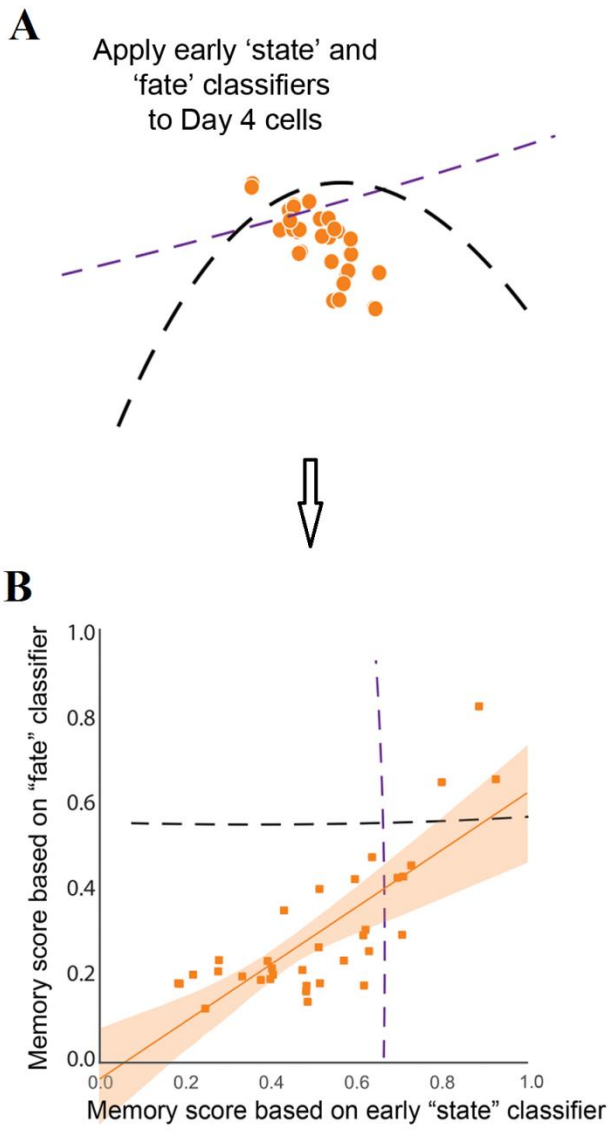


Figure 1.7 Early state and cell fate classifiers agree on the classification of intermediate-stage cells. (A) Schematic representation of the application of early state (purple dashed line) and cell fate (black dashed line) classifiers to Day 4 intermediate-stage cells (n = 34). **(B)** Memory score distribution of early state classifier (x-axis, purple dashed line, 0 = effector to 1 = memory) versus cell fate classifier (y-axis, black dashed line). Orange points represent individual Day 4 $CD8^+$ T lymphocytes. Early state and fate classifier scores correlate well in both linear (Pearson: r = 0.78, p = $4.8e^{-8}$) and monotonic sense (Spearman: r = 0.71, p = $2.2e^{-6}$). The orange shaded area around the orange linear regression line indicates the 95% confidence interval assuming Gaussian error.

CHAPTER 2: DIFFERENTIALLY-FATED CD8$^+$ T CELLS EXHIBIT DISTINCT LEVELS OF PROTEASOME ACTIVITY

2.1: Introduction

The generation of CD8$^+$ T cell heterogeneity can be attributed to asymmetric cell division. Previous studies have shown that CD8$^+$ T lymphocytes can asymmetrically segregate certain cellular components, including the proteasome machinery, during their first division in response to microbial infection [17]. We therefore asked whether asymmetric localization of the proteasome during mitosis might lead to distinct proteasome activity levels in the newly generated daughter cells following division. Activity of the proteasome catalytic subunits was assessed using an irreversible, covalent activity-based probe that has been previously described (**Fig. 2.1**) [34-36].

2.2: Results

2.2.1 Differentially-fated CD8$^+$ T cells emerging from the first cell division have distinct rates of proteasome activity

OT-I CD8$^+$ T cells, which have transgenic expression of T cell antigen receptors that recognize a specific ovalbumin (OVA) epitope, were labeled with CFSE then adoptively transferred into a mouse. 24 hours later, the mice were infected with *L. monocytogenes* that express OVA (Lm-OVA). 45 hours post-infection, splenocytes were harvested and analyzed by flow cytometry. Asymmetric CD8$^+$ T cell division has

been shown to yield one daughter cell (phenotypically $CD8^{hi}$IL-2R$\alpha^{hi}CD62L^{lo}$) exhibiting a predisposition toward the terminal effector fate ('pre-effector') and another daughter cell (phenotypically $CD8^{lo}$IL-2R$\alpha^{lo}CD62L^{hi}$) exhibiting a predisposition toward the long-lived memory fates ('pre-memory') [16]. We observed that pre-effector division 1 cells exhibited lower proteasome activity compared to pre-memory division 1 cells (**Fig. 2.2**). We observed that pre-effector 1^{st} division cells exhibited lower proteasome activity, compared to pre-memory 1^{st} division cells. Moreover, $CD8^+$ T cells exhibiting low proteasome activity expressed higher levels of effector lymphocyte-associated molecules (Granzyme B, T-bet) and lower levels of memory lymphocyte-associated molecules (Bcl-2, IL-7Rα, Tcf7) compared to their counterparts exhibiting low proteasome activity (**Fig. 2.3**).

2.2.2 Distinct rates of proteasome activity is a unique feature of differentially-fated $CD8^+$ T cells emerging from the first cell division

Notably, these patterns of proteasome activity observed in early differentiating cells that had undergone their first division were distinct from those of mature, fully differentiated T lymphocytes. $KLRG1^{hi}$IL7Rα^{lo} terminal effector cells exhibited proteasome activity similar to that of naïve ($CD62L^{hi}CD44^{lo}$) $CD8^+$ T cells, whereas effector memory ($CD44^{hi}CD62L^{lo}$) and central memory lymphocytes ($CD44^{hi}CD62L^{hi}$), assessed at 60 days post-infection, exhibited lower proteasome activity compared to naïve cells (**Fig. 2.4**). Taken together, these findings suggest the possibility that the eventual fates of $CD8^+$ T lymphocytes that have undergone their

first asymmetric division *in vivo* in response to microbial infection might be influenced by their levels of proteasome activity.

2.3:Discussion

Previous work has shown that proteasome activity is asymmetric in a $CD8^+$ T cell undergoing mitosis[17]. In data shown in this chapter, we explored the possibility that asymmetry in proteasome activity persists beyond mitosis and is inherited by the daughter cells generated by the first cell division. Our data shows that pre-effector and pre-memory cells emerging from the first cell division have distinctly low and high levels of proteasome activity, respectively. This pattern of differential proteasome activity was only observed at the first cell division; proteasome activity is not different between naïve, terminal effector, and T_{CM} populations and it is further decreased below to the level of naïve cell proteasome activity in the T_{EM} population. This finding suggests that proteasome activity plays a unique role in influencing $CD8^+$ T cell fate specification early in the process of differentiation.

Chapter 2, in full, is an adapted version of the material that has been submitted for publication. Widjaja, Christella E.; Metz, Patrick J.; Phan, Anthony T.; Savas, Jeffrey N.; de Bruin, Gerjan; Leestemaker, Yves; Berkers, Celia R.; de Jong, Annemeike; Florea, Bogdan I.; Fisch, Kathleen; Lopez, Justine; Kim, Stephanie H.; Garcia, Daniel A.; Searles, Stephen; Bui, Jack D.; Yates III, John R.; Goldrath, Ananda W.; Overkleeft, Hermen S.; Ovaa, Huib; Chang, John T. 2016. Proteasome

activity regulates $CD8^+$ T lymphocyte metabolism and fate specification. In revision. The dissertation was the primary author of all material.

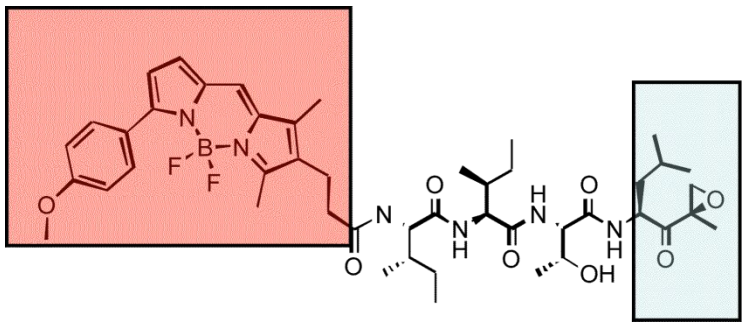


Figure 2.1 Structure of the pan-reactive proteasome probe MV003. Highlighted in blue is the epoxyketone warhead that covalently binds to proteasome activity subunits and in red is a BODIPY TMR fluorochrome reporter. MV003 has been previously described [34-36].

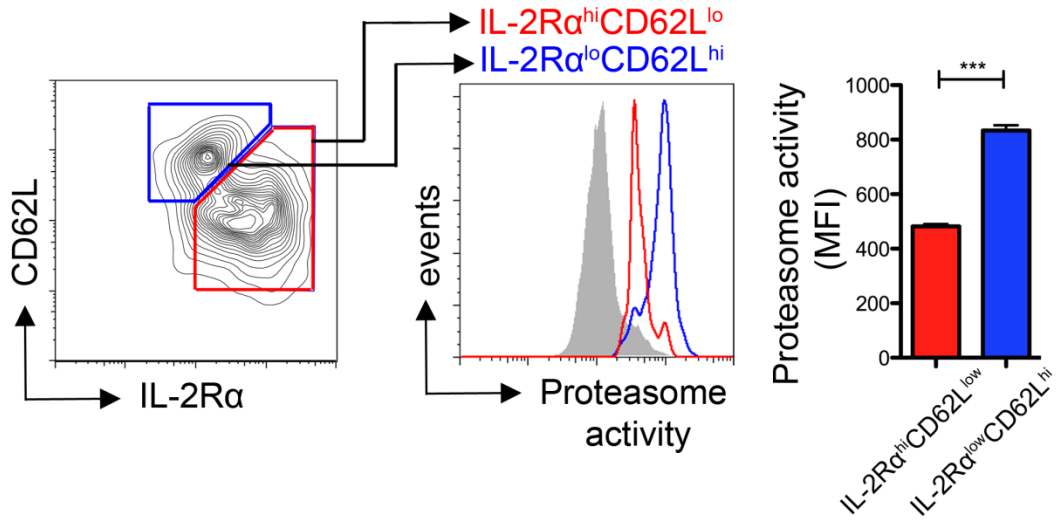


Figure 2.2 Differentially fated CD8$^+$ T cells exhibit distinct rates of proteasome activity. (A) Proteasome activity, assessed by flow cytometry, of gated first division (second CFSE peak) 'pre-effector' IL-2Rα^{hi}CD62L^{lo} and 'pre-memory' IL-2Rα^{lo}CD62L^{hi} OT-I CFSE-labeled CD8$^+$ T cells adoptively transferred into recipient mice that were infected 24 hours later with Lm-OVA. Splenocytes were harvested and analyzed using proteasome probe MV003 at 45 hours post-infection. Data are representative of at least 3 biological replicates from 3 independent experiments. Error bars represent S.E.M. of three replicates. *** $p < 0.001$ (Student's two-tailed *t*-test).

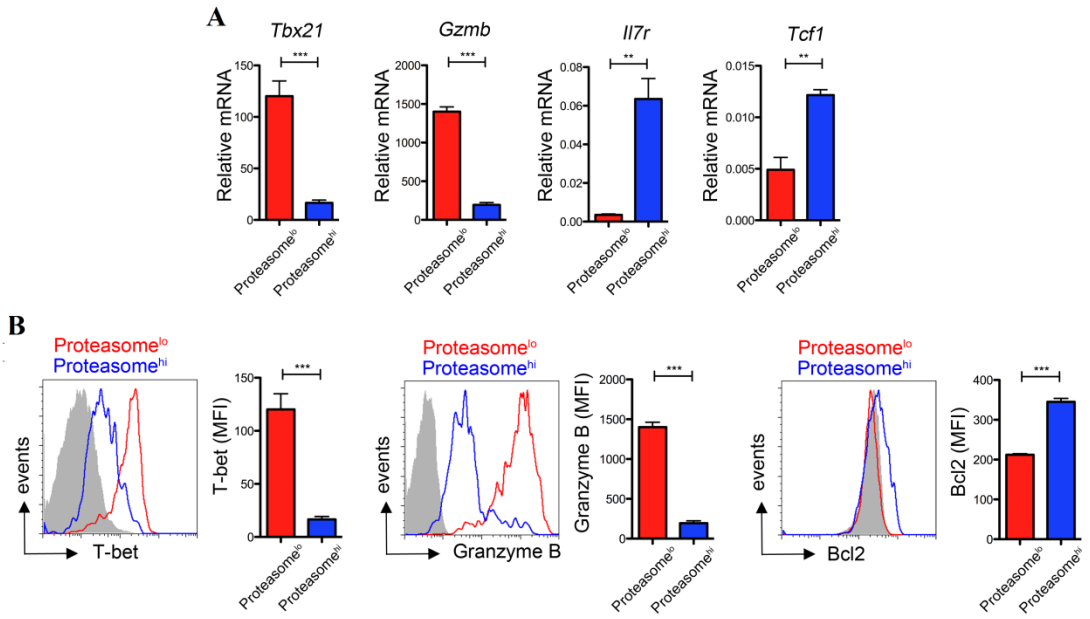


Figure 2.3 Cells with distinct levels of proteasome activity differ in effector and memory CD8$^+$ T cell marker expression. (A) Expression of *Gzmb*, *Tbx21*, *Il7r*, and *Tcf1* mRNA in FACS-sorted division 1 proteasome activity^{lo}IL-2Rα^{hi}CD62L^{lo} (red bars) and proteasome activity^{hi}IL-2Rα^{lo}CD62L^{hi} (blue bars) cells. Expression is measured by qPCR, normalized to the average of *Rpl13* and *Rn18s* mRNA expression. **(B)** Protein expression by flow cytometry expressed as MFI of Granzyme B, T-bet, and Bcl2 in division 1 proteasome activity^{lo}IL-2Rα^{hi}CD62L^{lo} (red) and proteasome activity^{hi}IL-2Rα^{lo}CD62L^{hi} (blue) cells. Gray histogram represents isotype control. Data are representative of at least 3 independent experiments **(A)** or 3 biological repleates from 3 independent experiments **(B)** with at least 4 mice per group. Error bars represent S.E.M. of at least 3 replicates. * $p < 0.05$, ** $p < 0.01$, *** $p < 0.001$ (Student's two-tailed *t*-test).

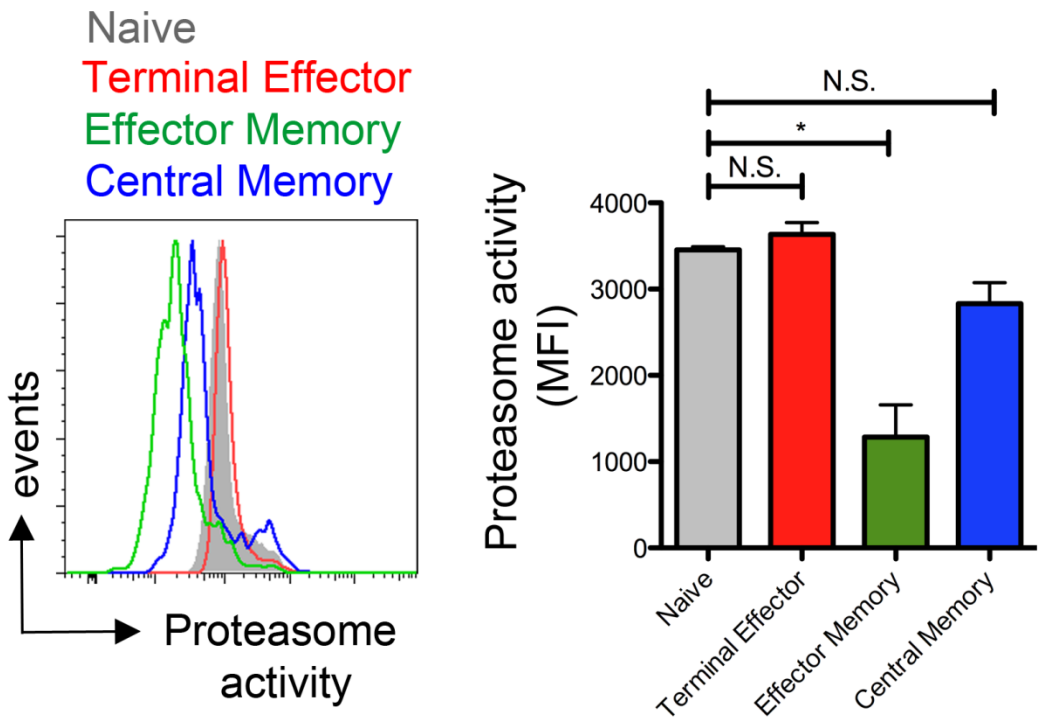


Figure 2.4 Proteasome activity of naïve, terminal effector cells, and memory cells are distinct from that of cells emerging from the first cell division. (A) Proteasome activity, assessed by MV003 fluorescence using flow cytometry, of gated naïve ($CD8^{+}CD45.1^{+}CD62L^{hi}CD44^{lo}$ cells; uninfected mice), terminal effector ($CD8^{+}CD45.1^{+}CD44^{hi}KLRG1^{hi}IL\text{-}7R^{lo}$ cells; 7 d post-infection), effector memory ($CD8^{+}CD45.1^{+}CD44^{hi}CD62L^{lo}$; 60 d post-infection), and central memory ($CD8^{+}CD45.1^{+}CD44^{hi}CD62L^{hi}$; 60 d post-infection) adoptively transferred into congenic mice that were infected with Lm-OVA 24 hours post transfer. Analysis was done at 7 or 60 days post-infection. Data are representative of at least 3 biological replicates from 3 independent experiments. Error bars represent S.E.M. of three replicates. N.S., not significant ($p > 0.05$), * $p < 0.05$ (Student's two-tailed *t*-test).

CHAPTER 3: PROTEASOME ACTIVITY INFLUENCES $CD8^+$ T CELL DIFFERENTIATION AND FUNCTION

3.1: Introduction

Because of our observation that 'pre-effector' and 'pre-memory' cells emerging from the first cell division had distinct levels of proteasome activity, we hypothesized that differences in proteasome activity could dictate the eventual fates of differentiating $CD8^+$ T cells. To experimentally model low and high levels of proteasome activity in $CD8^+$ T cells, we utilized epoxomicin, a pan-subunit proteasome inhibitor, and screen a panel of proteasome activator compounds that were able to increase proteasome activity in immortalized cell lines. Proteasome inhibitor molecules have been previously used in lymphocyte and non-lymphocyte systems to modulate proteasome activity and alter cell differentiation and function [27-30]. Knockdown or inhibition of deubiquitinating enzymes have been shown to increase proteasome activity [37], but the effect of increasing proteasome activity in $CD8^+$ T cells is currently unexplored. In our study, we utilize a panel of molecules predicted to increase proteasome activity (manuscript submitted).

3.2: Results

3.2.1: A screen to identify effective pharmacological modulators of proteasome activity

Naïve $CD8^+$ T cells were treated with proteasome inhibitor or activator for 4 hours, subsequently exposed to proteasome activity probe, then analyzed with flow cytometry. We found that epoxomicin was able to decrease proteasome activity and several proteasome activator molecules induced an increase in proteasome activity (**Fig 3.1**).

Next, we evaluated whether modulation of proteasome activity could influence effector and memory lymphocyte differentiation using a previously described *in vitro* system [38]. $CD8^+$ T cells were stimulated with their cognate peptide for 48 hours, followed by culture with either IL-2 or IL-15 along with proteasome inhibitor, proteasome activator, or vehicle control. In response to IL-2, vehicle-treated cells were able to differentiate into 'effector-like' lymphocytes characterized by high expression of IL-2Rα. Relative to vehicle-treated cells, reducing proteasome activity in IL-2 culture conditions increased the proportion of IL-2Rα^{hi} effector-like lymphocytes, whereas increasing proteasome activity reduced the proportion of these cells (**Fig. 3.2**, top row). In response to IL-15, vehicle-treated cells differentiated into 'memory-like' lymphocytes characterized by high expression of CD62L. Reducing proteasome activity in IL-15 culture conditions reduced the proportion of $CD62L^{hi}$ memory-phenotype cells, whereas increasing proteasome activity with certain proteasome activators (activators 1, 4, 5, and 9) increased the proportion of these cells (**Fig. 3.2**, bottom row).

We subsequently sought to determine whether modulation of proteasome activity might alter production of IFNγ, a proinflammatory effector cytokine characteristic of $CD8^+$ T cell effector function. We purified $CD8^+$ T cells and treated

them transiently with proteasome inhibitor, proteasome activators, or vehicle control. Cells were activated *in vitro* with platebound anti-CD3 and anti-CD28 antibodies. 48 hours later, we assessed the capacity of the cells to produce IFNγ. We observed that cells treated with proteasome inhibitor exhibited an enhanced capacity to produce cytokine relative to cells that received control treatment, while one of the proteasome activators (activator 9) reduced cytokine production by $CD8^+$ T cells (**Fig. 3.3**). We selected this proteasome activator, revealed to be cyclosporine, for subsequent experiments.

Cyclosporine is an immunosuppressive drug that is commonly used to treat transplant rejection [39]. However, it was not previously known to have effects on proteasome activity. A major mechanism of action of cyclosporine is by binding to its cognate intracellular receptor, cyclophilin, inhibiting the calcium/calmodulin-regulated phosphatase calcineurin and preventing nuclear translocation of the transcription factor NFAT [40,41]. Thus, to experimentally separate the effects of cyclosporine on NFAT and proteasome activity, we asked whether transient pre-treatment of $CD8^+$ T cells with cyclosporine, the experimental methodology used in Fig. 3.3, prevents nuclear translocation of NFAT. We found that continuous treatment with cyclosporine blocked NFAT nuclear translocation, but transient pre-treatment of cells prior to activation did not prevent NFAT nuclear translocation (**Fig. 3.4**). We also evaluated another calcineurin inhibitor, tacrolimus, for effects on proteasome activity and $CD8^+$ T cell differentiation. In contrast to cyclosporine, addition of tacrolimus did not increase proteasome activity in $CD8^+$ T cells or enhance differentiation into $CD8^+$ memory-like cells in IL-15 *in vitro* (**Fig. 3.5**). Together,

these results provide evidence that the observed effects of transient cyclosporine treatment on $CD8^+$ T cell differentiation may be mediated by increasing proteasome activity.

In subsequent experiments, epoxomicin ('proteasome inhibitor') and cyclosporine ('proteasome activator') will be used to experimentally test the effects of proteasome activity modulation on $CD8^+$ T cell differentiation. Using an in-gel proteasome activity assay and a luminescent substrate assay, we confirmed our flow cytometry finding that proteasome activity could be modulated in $CD8^+$ T cells with proteasome inhibitor and activator (**Fig. 3.6**).

3.2.2: Proteasome activity influences $CD8^+$ T cell differentiation and function in vitro

We asked whether modulation of proteasome activity might alter other attributes of effector $CD8^+$ T cell differentiation and function in addition to cytokine production. Compared to control-treated cells, proteasome inhibitor-treated cells exhibited higher levels of T-bet and IRF4, key transcription factors that have been linked with terminal effector cell differentiation and function (**Fig. 3.7**) [1,7]. Proteasome inhibitor-treated $CD8^+$ T cells also exhibited increased cytotoxicity when incubated with peptide-pulsed target cells compared to vehicle-treated cells, whereas $CD8^+$ T cells with increased proteasome activity exhibited decreased levels of cytotoxic function (**Fig. 3.8**). These observations suggest that level of proteasome activity might influence $CD8^+$ T lymphocyte fate specification and function *in vitro*.

3.2.3: Proteasome activity influences CD8$^+$ T cell differentiation and memory formation in vivo

After observing that proteasome activity alter CD8$^+$ T cell differentiation and function *in vitro*, we next sought to determine whether an *in vivo* CD8$^+$ T cell response could be affected by level of proteasome activity. We utilized an experimental approach that enabled us to selectively modulate proteasome activity within early differentiating CD8$^+$ T lymphocytes without affecting the cells and tissues of recipient mice. OT-I cells were pre-treated with proteasome inhibitor, proteasome activator, or vehicle control followed by drug washout prior to adoptive transfer into congenically marked recipients that were subsequently infected with 10^3 CFU Lm-OVA. Donor-derived CD8$^+$ T cells were then analyzed at days 7 and 50 post-infection. **Fig. 3.9**).

CD8$^+$ T cells treated with proteasome inhibitor expanded to the same degree as control cells at day 7 post-infection. However, at day 50 post-infection, cells that had received proteasome inhibitor gave rise to fewer memory cells (**Fig. 3.10**). Profiling of the remaining OT-I cells during the contraction phase post-infection revealed that CD8$^+$ T cells treated with proteasome inhibitor have a decreased formation of KLRG1-IL-7R$^+$ cells, effector cells that are thought to be memory precursors that have potential to give rise to long-lived memory cells (**Fig. 3.11**). To confirm the observation of reduced memory differentiation in the recipients that had received inhibitor-treated cells, mice were rechallenged with 10^5 CFU Lm-OVA. We observed that inhibitor-treated cells expanded to a lesser degree than control-treated cells upon rechallenge (**Fig. 3.12**), demonstrating that reducing proteasome activity in CD8$^+$ T cells resulted in a defect in their differentiation into memory lymphocytes.

Treatment of $CD8^+$ T cells with proteasome activator also did not affect their ability to expand by day 7 post-infection. However, proteasome activator-treated cells gave rise to equivalent numbers of total memory cells at day 50 post-infection compared to control cells (**Fig. 3.13**). When these cells were profiled, we found that proteasome activator-treated cells gave rise to memory cells that had an increased proportion of $CD62L^{hi}$ T_{CM} cells, a lower proportion of cells expressing KLRG1, a marker associated with terminal differentiation, and enhanced expression of CD27 and Bcl2, molecules associated with memory cell survival (**Fig. 3.14**) [42,43]. When rechallenged with 10^5 CFU Lm-OVA, mice that had received proteasome activator-treated cells had greater re-expansion in response to the secondary infection (**Fig. 3.15**). Taken together, these results suggest that the level of proteasome activity in $CD8^+$ T cells early during their differentiation may play a critical role in regulating memory lymphocyte fate specification and function.

3.3 Discussion

The observation that $CD8^+$ T cells emerging from the first cell division had differential levels of endogenous proteasome activity led us to hypothesize that pharmacologically decreasing or increasing level of proteasome activity could alter effector or memory differentiation in $CD8^+$ T cells. Using an *in vitro* system, we demonstrated that decreasing proteasome activity polarized $CD8^+$ T cells toward an effector phenotype and that increasing proteasome activity resulted in polarization toward a memory-like cell. In addition to alteration of phenotypic markers, modulation

of proteasome activity was also able to regulate cell functions like cytokine production and cytotoxicity.

In a $CD8^+$ T cell-dependent intracellular bacterial infection, effector cells at the peak of infection were largely unaffected, but proteasome inhibition resulted in a significant decrease in the formation of memory precursors and a decrease in memory cell formation. Proteasome activation increased the proportion of T_{CM} cells, which significantly contribute to the recall response. Most interestingly, the effects of proteasome activity modulation on these differentiating $CD8^+$ T cells was caused by short-term, transient pre-treatment of the cells prior to adoptive transfer. This demonstrates that modulation of cell-intrinsic proteasome activity at an early stage of differentiation is sufficient to drive phenotyping changes observable at a memory timepoint in an *in vivo* response.

Chapter 3, in full, is an adapted version of the material that has been submitted for publication. Widjaja, Christella E.; Metz, Patrick J.; Phan, Anthony T.; Savas, Jeffrey N.; de Bruin, Gerjan; Leestemaker, Yves; Berkers, Celia R.; de Jong, Annemeike; Florea, Bogdan I.; Fisch, Kathleen; Lopez, Justine; Kim, Stephanie H.; Garcia, Daniel A.; Searles, Stephen; Bui, Jack D.; Yates III, John R.; Goldrath, Ananda W.; Overkleeft, Hermen S.; Ovaa, Huib; Chang, John T. 2016. Proteasome activity regulates $CD8^+$ T lymphocyte metabolism and fate specification. In revision. The dissertation was the primary author of all material.

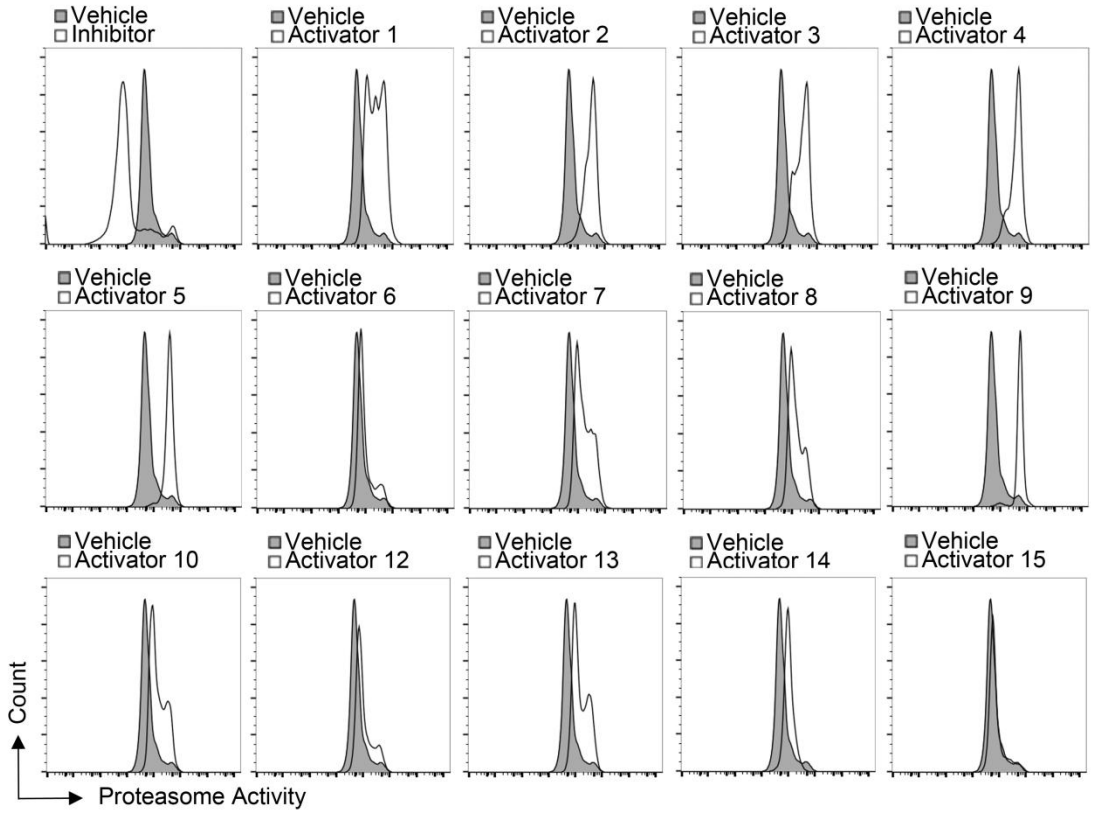


Figure 3.1 Level of proteasome activity can be modulated pharmacologically. Proteasome activity, assessed using MV003 MFI by flow cytometry, of naïve $CD8^+$ T cells following 4 hours culture with vehicle, 0.5 µM proteasome inhibitor, or 5 µM proteasome activators. Data are representative of at least two independent experiments.

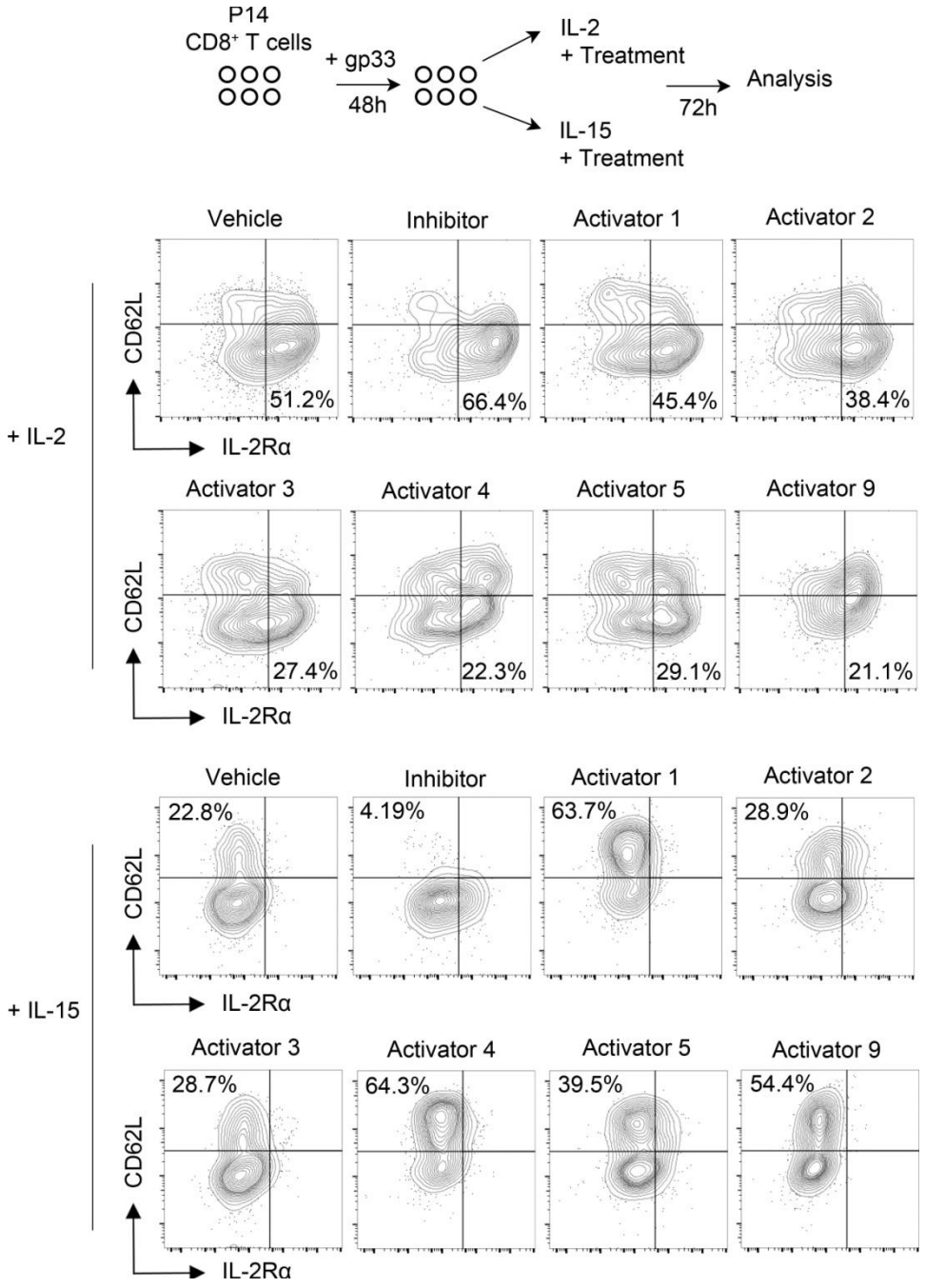


Figure 3.2 Proteasome inhibiton or activation can influence CD8$^+$ T cell differentiation *in vitro*. Experimental design and flow cytometry analysis of *in vitro* IL-2Rα^{hi}CD62L^{lo} 'effector-like' and IL-2Rα^{lo}CD62L^{hi} 'memory-like' P14 CD8$^+$ T cells. Cells were activated for 2 days with gp33 peptide and T-depleted splenocytes, then cultured in IL-2 (top row) or IL-15 (bottom row) in the presence of vehicle, proteasome inhibitor, or indicated proteasome activators for an additional 3 days. Data are representative of at least two independent experiments.

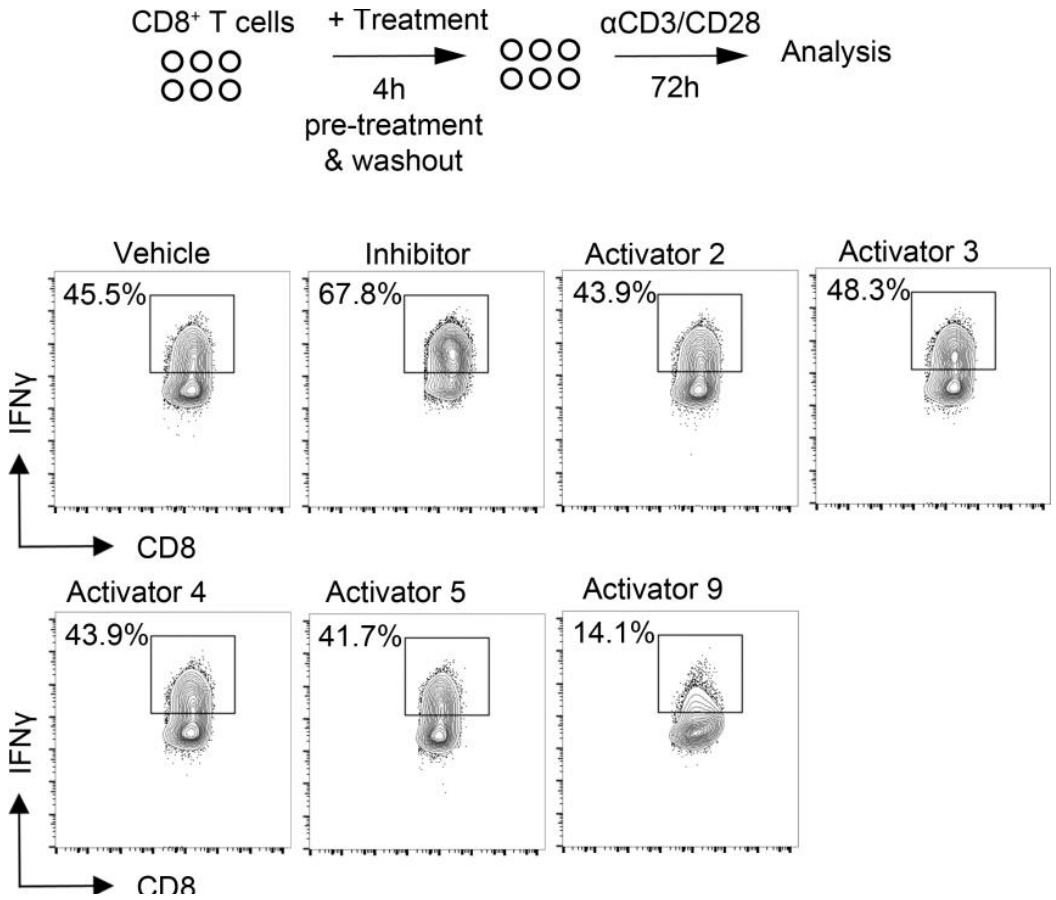


Figure 3.3 Proteasome inhibition or activation affects production of IFNγ. Experimental design and flow cytometry analysis of intracellular IFNγ and TNFα at 3 days post-activation in $CD8^+$ T cells transiently treated for 4 hours with vehicle, proteasome inhibitor, or proteasome activators followed by drug washout prior to activation with anti-CD3 and anti-CD28 antibodies. Data are representative of at least two independent experiments.

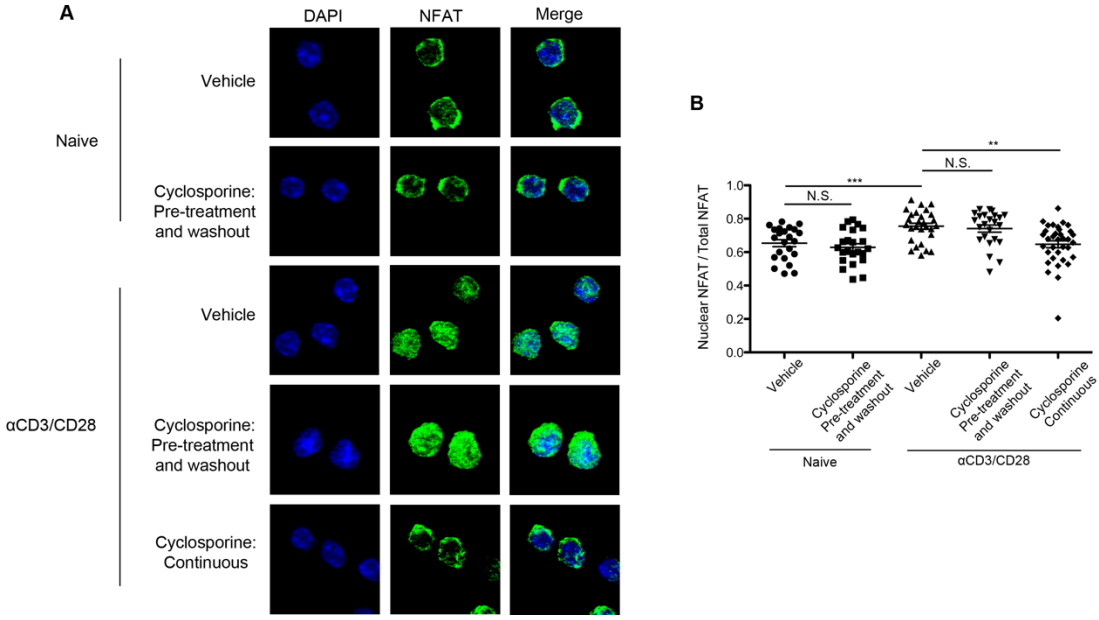


Figure 3.4 Transient pre-treatment of CD8$^+$ T cells with cyclosporine does not block NFAT nuclear translocation. (A) Immunofluorescence staining of NFAT (green) in naïve CD8$^+$ T cells or CD8$^+$ T cells that were activated *in vitro* with 10 µg/ml immobilized anti-CD3 and anti-CD28 for 10 minutes. Prior to imaging, activated CD8$^+$ T cells were pre-treated with DMSO (n = 27) for 4 h; pre-treated for 4 h with cyclosporine followed by drug washout (n = 35); or pre-treated for 4 h with cyclosporine without drug washout during activation (n = 23) ('continuous cyclosporine'). Nuclei were stained with DAPI (blue). **(B)** Nuclear localization was measured by the ratio of nuclear NFAT over total NFAT. Quantification was performed using NIH ImageJ software. Error bars represent S.E.M., * $p < 0.05$, ** $p < 0.01$, *** $p < 0.001$ (Student's two-tailed *t*-test).

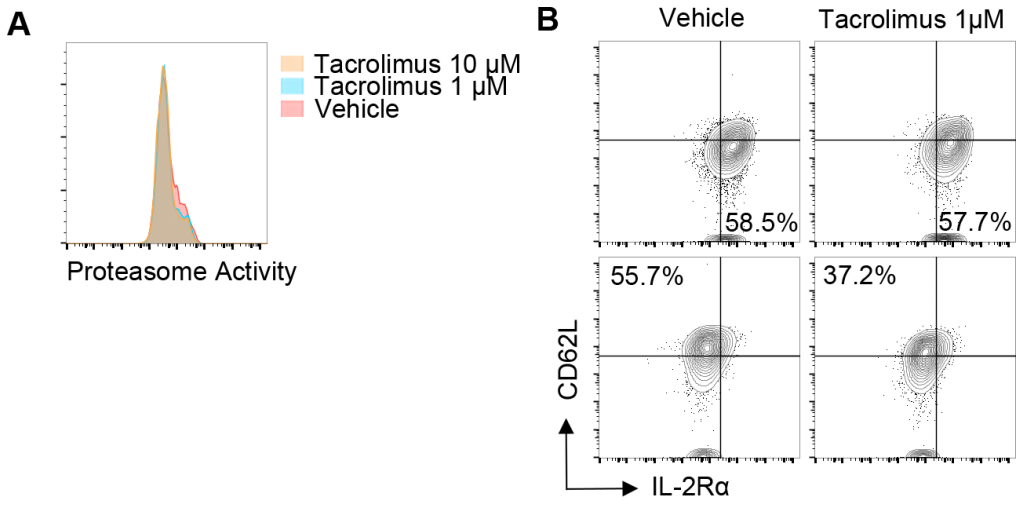


Figure 3.5 Effects on proteasome activity and CD8$^+$ T cell differentiation are not a general feature of calcineurin inhibitors. (A) Proteasome activity, assessed by flow cytometry, of naïve CD8$^+$ T cells following 4 h culture with vehicle (red) or calcineurin inhibitor tacrolimus at 1 μM (blue) and 10 μM (yellow). **(B)** Flow cytometry analysis of *in vitro* IL-2Rα^{hi}CD62L^{lo} 'effector-like' and IL-2Rα^{lo}CD62L^{hi} 'memory-like' P14 CD8$^+$ T cells. Cells were activated for 2 days with gp33 peptide and T-depleted splenocytes, then cultured in IL-2 (top row) or IL-15 (bottom row) in the presence of vehicle or tacrolimus. Data are representative of at least two independent experiments.

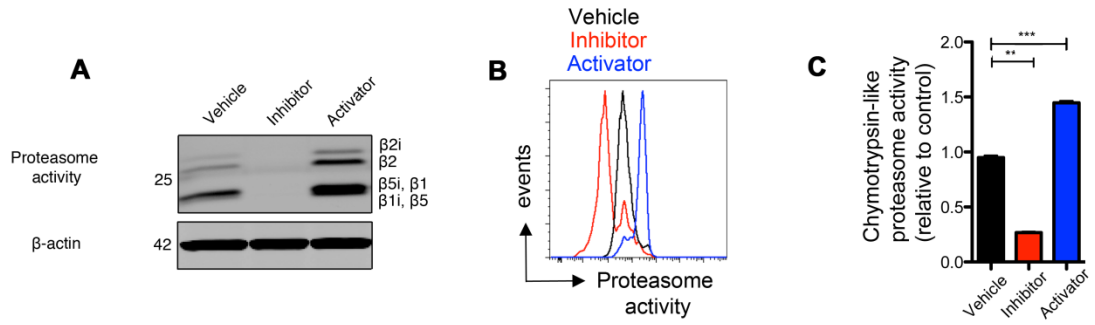


Figure 3.6 Validation of selected proteasome inhibitor and activator in modulation of proteasome activity. (**A**) Proteasome activity, assessed by in-gel assay, of naïve $CD8^+$ T cells following 4 hours culture with vehicle, proteasome inhibitor, or proteasome activator. Immunoblotting was performed with anti-β-actin antibodies to confirm equal loading of samples. (**B**) Proteasome activity, assessed by flow cytometry, of cells cultured with vehicle (black line), proteasome inhibitor (red line), or proteasome activator (blue line). (**C**) Proteasome activity, assessed by bioluminescent chymotrypsin-like proteolytic assay, of cells cultured with proteasome inhibitor (red bar) or proteasome activator (blue line) and normalized to vehicle control (black bar). Data are representative of at least two independent experiments with at least 3 biologic replicates. Error bars represent S.E.M. of three replicates. ** $p < 0.01$, *** $p < 0.001$ (Student's two-tailed *t*-test).

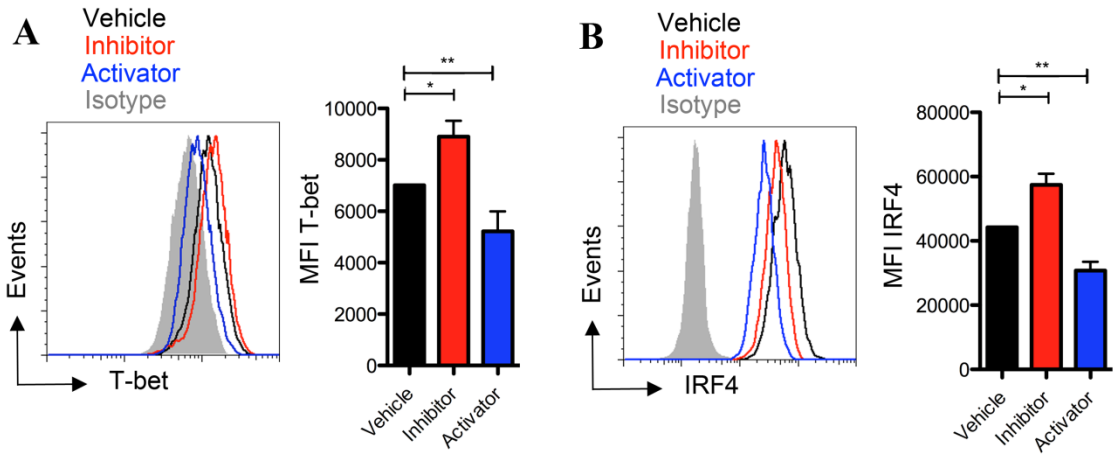


Figure 3.7 Modulation of proteasome activity affects effector CD8$^+$ T cell differentiation. Flow cytometry analysis (left) and mean fluorescence intensity (right) of **(A)** T-bet **(B)** IRF4 at 3 days post-activation in CD8$^+$ T cells transiently treated for 4 hours with vehicle, proteasome inhibitor, or proteasome activator prior to activation with anti-CD3 and anti-CD28 antibodies. Data are representative of at least two independent experiments with at least 3 biologic replicates. Error bars represent S.E.M. of three replicates. * $p < 0.05$, ** $p < 0.01$ (Student's two-tailed *t*-test).

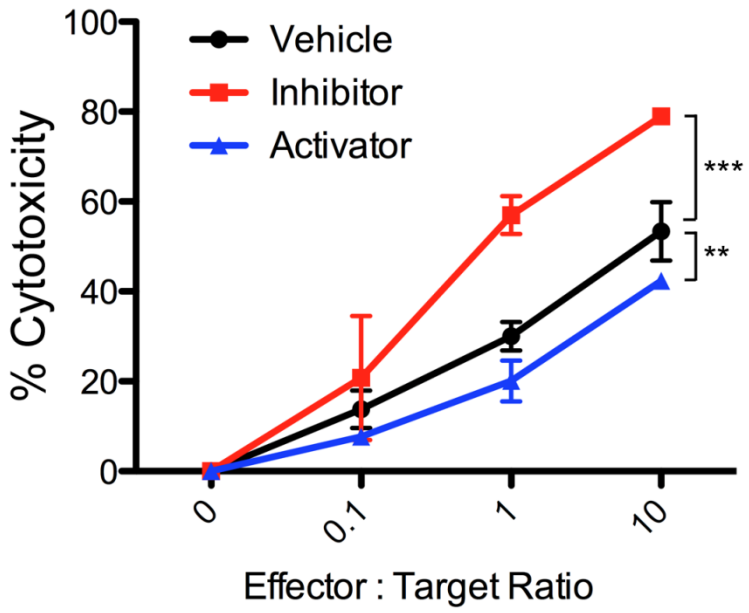


Figure 3.8 Proteasome activity regulates effector CD8$^+$ T cell cytotoxic function. Percent specific cytotoxicity of OT-I CD8$^+$ T cells treated transiently with vehicle (black line), proteasome inhibitor (red line), or proteasome activator (blue line) prior to culture with T depleted-splenocytes and ovalbumin peptide. CD8$^+$ T cells were incubated with an equal ratio of peptide-pulsed and unpulsed splenocytes in varying effector cell to target cell ratios. Cytotoxicity was calculated by subtracting the difference in live cell percentage between pulsed and unpulsed target cells, normalized to the live percentage of unpulsed target cells. Data are representative of at least 3 biologic replicates from 3 independent experiments. ** $p < 0.01$, *** $p < 0.001$ (one-way ANOVA).

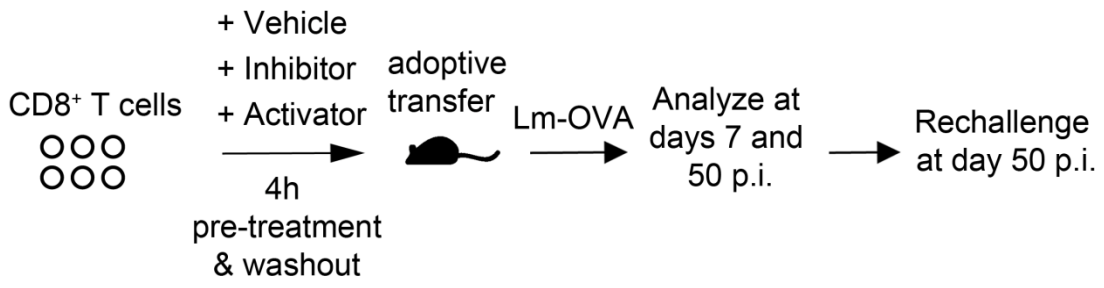


Figure 3.9 Experimental approach in analysis of the effect of proteasome activity modulation on the CD8$^+$ T cell response to infection. TCR transgenic CD8$^+$ T cells are pre-treated with vehicle, proteasome inhibitor, or proteasome activator. Then, cells are adoptively transferred into a recipient mouse that is subsequently infected with 10^3 CFU Lm-OVA. Mice are sacrificed and splenocytes are analyzed at days 7 and 50 post infection. At day 50 post infection, some mice are rechallenged with 10^5 CFU Lm-OVA.

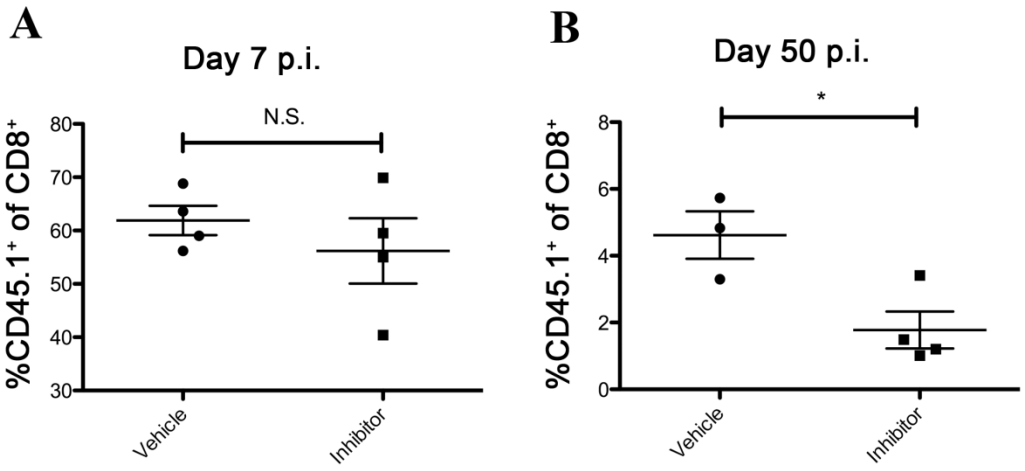


Figure 3.10 Proteasome inhibition does not affect percentage of effector CD8$^+$ T cells but decreases percentage of memory CD8$^+$ T cells. Percentages of CD45.1$^+$ vehicle- and proteasome inhibitor-treated CD8$^+$ T cells, analyzed by flow cytometry at days **(A)** 7 and **(B)** 50 post-infection. Data are representative of two independent experiments with n = 4 mice per group; error bars represent S.E.M. of four replicates. N.S., not significant ($p > 0.05$), * $p < 0.05$ (Student's *t*-test).

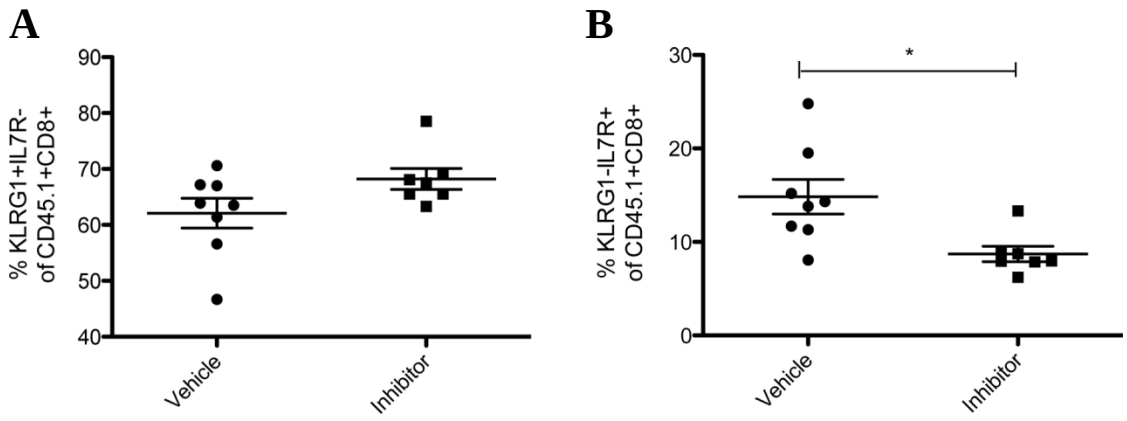


Figure 3.11 CD8$^+$ T cells with decreased proteasome activity have a decreased percentage of memory precursor cells during contraction. Percentages of **(A)** KLRG1$^+$IL-7R$^-$ terminal effector cells and **(B)** KLRG1$^-$IL-7R$^+$ memory precursor effector cells analyzed by flow cytometry at day 21 post-infection. Data are representative of at least two independent experiments with n ≥ 4 mice per group; error bars represent S.E.M. N.S., not significant ,p > 0.05, * p < 0.05 (Student's *t*-test).

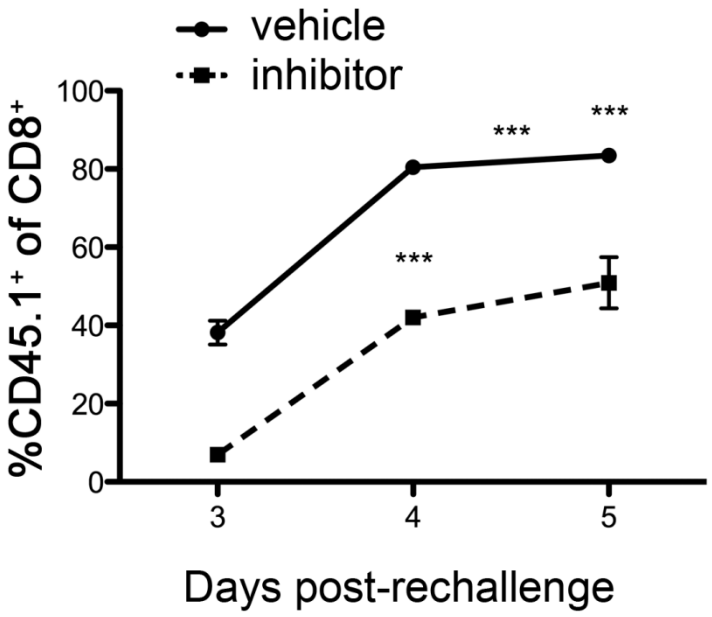


Figure 3.12 CD8$^+$ T cells with decreased proteasome activity have a reduced recall response to a secondary infection. Proliferative response of CD45.1$^+$ CD8$^+$ T cells in response to reinfection with 10^5 CFU LM-ova in immune mice that had received cells treated with vehicle or proteasome inhibitor 50 days prior. Data are representative of at least two independent experiments with $n \geq 4$ mice per group; error bars represent S.E.M. of four replicates. *** $p < 0.001$ (Student's *t*-test).

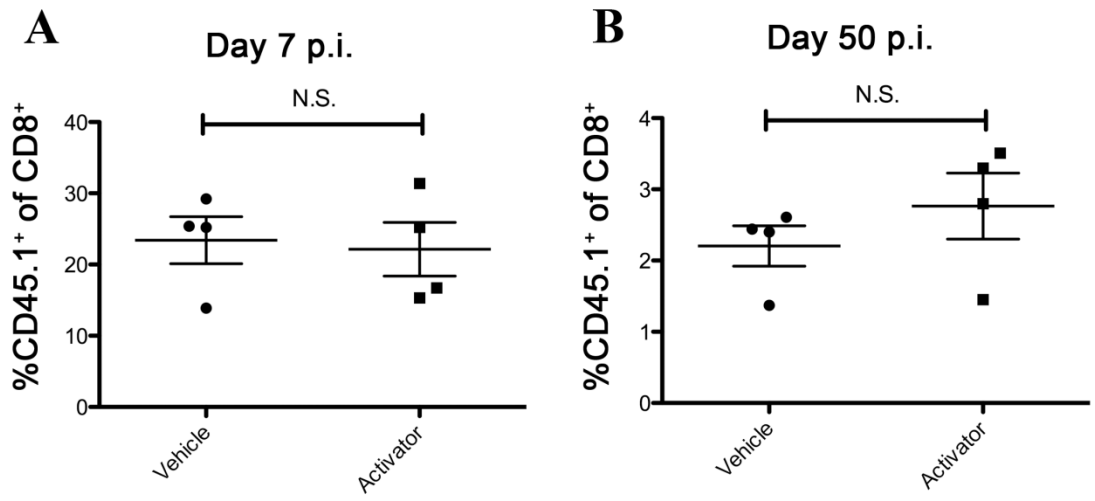


Figure 3.13 Increasing proteasome activity does not affect percentage of effector or memory CD8$^+$ T cells. Percentages of CD45.1$^+$ vehicle- and proteasome activator-treated CD8$^+$ T cells, analyzed by flow cytometry at days **(A)** 7 and **(B)** 50 post-infection. Data are representative of two independent experiments with n = 4 mice per group; error bars represent S.E.M. of four replicates. N.S., not significant, $p > 0.05$, (Student's *t*-test).

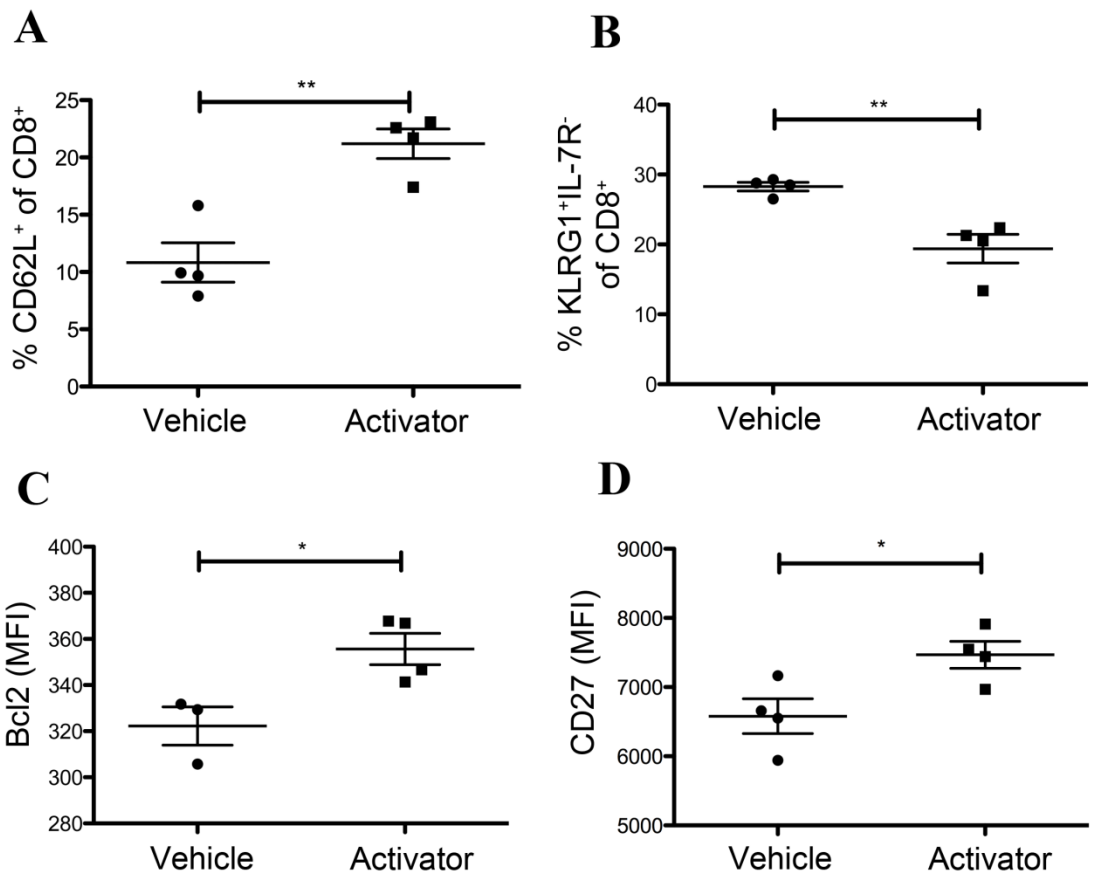


Figure 3.14 CD8$^+$ T cells with increased proteasome activity have increased generation of central memory cells. Flow cytometry analysis of **(A)** CD62L and (B) KLRG1 percentage of CD45.1$^+$ vehicle- and proteasome activator-treated CD8$^+$ T cells and (C) Bcl2 and (D) CD27 MFI at 50 days post-infection. Data are representative of two independent experiments with n = 4 mice per group; error bars represent S.E.M. of four replicates. * $p < 0.05$, ** $p < 0.01$ (Student's *t*-test).

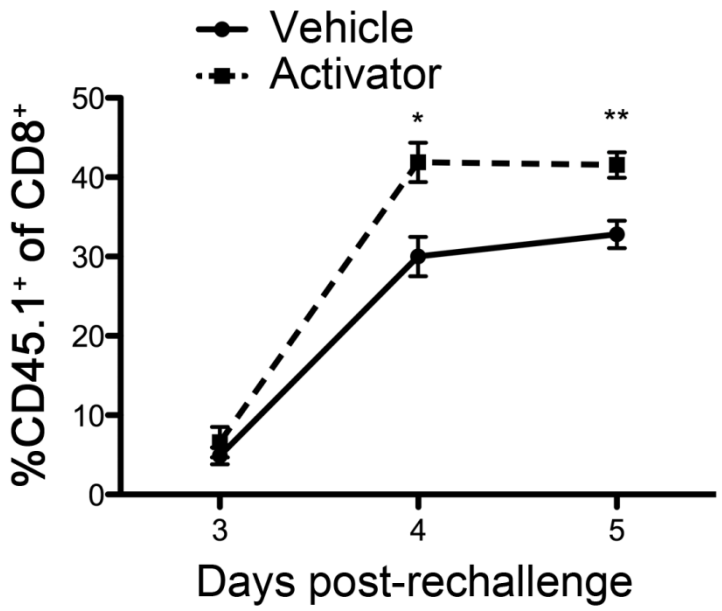


Figure 3.15 Memory CD8$^+$ T cells generated from proteasome activator-treated cells have an increased recall response. Proliferative response of CD45.1$^+$ CD8$^+$ T cells in response to reinfection with 10^5 CFU Lm-OVA in immune mice that had received cells treated with vehicle or proteasome activator 50 days prior. Data are representative of two independent experiments with n = 4 mice per group; error bars represent S.E.M. of four replicates. * $p < 0.05$, ** $p < 0.01$ (Student's *t*-test).

CHAPTER 4: PROTEASOME ACTIVITY REGULATES $CD8^+$ T CELL DIFFERENTIATION THROUGH EFFECTS ON CELLULAR METABOLISM

4.1: Introduction

Early changes in proteasome activity results in profound changes in memory $CD8^+$ T cell phenotype and function in response to *in vivo* infection. Protein degradation is a process that can affect a variety of cellular processes, including lymphocyte activation, proliferation, metabolism, and apoptosis. In order to identify the processes that are affected by proteasome-mediated degradation, we employed a transcriptomic analysis and a quantitative shotgun proteomic screen. From these methods, we identified that cellular metabolism was one of the processes affected by modulation of proteasome activity. It is known that upon activation and effector differentiation, T cells undergo a metabolic switch to aerobic glycolysis in order to generate more biosynthetic precursors support growth and proliferation [44,45]. In this chapter we explore the different processes that are affected by proteasome activity as well as a candidate degradation target by which proteasome activity influences cellular metabolism.

4.2: Results

4.2.1: Transcriptomic and proteomic analyses identify that proteasome activity alters cellular metabolism

To begin to investigate the molecular mechanisms underlying proteasome-mediated regulation of terminal effector and memory lymphocyte differentiation, we performed microarray analysis of $CD8^+$ T cells treated with proteasome inhibitor, proteasome activator, or vehicle control activated for 24 hours *in vitro*. 470 and 1,461 genes were significantly differentially expressed in inhibitor-treated and activator-treated cells, respectively, compared to vehicle-treated cells (**Fig. 4.1**). Proteasome activator-treated cells differentially expressed several transcriptions previously reported to be important for T cell function, survival, and memory function, including *Ifng, Il2, Tbx21, Eomes, Bcl2, Klf2*, and *Il7r* (**Fig. 4.2**).

Differentially expressed genes were subjected to pathway analysis to determine relevant Gene Ontology Biological Processes categories. This analysis identified metabolic processes among the most significantly affected pathways, including apoptosis, lipid metabolism, cellular protein metabolism, and cell proliferation (**Fig. 4.3**). Gene set enrichment analysis (GSEA) revealed that transcripts expressed in proteasome inhibitor-treated cells were significantly enriched within the set of genes associated with effector $CD8^+$ T cells obtained from Molecular Signatures Database (MSigDB) (**Fig. 4.4, Supplementary Table 1**). Conversely, transcripts upregulated in proteasome activator-treated cells were significantly enriched within the set of genes associated with naïve and memory $CD8^+$ T cells (**Fig. 4.4**). Taken together, these data suggest that low and high proteasome activity levels induced by proteasome inhibitor and activator resulted in gene expression patterns resembling those found in effector and memory $CD8^+$ T cells, respectively.

Next we aimed to identify categories of proteins affected by differential levels of proteasome activity. We performed a quantitative shotgun proteomic screen using stable isotope labeling by amino acids in cell culture (SILAC), a method in which newly synthesized proteins are differentially labeled with different isotopes. $CD8^+$ T cells treated with proteasome inhibitor, proteasome activator, or vehicle control were cultured for 52 hours (6 cell divisions) in media containing unlabeled or labeled 'heavy' L-lysine andL-arginine to allow metabolic incorporation of these amino acids into proteins. After cell lysis, peptides were analyzed by multi-dimensional liquid chromatography mass spectrometry (LC-MS/MS). Differentially expressed proteins were compared between experimental groups. Relative to control-treated cells, 337 proteins were found at higher levels in proteasome inhibitor-treated cells, whereas 341 proteins were found at lower levels in proteasome activator-treated cells (**Fig. 4.5**). Pathway analysis of differentially abundant proteins suggested that proteasome inhibition significantly affected several metabolic processes, including ribonucleoprotein complex biogenesis, generation of precursor metabolites, and electron transport chain activity. Proteasome activation had the most pronounced effects on pathways involving lymphocyte activation and differentiation (**Fig. 4.6**). Taken together, the findings from the transcriptomic and proteomic analyses suggested the possibility that level of proteasome activity within early differentiating $CD8^+$ T cells might play a role in regulating lymphocyte fate specification by virtue of effects on cellular metabolism.

4.2.2: $CD8^+$ T cells with altered levels of proteasome activity utilizle different methods of cellular metabolism

Previous studies have shown that effector $CD8^+$ T cells increase the use of aerobic glycolysis, the process by which glucose is converted to lactate in the presence of oxygen, whereas memory $CD8^+$ T cells preferentially utilize oxidative phosphorylation to meet metabolic demands [44,45]. To test the possibility that differential levels of proteasome activity, we examined the levels of glycolysis and oxidative phosphorylation in $CD8^+$ T cells transiently treated with proteasome inhibitor, proteasome activator, or vehicle prior to activation in vitro for 72 hours. Proteasome inhibitor-treated cells exhibited an increased extracellular acidification rate (ECAR), maximal glycolytic capacity, and glucose uptake compared to control-treated cells (**Fig. 4.7**). Conversely, proteasome inhibitor-treated cells exhibited a decreased maximal respiratory capacity, while proteasome activator-treated cells exhibited a significant increase (**Fig. 4.8**). In support of the hypothesis that low levels of proteasome activity may promote glycolysis, we observed that inhibitor-treated cells exhibited increased expression of genes associated with glycolysis and glutaminolysis, such as Glut1, Hk2, Eno1, Ldha, and Pfkp (**Fig. 4.9**). These results suggest that low levels of proteasome activity may promote metabolic reprogramming by enhancing the expression *of key metabolic genes involved in the glycolytic program.*

4.2.3 Myc is a target of proteasome-mediated regulation of cellular metabolism

We next sought to determine the mechanism by which proteasome activity influences the glycolytic transcriptional program. Several key transcription factors, including Myc, estrogen-related receptor α (ERRα), and hypoxia-inducible factor 1-

α (HIF1α), have been shown to facilitate metabolic reprogramming by upregulating genes associated with the glycolytic pathway [3,46-48]. Conversely, Bcl-6 directly represses genes encoding the glycolytic pathway while Foxo1 positively regulates genes involved in mitochondrial function and fatty acid metabolism [49,50]. Relative to control-treated cells, proteasome inhibitor-treated cells exhibited increased expression of Myc; however, no significant changes in the levels of Hif1α, ERRα, Bcl-6, or Foxo1 were observed in the setting of proteasome inhibition (**Fig. 4.10**).

Because we observed increased expression of Myc in $CD8^+$ T cells exhibiting low proteasome activity, we asked whether Myc expression was functionally required for the proteasome inhibitor-mediated effects on effector $CD8^+$ T cell differentiation. We assessed IFNγ as a proxy of effector cell differentiation because its expression is dependent on the induction of glycolysis [51]. We activated wild-type $CD8^+$ T cells treated with proteasome inhibitor or vehicle control and added a Myc inhibitor at 24 hours following activation to avoid potential confounding effects on cell activation and proliferation [46]. Strikingly, addition of Myc inhibitor prevented the increase in IFNγ production induced by proteasome inhibition, suggesting that the proteasome-mediated effect on effector differentiation was dependent on Myc (**Fig. 4.11**). By contrast, analogous experiments performed with Hif1α-deficient $CD8^+$ T cells suggested that Hif1α might be dispensable for the proteasome-mediated effects on early T cell effector differentiation (**Fig. 4.12**).

Although we did not observe changes in the expression level of Bcl-6 and Foxo1 in $CD8^+$ T cells treated with proteasome inhibitor or activator, it remained

possible that these molecules could nonetheless play a functional role in mediating decreased effector $CD8^+$ T cell differentiation induced by the proteasome activator. We activated Bcl-6-deficient, Foxo1-deficient, or wild-type $CD8^+$ T cells treated with proteasome activator or vehicle control. Bcl-6-deficient and Foxo1-deficient $CD8^+$ T cells exhibited a proteasome activator-mediated reduction in IFNγ production comparable to that observed with control cells, suggesting that both Bcl-6 and Foxo1 may be dispensable for proteasome-mediated effects on effector differentiation (**Fig. 4.13**). Taken together, these results suggest that proteasome-mediated effects on metabolic reprogramming and effector differentiation may be predominantly dependent on Myc.

The observation of distinct proteasome activity levels within daughter cells emerging from the first T cell division *in vivo*, together with the finding that proteasome activity-mediated effects on effector differentiation were Myc-dependent, prompted us to hypothesize that Myc might also be unequally expressed in the first daughter cells by virtue of differential degradation. OT-I $CD8^+$ T cells were labeled with CFSE and adoptively transferred into recipient mice, which were subsequently infected with Lm-OVA. Splenocytes were harvested and analyzed 48 hours post-infection. When gating on cells that had undergone their first division, $CD8^{hi}$ 'pre-effector' cells exhibiting low proteasome activity expressed higher levels of My compared to $CD8^{lo}$ 'pre-memory' cells exhibiting high proteasome activity (**Fig. 4.12**).

Next, we wanted to experimentally determine that the differential levels of Myc observed in division 1 'pre-effector' and 'pre-memory' cells were dependent on

level of proteasome activity. To experimentally model distinct levels of proteasome activity in division 1 daughter cells, polyclonal $CD8^+$ T cells were CFSE labeled then activated for 24 hours using anti-CD3 and anti-CD28 antibodies. Undivided parental cells (first CFSE peak) were sorted using flow cytometry. Sorted cells were re-cultured for an additional 4 hours along with proteasome inhibitor or activator to model the low and high proteasome activity experienced by the 'pre-effector' and 'pre-memory' cells. Myc protein was then assessed by flow cytometry in the cells that had undergone cell division (second CFSE peak). We observed that nascent daughter cells pharmacologically induced to exhibit low proteasome activity expressed higher levels of Myc, whereas daughter cells induced to exhibit high proteasome activity expressed lower levels of Myc (**Fig. 4.13**). Taken together, these data suggest that the low proteasome activity observed in first division pre-effector daughter cells may result in reduced degradation and consequently increased abundance of Myc, leading to increased glycolytic activity and effector differentiation.

4.3: Discussion

Transcriptional and proteomic analysis both revealed that in $CD8^+$ T cells treated with proteasome inhibitor, apoptosis, cellular metabolism, and proliferation were among the categories of pathways that were affected. However, in $CD8^+$ T cells treated with proteasome activator, we found that categories involving lymphocyte activation, function, survival, and differentiation were most significantly affected. An explanation for this discrepancy could be that $CD8^+$ T cells treated with proteasome activator were more similar to vehicle-treated cells in that they had just become better

effector cells; thus, the most significant differences between the two groups are the processes involving metabolism since they are similar in function and differentiative state. In contrast, activator-treated $CD8^+$ T cells are skewed away from the effector phenotype. Therefore, any changes in lymphocyte activation, differentiation, and function are much more detectable.

When directly assaying cellular metabolism, we found that proteasome inhibitor-treated $CD8^+$ T cells are significantly more glycolytic than control $CD8^+$ T cells. We found that Myc is the primary transcription factor whose level is regulated by proteasome activity. Previous studies have shown that upon T cell activation, Myc drives a rapid increase in glycolysis and glutaminolysis, which was also shown to de-repress genes associated with effector function, including IFNγ [46]. Further, we also found that Myc is asymmetric at the first cell division and that Myc levels could be altered by decreasing or increasing proteasome activity [52]. This is consistent with other findings that PI3K signaling and mTORC1 kinase activity, which also drive the metabolic switch to glycolysis, are asymmetric at the first cell division [53,54]. One study notes that Myc expression is regulated by mTORC1 activity and asymmetric segregation of amino acid transporters [52]. Proteasome-mediated degradation could be an alternative mechanism that contributes to asymmetric expression of Myc in differentially fated cells emerging from the first cell division.

Chapter 4, in full, is an adapted version of the material that has been submitted for publication. Widjaja, Christella E.; Metz, Patrick J.; Phan, Anthony T.; Savas, Jeffrey N.; de Bruin, Gerjan; Leestemaker, Yves; Berkers, Celia R.; de Jong, Annemeike; Florea, Bogdan I.; Fisch, Kathleen; Lopez, Justine; Kim, Stephanie H.;

Garcia, Daniel A.; Searles, Stephen; Bui, Jack D.; Yates III, John R.; Goldrath, Ananda W.; Overkleeft, Hermen S.; Ovaa, Huib; Chang, John T. 2016. Proteasome activity regulates $CD8^+$ T lymphocyte metabolism and fate specification. In revision. The dissertation was the primary author of all material.

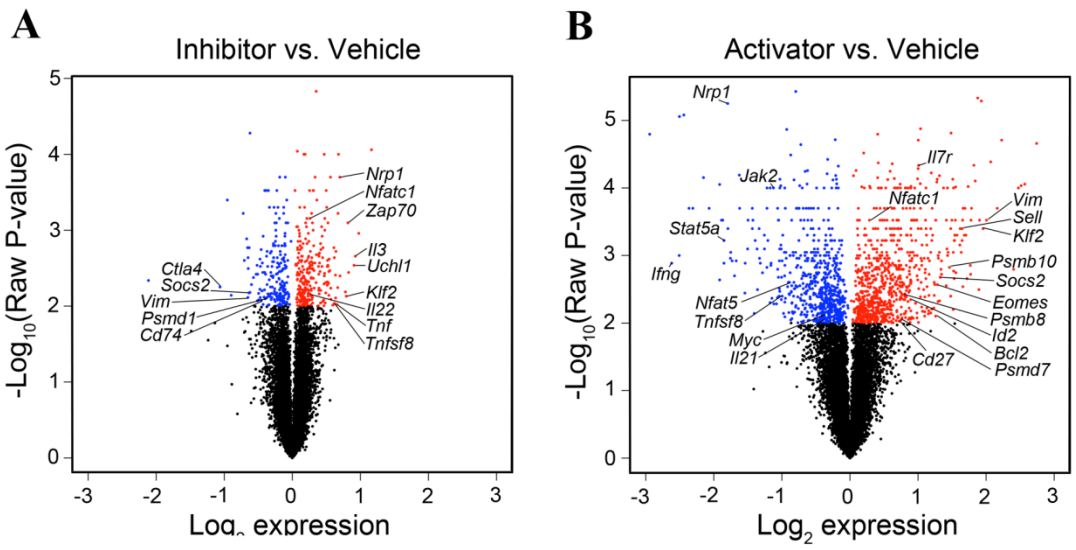


Figure 4.1 Transcriptional profiling of CD8$^+$ T cells with decreased or increased proteasome activity reveals differential gene expression. Volcano plots depicting differentially expressed genes derived from microarray gene expression analysis in CD8$^+$ T cells treated with **(A)** proteasome inhibitor or **(B)** proteasome activator prior to activation with anti-CD3 and anti-CD28 antibodies for 24 hours, compared to gene expression of vehicle-treated cells. X axis represents normalized Log_2 expression and y axis represents significance as $–Log_{10}$ (*t*-test p-value). Each dot represents an individual gene; red or blue coloration represents significantly differentially upregulated or downregulated genes, respectively. Microarray data are derived from two biological replicates.

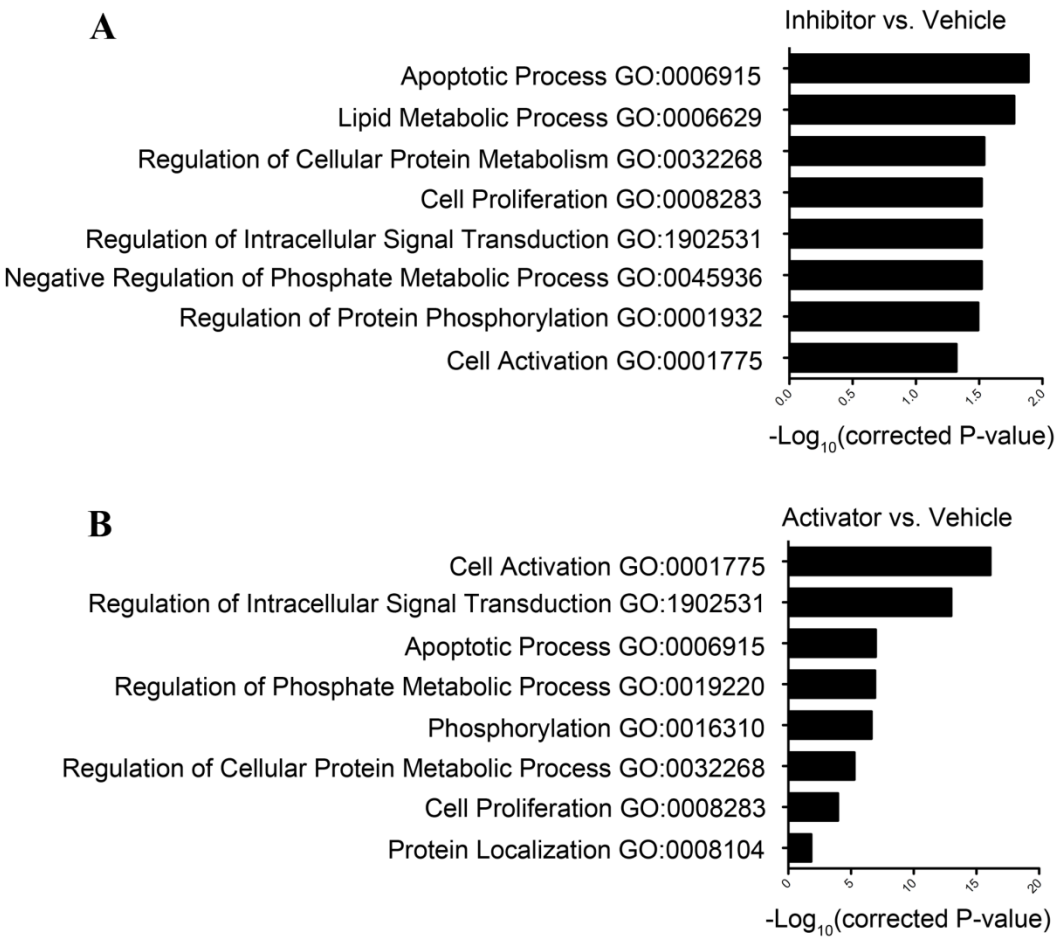


Figure 4.2 Pathway analysis reveals that modulation of proteasome activity affects many CD8$^+$ T cell functions including apoptosis, metabolic processes, and signal transduction. Gene Ontology Biological Processes of differentially expressed gene sets in **(A)** proteasome inhibitor-treated or **(B)** proteasome activator-treated CD8$^+$ T cells activated for 24 hours by anti-CD3 and anti-CD28 antibodies are shown in order of significance as $-\text{Log}_{10}$ (corrected p-value).

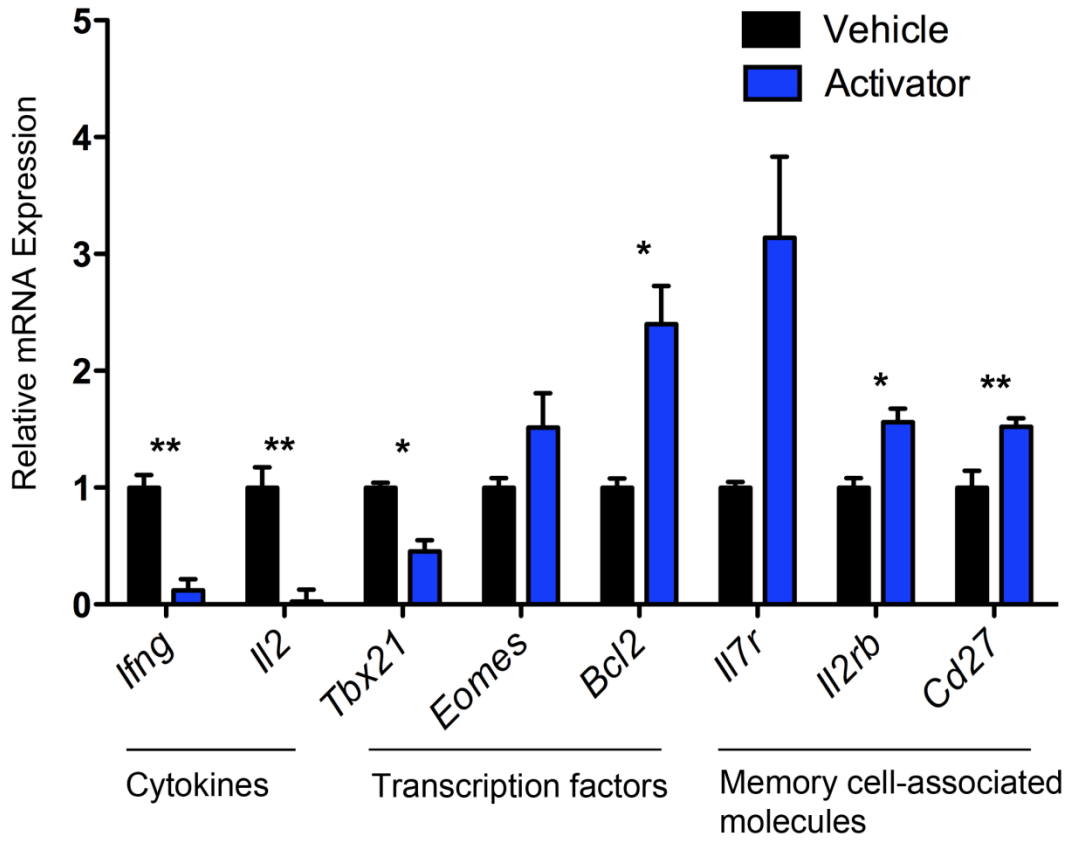


Figure 4.3 Memory-associated genes have increased expression in proteasome activator-treated CD8$^+$ T cells. mRNA expression of selected cytokines, transcription factors, and memory-associated genes in proteasome activator-treated CD8$^+$ T cells 24 hours following activation with anti-CD3 and anti-cD28 antibodies. Expression is shown relative to vehicle-treated cells and normalized to the average of *Rpl13* and *Rn18s* RNA. Data are representative of 3 biologic replicates from 3 independent experiments. Error bars represent S.E.M. of three replicates. N.S., not significant, $p > 0.05$, * $p < 0.05$, ** $p < 0.01$, *** $p < 0.001$ (Student's two-tailed *t*-test).

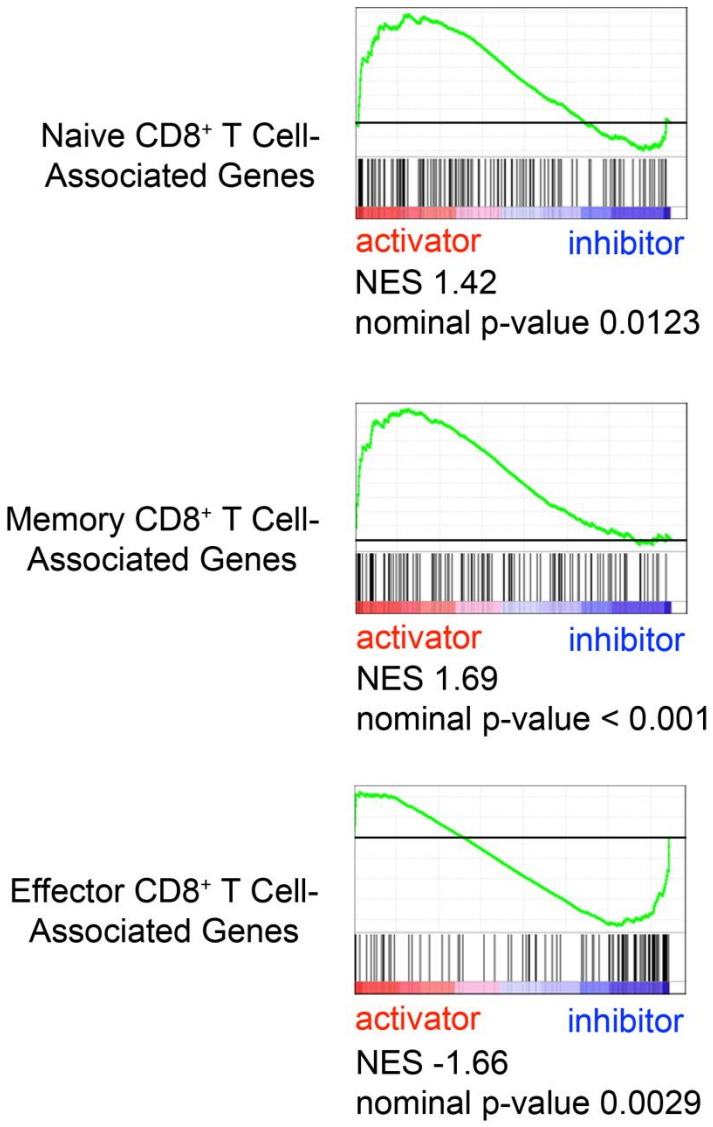


Figure 4.4 Transcriptional profile of proteasome inhibitor-treated cells resemble effector CD8$^+$ T cells while proteasome activator-treated cells resemble memory CD8$^+$ T cells. Gene Set Enrichment Analysis of functional enrichment of differentially expressed genes in proteasome inhibitor-treated vs. proteasome activator-treated cells activated for 24 hours by anti-CD3 and anti-CD28 antibodies; naïve, effector, and memory enrichment datasets were obtained from MSigDB. Normalized Enrichment Score (NES) is visualized in green.

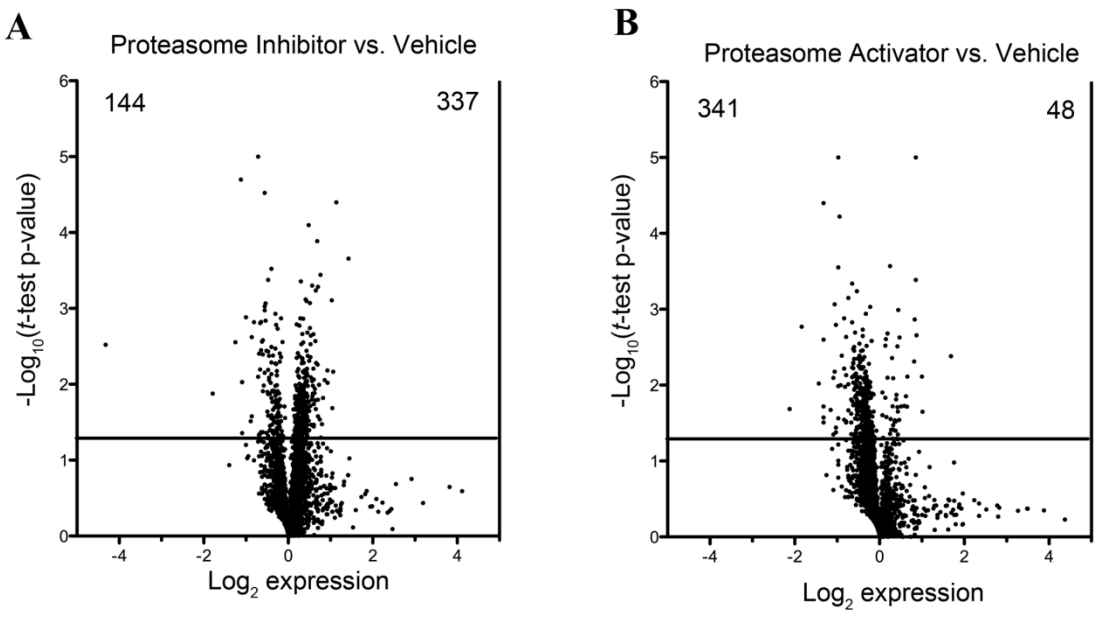


Figure 4.5 Mass spectrometry analysis reveals that proteasome activity modulation alters global proteome of CD8$^+$ T cells. Volcano plots depicting differentially expressed proteins derived from quantitative analysis in CD8$^+$ T cells treated with **(A)** proteasome inhibitor or **(B)** proteasome activator prior to activation with anti-CD3 and anti-CD28 antibodies for 72 hours, compared to vehicle-treated cells. Data are representative of 3 biologic replicates. Numbers in the top left and right corners represent the number of proteins whose abundance was decreased or increased, respectively, relative to vehicle treatment. Black horizontal line represents the threshold of significance ($p < 0.05$).

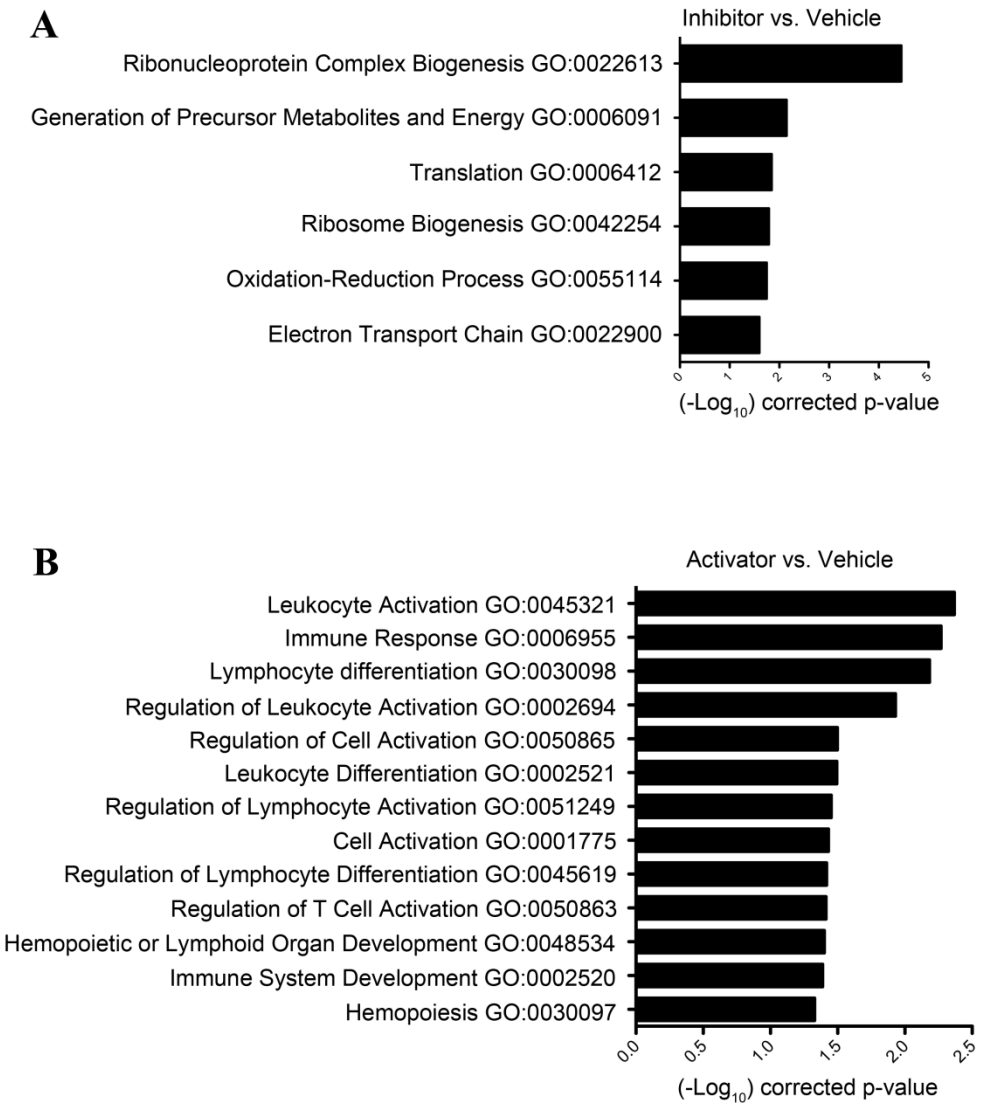


Figure 4.6 Functional characterization of differentially expressed proteins reveals that proteasome inhibition alters processes associated with cellular metabolism. Gene Ontology Biological Processes categories enriched in proteins that were differentially expressed by **(A)** proteasome inhibitor-treated or **(B)** proteasome activator-treated $CD8^+$ T cells activated for 72 hours by anti-CD3 and anti-CD28 antibodies, shown in order of significance as $-Log_{10}$(*t*-test p-value).

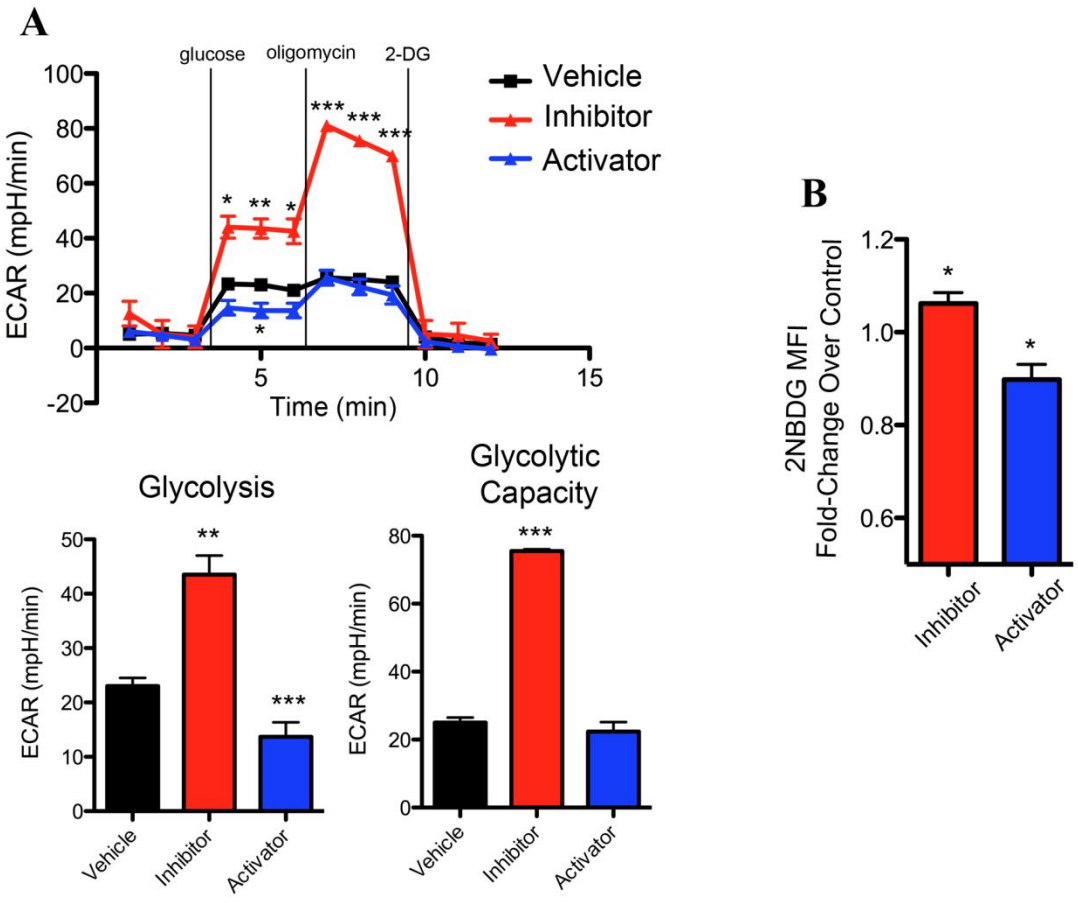


Figure 4.7 CD8$^+$ T cells with decreased proteasome activity have an increased rate of glycolysis and glucose uptake. (A) Glycolytic activity, expressed as extracellular acidification rate (ECAR) of CD8$^+$ T cells transiently treated with vehicle (black), proteasome inhibitor (red), or proteasome activator (blue) prior to activation with anti-CD3 and anti-CD28 antibodies for 72 hours. Glucose, oligomycin, and 2-DG are added at specified time points. Bar graphs represent glycolysis and maximal glycolytic capacity. **(B)** Glucose uptake, as measured by uptake of 2-NBDG, in CD8$^+$ T cells transiently treated with proteasome inhibitor (red) or proteasome activator (blue), relative to control-treated cells, as in **(A)**. Data are representative of 3 independent experiments, n ≥ 3 replicates per group. Error bars represent S.E.M. of three replicates. * $p < 0.05$, ** $p < 0.01$, *** $p < 0.001$ (Student's two-tailed *t*-test).

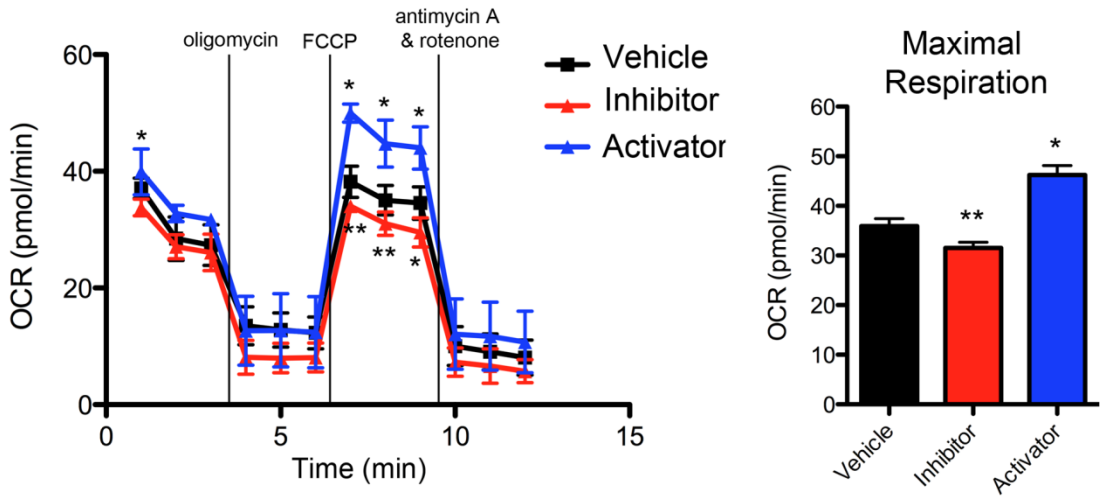


Figure 4.8 CD8$^+$ T cells with increased proteasome activity have an increased maximal respiratory capacity. Oxidative phosphorylation, expressed as oxygen consumption rate (OCR), in CD8$^+$ T cells transiently treated with vehicle (black), proteasome inhibitor (red), or proteasome activator (blue) prior to activation with anti-CD3 and anti-CD28 antibodies for 72 hours. Oligomycin, FCCP, antimycin A, and rotenone are added at specified time points. Bar graph represents maximal respiratory capacity. Data are representative of 3 independent experiments, n ≥ 3 replicates per group. Error bars represent S.E.M. of three replicates. * $p < 0.05$, ** $p < 0.01$ (Student's two-tailed *t*-test).

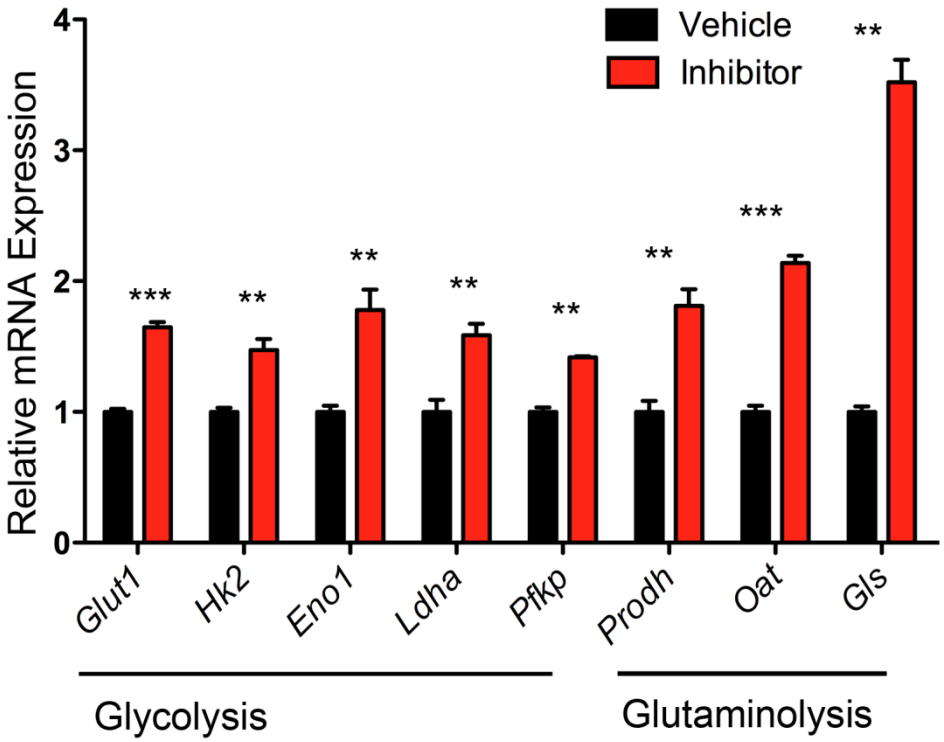


Figure 4.9 Proteasome inhibitor treatment of CD8$^+$ T cells results in increased expression of glycolysis genes. Relative mRNA expression of genes involved in glycolysis and glutaminolysis in FACS-sorted vehicle- or proteasome inhibitor-treated CD8$^+$ T cells activated with anti-CD3 and anti-CD28 antibodies for 72 hours. Expression is shown relative to vehicle-treated cells and normalized to *Actb* RNA. Data are representative of 3 independent experiments, $n \geq 3$ replicates per group. Error bars represent S.E.M. of three replicates. ** $p < 0.01$, *** $p < 0.001$ (Student's two-tailed *t*-test).

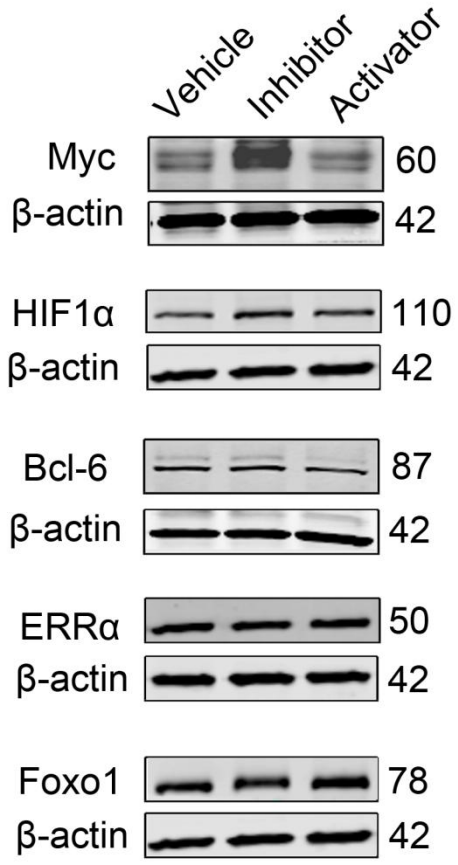


Figure 4.10 Proteasome inhibitor treatment of CD8$^+$ T cells results in increased Myc expression. Immunoblot analysis of Myc, HIF1α, Bcl-6, ERRα, and Foxo1 in vehicle-, proteasome inhibitor-, and proteasome activator-treated CD8$^+$ T cells activated by anti-CD3 and anti-CD28 antibodies for 72 hours. Actin was assessed to ensure equal loading. Molecular weight of each protein is displayed. Data are representative of two independent experiments.

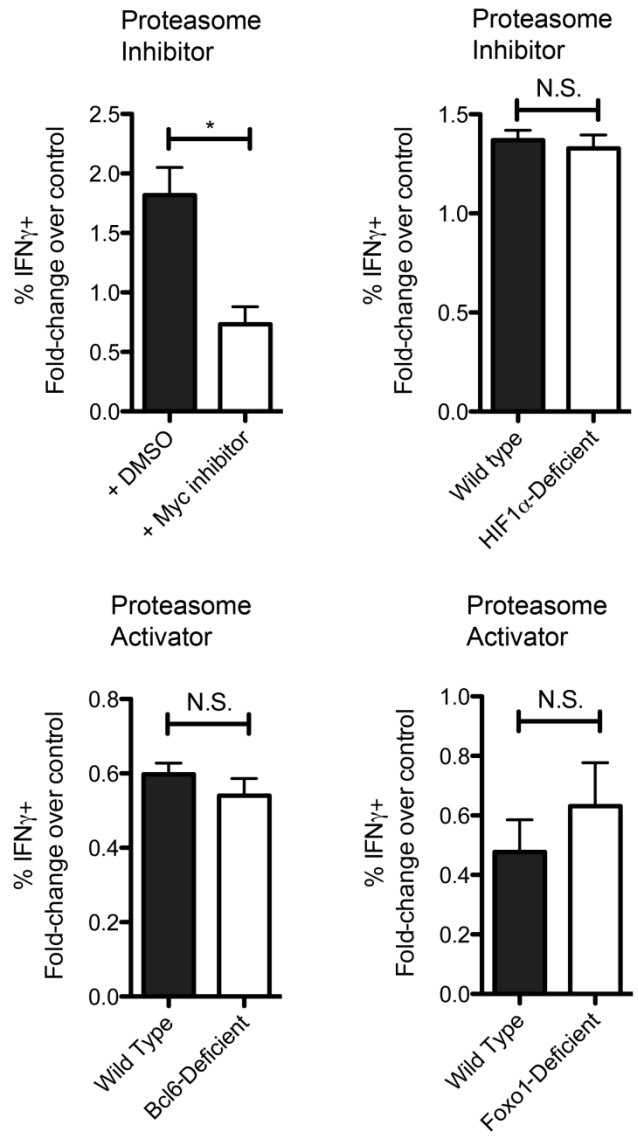


Figure 4.11 Enhanced CD8$^+$ T cell effector function induced by proteasome inhibitor is dependent on Myc expression. (A) Flow cytometry analysis of IFNγ production in CD8$^+$ T cells transiently treated with proteasome inhibitor, relative to vehicle control, prior to activation by antibodies against CD3 and CD28, followed by addition of DMSO or Myc inhibitor at 24 h post-activation. **(B)** Flow cytometry analysis of IFNγ production in wild-type or HIF1α-deficient CD8$^+$ T cells transiently treated with proteasome inhibitor, relative to vehicle control, prior to activation. **(C, D)** Flow cytometry analysis of IFNγ production in wild-type, Bcl6-deficient **(C)**, or Foxo1-deficient **(D)** CD8$^+$ T cells transiently treated with proteasome inhibitor, relative to vehicle control, prior to activation. Data are representative of 2 independent experiments, $n \geq 3$ replicates per group. Error bars represent S.E.M. of three replicates. * $p < 0.05$ (Student's two-tailed *t*-test).

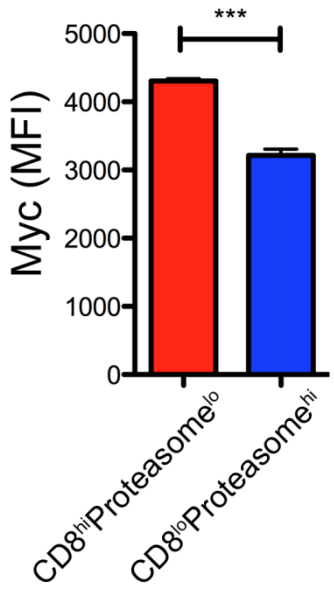


Figure 4.12 Pre-effector and pre-memory cells emerging from the first cell division express differential levels of Myc. MFI of Myc in first division proteasome activity^{lo}CD8^{hi} (red) and proteasome activity^{hi}CD8^{lo} (blue) cells, measured by flow cytometry, gated by CFSE dilution. Data are representative of 2 independent experiments, n ≥ 3 replicates per group. Error bars represent S.E.M. of three replicates. *** $p < 0.001$ (Student's two-tailed *t*-test).

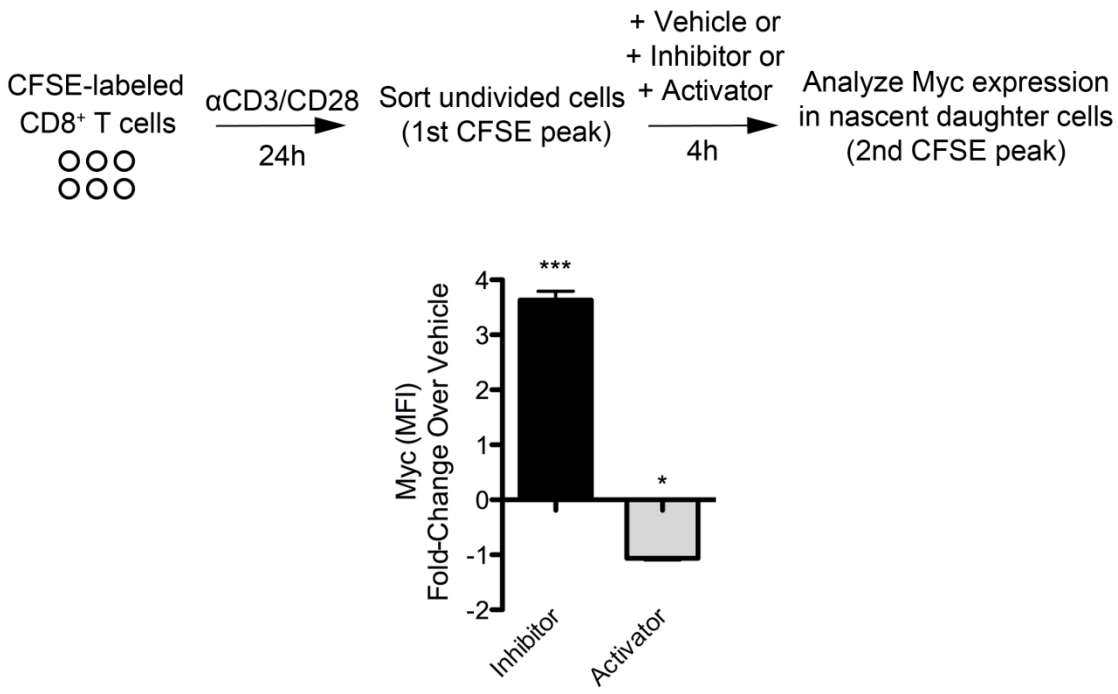


Figure 4.13 Myc degradation is dependent on level of proteasome activity. MFI of Myc in recently divided (2nd CFSE peak) cells arising from sorted undivided (1st CFSE peak) $CD8^+$ T cells treated with vehicle, proteasome inhibitor, or proteasome activator. Undivided cells were cultured for 4 hours to allow them to divide. MFI of inhibitor- or activator-treated relative to control-treated cells is shown. Data are representative of 3 independent experiments, $n \geq 3$ replicates per group. Error bars represent S.E.M. of three replicates. * $p < 0.05$, *** $p < 0.001$ (Student's two-tailed *t*-test).

CHAPTER 5: Conclusions

$CD8^+$ T cell differentiation in response to microbial infection is a complex process with many layers of regulation. In this dissertation, we observed transcriptional heterogeneity at the single-cell level, which we have shown to be predictive of $CD8^+$ T cell fate later in the course of differentiation. Using the transcriptional profile of $Div1_{TE}$ and $Div1_{MEM}$ cells, we were able to classify intermediate-stage Day 4 cells into effector-like or memory-like cells. What was most significant about this finding was that when we used the transcriptional profile of Day 7 terminal effector and total circulating memory cells to classify the same Day 4 cells, both early state and late-stage cell fate classifiers agreed on the identity of the Day 4 intermediate cells. This suggests the possibility that unique sets of genes regulate the early process of differentiation and the maintenance of differentiated cells.

Another significant finding from our single-cell transcriptional profiling is that $Div1_{TE}$ are much more transcriptionally active than $Div1_{MEM}$ cells. Many genes known to be important for $CD8^+$ T cell memory specification are highly expressed in $Div1_{TE}$ cells. This finding suggests that early in the differentiation process, terminal effector differentiation is characterized by a large transcriptional burst, while memory differentiation is characterized by the expression of a few specific $CD8^+$ T cell memory-associated genes. Another possibility is that gene expression is post-translationally regulated in order to more specifically downregulate the expression of memory-associated genes in cells differentiating into terminal effectors.

Previous studies have suggested that asymmetric partitioning of cellular components is an important mechanism for the generation of the heterogeneous $CD8^+$ T cell response that we have characterized using single-cell RNA-seq [14-16]. One of the cellular components that is asymmetrically localized is the proteasome [17]. In a previous study, it was shown that proteasome activity is asymmetric during mitosis. In this dissertation, we have observed that distinct levels of proteasome activity is maintained in the daughter cells emerging from the first $CD8^+$ T cell division in response to infection, which are shown in Chapters 1 and 2 to be differentially fated.

Endogenous proteasome activity has been studied in many biological contexts to regulate cell differentiation. Pluripotent stem cells have high proteasome activity relative to their differentiated progeny [24,25]. In these contexts, maintenance of high proteasome activity is critical for expression of factors that preserve the expression of transcription factors that uphold pluripotency. Proteasome activity has been shown to influence differentiation and function of cancer stem cells, a subset of cancer stem cells that have a capacity for self-renewal and tumor initiation [34,55]. Other components of the ubiquitin-proteasome system have also been demonstrated to influence lymphocyte differentiation and function. Stability of the transcription factor FoxP3 has been shown to undergo UPS-mediated regulation [56,57].

Many studies in lymphocytes have shown that decreasing proteasome activity attenuates T cell responses [27-29]. However, this could be due to effects on antigen processing or because only a single immunosubunit was inhibited. One study contrastingly showed that inhibition of all immunosubunits enhanced the T cell response [30]. In accordance with this study, our work has found that transient inhibition

of $CD8^+$ T cell proteasome activity resulted in an increase in the expression of effector-associated transcription factors and the production of inflammatory cytokines.

Metabolic reprogramming is another biological process that has recently been shown to be crucial in $CD8^+$ T cell fate specification [44,45]. Early post-activation, T cells undergo a rapid increase in glycolysis and glutaminolysis driven by Myc-dependent metabolic reprogramming [46]. At later time points, additional factors, such as HIF1α, sustain the glycolytic program [48]. Engagement of glycolysis by activated $CD8^+$ T cells is essential for de-repression of mRNA associated with effector function, such as IFNγ [46]. Our findings suggest that different levels of endogenous proteasome activity in $CD8^+$ T cells generated by the first cell division *in vivo* regulate levels of Myc. In addition, increased Myc expression in $CD8^+$ T cells that have been treated with proteasome inhibitor is consistent with the findings that a metabolic switch toward glycolysis drives effector $CD8^+$ T cell differentiation. PI3K signaling and mTORC1 activity have also been found to be asymmetric at the first cell division. In addition to proteasome-mediated degradation, these signals may also enforce Myc expression to promote the metabolic switch and effector differentiation [52-54].

Generation of immunologic memory is an important goal of vaccination. Inhibition of the mTORC1 pathway was found to enhance the development of T_{CM} [58]. Treatment of mice with metformin promoted fatty acid oxidation and oxidative phosphorylation through an AMPK-dependent mechanism, resulting in an enhanced memory $CD8^+$ T cell response [44]. Inhibition of glycolysis in $CD8^+$ T cells using 2-deoxyglucose resulted in increased formation of T_{CM} [59]. These studies suggest that increasing fatty acid oxidation and oxidative phosphorylation while reducing

glycolysis can potentially enhance the generation of $CD8^+$ T cell memory. In our study, we have found that increasing proteasome activity pharmacologically resulted in a decrease in glycolysis and an increase in maximal respiratory capacity. In response to infection, proteasome activator-treated cells had a higher rate of T_{CM} generation as well as an increased response to rechallenge. These findings suggest that increasing proteasome activity in $CD8^+$ T cells may be a useful strategy in boosting T_{CM} generation during vaccination.

In summary, we have demonstrated the novel finding that distinct levels of proteasome activity in differentially fated $CD8^+$ T cells regulate their effector and memory fate specification through alteration of cellular metabolism, dictated in part by levels of the transcription factor Myc.

APPENDIX A: MATERIALS AND METHODS

Mice

All animal work was approved by the Institutional Animal Care and Use Guidelines of the University of California, San Diego. All mice were housed in specific pathogen-free conditions before use. Wild-type C57/BL6, OT-I, and P14 mice were purchased from the Jackson Laboratories. $Cd4^{Cre}Hif1\alpha^{fl/fl}$ mice have been previously described [48]. $Cd4^{Cre}Bcl6^{fl/fl}$ mice were provided by Dr. Shane Crotty (La Jolla Institute for Allergy and Immunology) and $dLck^{Cre}Foxo1^{fl/fl}$ mice were provided by Dr. Stephen Hedrick (UCSD).

Adoptive transfer and infection

For analysis of 1st division cells, OT-I or P14 $CD8^+$ T cells were labeled with carboxyfluorescein diacetate succinimidyl ester (CFSE), and 3×10^6 cells were transferred intravenously into recipient mice. 24 hours later, mice were infected intravenously with 5×10^3 cfu of Lm-OVA or 2×10^5 pfu of LCMV-Arm. 45-48 hours post-infection, spleens were harvested and analyzed by flow cytometry. For analysis of cells 7 and 50 days post-infection, 5×10^3 congenically marked $CD45.1^+$ OT-I or P14 $CD8^+$ T cells were transferred into $CD45.2^+$ recipient mice that were infected 24 hours later with Lm-OVA. Blood and splenocytes were analyzed at days 7 and 50 post- infection. When applicable, cells were transiently treated with

proteasome inhibitor or activator. Mice were re-challenged ≥ 50 days post-infection with 5×10^5 cfu Lm-OVA.

Single-cell transcriptome amplification and RNA-sequencing

The C_1 Single-Cell Auto Prep System (Fluidigm) was used to perform whole transcriptome amplification (WTA) of up to 96 single cells simultaneously. After cell isolation, FACS sorted 2.5 x 10^5 to 2 x 10^6 P14 $CD8^+$ T cells were loaded onto the C_1 Single-Cell Auto Prep mRNA Array IFC for single-cell capture on chip. Live/dead stain (Invitrogen) was included to exclude dead cells. Viable single cells captured on chip were manually imaged. Cell lysis and RT-PCR were performed on chip. SMARTer chemistry (Clontech) WTA was performed according to the manufacturer's instructions. Illumina Nextera XT single-cell complementary DNA (cDNA) libraries were generated according to the manufacturer's instructions (Illumina). Quality control measures of the single-cell cDNA libraries were performed on the 2100 Bioanalyzer (Agilent Technologies), Qubit 3.0 Fluorometer (Thermo Fisher Scientific), and MiSeq Sequencing System (Illumina). Single-cell cDNA libraries were sequenced (paired-end 100 or single-end 100) on the HiSeq2500 Sequencing System at the UCSD Institute for Genomics Medicine (IGM) Center.

Single-cell RNA-seq data pre-processing

Single-cell mRNA sequencing data from 256 murine $CD8^+$ T cells were processed with a bioinformatics pipeline focusing on quality control (QC) and robust expression quantification. For each cell, raw RNA-seq reads were: checked for quality metrics with fastqc (v0.10.1) [60]; poly-A and adaptor-trimmed with cutadapt (v1.8.1) [61]; quantified by kallisto (v0.42.1) [62] to a reference transcriptome (Gencode vM3) [60] without bias correction; and aligned by STAR (v2.4.1b) [63] to the reference mouse genome (mm10) [64] with default parameters for quality control and downstream analysis. Next, the transcript per million (TPM) outputs of kallisto for all cells were combined into a cell-by-gene expression matrix (C=288 cells=rows, G=22425 genes=columns) by summing the expression values for all quantified transcripts of a given gene. Finally, the TPM value for each cell *c* and gene *g* was natural log-transformed to yield a normalized expression value: $EXPR_{c,g} = ln(1^+TPM_{c,g})$.

Dimensionality reduction and cell heterogeneity visualization

To reduce the dimensionality of the cell-by-gene expression matrix EXPR and visualize the diversity of gene expression among $CD8^+$ T cells of different subtypes in a 2-dimensional scatter plot, we applied the t-distributed Stochastic Neighborhood Embedding (tSNE)[60] algorithm via its Barnes-Hut approximation (bhSNE) [65]. tSNE is an unsupervised technique based on a non-convex objective which solves the so-called crowding problem, and has been successfully used to visualize millions of single-cell cytometry measurements where the original dimension is D≈40 approximately [66-69]. In contrast, our total RNA sequencing data for each cell gave signal for over 22,000

genes (6000 of which had a mean expression over all cells greater than 1 TPM). Therefore, we first applied standard Principal Components Analysis (PCA) to reduce the dimensionality down to D=10, and only then applied bhSNE to visualize in D=2 (with perplexity=30 and theta=0.75 parameters). This composition of transformations is standard practice and results in a dimensionality reduction that is invariant to reflection [69]. After dimensionality reduction, each point on the resulting 2-dimensional scatter plot was colored by the stage of its corresponding T cell population. Since we observed two distinct clusters of Division 1 T cells (red dots) in our tSNE plot (**Fig. 1.4**), we re-colored those cells distinctly for the inset scatterplot according to their proximity to the centroids of the terminally differentiated effector (T_{SLE}) and memory (T_{MEM}) T cell clusters. Specifically, the proposed $Div1_{MEM}$ cells (inset) were re-colored blue because they were closer (in tSNE space) to the overall centroid of all T_{CM} (purple) and all T_{EM} (green) cells than to that of all Day 7 cells (yellow). The remaining $Div1_{TE}$ cells remained red because they were closer (in tSNE space) to the centroid of all Day 7 cells (yellow) than to that of the memory T cells (purple and green).

Supervised analysis of gene expression data

In contrast to the unsupervised dimensionality reduction (PCA, tSNE) and hierarchical clustering methods which are blind to the cell type labels, we also applied two supervised methods which utilize the extra information to give more interpretable results: (1) Differential gene expression analysis. We performed differential gene

expression analysis between all pairs of T cell sub-populations from two non-overlapping sets of rows in the log-transformed expression matrix EXPR. Since single-cell gene expression does not conform to the usual negative binomial distribution [70,71] and can even be bimodal due to dropout [72] we used two non-parametric statistical tests for heterogeneity of expression: Mann Whitney Wilcoxon (MWW, also known as MWU) which is a rank-sum test but relies on a large sample to approximate normality, and Kolmogorov-Smirnov 2-sample (KS2) test[70] which finds the largest difference between the empirical cumulative distributions, even between two small samples such as our 1st division sub-types $Div1_{TE}$ (n =36) and $Div1_{MEM}$ (n =24). (2) Cell type classifier. We trained two binary T cell classifiers to identify gene expression signatures that not only differentiate the examined T cell sub-populations (like the differential gene expression described above) but can also be used to predict the 'memory-' or 'effector-ness' of previously unseen cells. Each classifier constructed an independent ensemble of Extremely Randomized Trees[71]. Using the terminally differentiated effector and memory (T_{CM}, T_{EM}) populations, we built a training set for a fate classifier for $CD8^+$ T cells. Using the newly observed segregation of daughter T cells into $Div1_{TE}$ and $Div1_{MEM}$ subpopulations after the first division, we built a second training set for another early state classifier. Both classifiers were fed their respective training sets using 10-fold cross-validation. To evaluate their overall accuracy and precision, a Receiver Operating Characteristic (ROC) curve was computed by combining the predictions on each 10% test fold while training on the remaining 90%[72]. After both the fate and early state classifiers were trained on their respective subpopulations, they were both applied on previously

unseen intermediate Day 4 $CD8^+$ T cells [73]. Their predicted 'memory-ness' scores were scatter-plotted and shown to correlate (**Fig. 1.5**). For each T cell, its 'effector-ness' scores is 1 minus the 'memory-ness' score and is redundant for this analysis. The signature genes for each classifier were selected from all G=22,425 genes by their GINI score [74]. The surprisingly small overlap in gene expression signatures between the two classifiers was computed to contrast with their seeming agreement in their 'memory-ness' score predictions.

Cell culture

Single-cell suspensions were prepared from spleens and peripheral lymph nodes of C57BL/6, OT-I, or P14 mice. For *in vitro* memory differentiation, TCR transgenic $CD8^+$ T cells were isolated using the $CD8^+$ T cell isolation kit II (Miltenyi Biotec) and then cultured for 2 days with their cognate peptide and wild-type T-depleted splenocytes. Cells were then washed and resuspended in media containing IL-2 or IL-15 (PeproTech), along with DMSO (Sigma-Aldrich), 100 nM epoxomicin (Enzo), 1 µM proteasome activator, or 1 µM tacrolimus (Sigma-Aldrich); cells were analyzed 3 or 5 days later. In pre-treatment experiments, $CD8^+$ T cells were isolated with $CD8^+$ T Cell Isolation Kit II (Miltenyi Biotec), treated with DMSO, 0.5 µM epoxomicin, or 1 µM proteasome activator for 4 hours, washed with culture media, then cultured with immobilized anti-CD3 and anti-CD28 (Bio X Cell) antibodies and IL-2 for 3 days. In some experiments, Myc inhibitor was added 24 hours post-activation at a dose of 10 µM (ref).

Proteasome activity assays

Cells were incubated with 5 μM activity-based proteasome probe for 2 hours at 37°C, then washed and analyzed with flow cytometry. To analyze probed cells using SDS-PAGE, cells were lysed with cold lysis buffer (50 mM Tris-HCl, pH 8.5, 150 mM NaCl, 1% Triton-X-100) for 30 minutes at 4°C with vortexing. 50 μg of protein was incubated with 0.5 μM of activity-based probe for 1 hour at 37°C then resolved on a 4-20% Tris-Glycine gel (Life Technologies). Fluorescence was detected directly from the gel using a FluorChem Q (Cell Biosciences). Proteasome activity was also measured using Proteasome-Glo Cell-Based Assay (Promega) according to manufacturer's instructions.

Flow cytometry, cell sorting, and antibodies

Cells were stained with fluorochrome-conjugated antibodies and analyzed on an Accuri C6 or FACSCanto II (BD Biosciences). Cell sorting was done on a FACS Aria II (BD Biosciences). The following antibodies were used: anti-CD8α (53-6.7), anti-CD45.1 (A20), anti-CD25 (PC61), anti-CD62L (MEL-14), anti-CD44 (IM7), anti-IFNγ (XMG1.2), anti-TNFα (MP6-XT22), anti-KLRG1 (2F1), anti-IL-7R (A7R34), anti-CD27 (LG.7F9), anti-T-bet (4B10), anti-Bcl2 (BCL/10C4, all from Biolegend), anti-Gzmb (GB11, Life Technologies). Intracellular antigens were stained with Transcription Factor Staining Buffer Set (eBioscience) according to manufacturer's

instructions. For intracellular cytokine staining, cells were stimulated for 4 hours at 37°C with 0.5 μg/ml phorbol 12-myristate 13-acetate, 5 μg/ml ionomycin (Sigma-Aldrich) in the presence of 10 μg/ml brefeldin A (Sigma-Aldrich). Cells were fixed in 4% paraformaldehyde (Electron Microscopy Services) and permeabilized with PBS (Mediatech) containing 1% FBS (Life Technologies), 1% saponin (Sigma-Aldrich), and 0.1% sodium azide (Sigma-Aldrich), followed by staining with antibodies. Analysis was performed with FlowJo software (TreeStar).

Immunoblotting and antibodies

Cells were lysed with RIPA lysis buffer (50 mM Tris pH 8.5, 150 mM NaCl, 1% Triton-X-100, 0.5% sodium deoxycholate, 0.1% SDS) in the presence of Protease Inhibitor Cocktail (Sigma-Aldrich). Protein concentration was quantitated using DC protein assay (Bio-Rad). 20 μg of protein was resolved on 4-20% Tris-Glycine gels (Life Technologies) and transferred onto nitrocellulose membranes. Membranes were probed with the following antibodies: anti-Myc (D84C12), anti-Bcl6 (polyclonal), anti-ERRα (E1G1J), Foxo1 (C29H4, all from Cell Signaling), anti-HIF1α (polyclonal, Novus Biologicals), anti-β-actin (AC-74, Sigma-Aldrich). Fluorochrome-conjugated secondary antibodies used were anti-rabbit Alexa Fluor 680 (Life Technologies) and anti-mouse IRDye 800 (Rockland). Fluorescent signals were detected using Odyssey imaging system (LI-COR Biosciences).

Cytotoxicity assay

OT-I $CD8^+$ T cells were pre-treated with DMSO, 0.5 μM epoxomicin, or 1 μM proteasome activator for 4 hours, washed, and then cultured with ovalbumin peptide for 3 days. Mouse splenocytes were harvested, labeled with 5 μM and 0.5 μM of eFluor 670 (eBioscience), for use as target cells. One group of labeled cells was pulsed with 1 nM peptide for 1 hour, while the other group served as an unpulsed control. $CD8^+$ T cells were co-cultured in various ratios with unpulsed and pulsed target cells for 4 hours. Specific killing was shown as the difference in live percentage between pulsed and unpulsed target cells, normalized to the live percentage of unpulsed target cells.

Gene expression microarray

RNA was extracted using TRIzol with GlycoBlue, then processed using RNA Clean and Concentrator Kit (Zymo Research). RNA quality was assessed using the Agilent 2100 Bioanalyzer (Agilent Technologies). Microarray analysis was performed using the Illumina Mouse WG-6 v2.0 Expression BeadChip (Illumina) following the manufacturer's instructions. Array data was loaded into the Array Studio analysis suite (Omicsoft, Inc.) to perform data visualization and management of analyzed datasets on the cloud. Data was normalized at the gene level and log-transformed before computing one-way ANOVA statistics between treatment and control groups (inhibitor vs. vehicle and activator vs. vehicle). Samples were quality-controlled using

principal component analysis to detect possible outliers and batch effects across samples. Differentially expressed gene signatures representing 1-5% of the coding transcriptomes were generated using a log2 (fold change) value > 1 and a raw p-value of < 0.01. Functional enrichment of differentially expressed genes was performed using the ToppGene Suite and WebGestalt [75,76]. Gene Set Enrichment Analysis [77,78] was performed using genes differentially expressed in drug treatment versus normal conditions. These differentially expressed genes were compared to an annotated gene set on Molecular Signatures Database representing genes that were upregulated in naïve, effector, or memory $CD8^+$ T cells compared to other $CD8^+$ T cell populations (**Supplementary Table 1**) [79].

SILAC metabolic labeling and sample processing

To generate labeled $CD8^+$ T cells with stable isotope-labeled amino acids [80], cells were cultured for 72 hours (approximately 6 population doublings) in arginine- and lysine-depleted IMDM media (Cellgro), supplemented at a final concentration of 100 mg/L either with regular 'light' L-Arg and L-Lys (Cambridge Isotopes) or 'heavy' isotope-enriched [U-13C6, 15N2]-L-Arg and [U-13C6, 15N4]-L-Lys (Cambridge Isotopes). $CD8^+CD44^+$ cells were sorted and equal cell numbers were mixed 1:1 in the following way for both drug treatments: (1) control labeled / drug unlabeled; (2) control labeled / drug labeled; and (3) (drug unlabeled / control labeled) / (control unlabeled / control labeled). Cell mixtures were lysed with RIPA lysis buffer (50 mM Tris pH 8.5, 150 mM NaCl, 1% Triton-X-100, 0.5% sodium deoxycholate, 0.1% SDS)

in the presence of Protease Inhibitor Cocktail (Sigma) and precipitated with methanol and chloroform. 8M urea (in 50 mM ammonium bicarbonate) was added to the protein pellets and extracts were processed with ProteasMAX (Promega) as described by the manufacturer's instructions. The peptides were subsequently reduced with 5 mM Tris(2 carboxyethyl)phosphine at room temperature for 30 min, alkylated in the dark by 10 mM iodoacetamide for 20 min, and digested with Sequencing Grade Modified Trypsin (Promega) overnight at 37°C at an enzyme to sample protein ratio of 1:100, and the reaction was stopped by acidification.

MudPIT and LTA Orbitrap MS analysis

The peptides were pressure-loaded into a 250-μm i.d. capillary packed with 2.5 cm of 10-μm Jupiter C18 resin (Phenomenex) followed by an additional 2.5 cm of 5-μm Partisphere strong cation exchanger (Whatman). The column was washed for 15 minutes with buffer containing 95% (vol/vol) water, 5% (vol/vol) acetonitrile, and 0.1% formic acid. After washing, a 100-μm i.d capillary with a 5-μm pulled tip packed with 15 cm of 4-μm Jupiter C18 resin was attached to a union, and the entire split column (desalting column–union–analytical column) was placed directly inline with an Agilent 1100 or 1200 quaternary HPLC and analyzed using a modified 11-step separation described previously [81]. The data was acquired on a LTQ Orbitrap XL.

Analysis of tandem mass spectra

Protein identification and quantification and analysis were performed with Integrated Proteomics Pipeline - IP2 (Integrated Proteomics Applications, Inc.) using ProLuCID/Sequest , DTASelect2, and Census [82,83]. Mass spectrum raw files were extracted into ms1 and ms2 files from raw files using RawExtract 1.9.9 [82], and the tandem mass spectra were searched against the European Bioinformatic Institute (IPI) mouse protein database. To estimate peptide probabilities and FDRs accurately, we used traditional target/decoy database containing the reversed sequences of all the proteins appended to the target database [84]. Tandem mass spectra were matched to sequences using the ProLuCID algorithm done on an Intel Xeon cluster running under the Linux operating system. The search space included all fully and half-tryptic peptide candidates that fell within the mass tolerance window with no miscleavage constraint. Carbamidomethylation ($^{+}$57.02146 Da) of cysteine was considered as a static modification. The validity of peptide/spectrum matches (PSMs) was assessed in DTASelect using two SEQUEST-defined parameters, the cross-correlation score (XCorr), and normalized difference in cross-correlation scores (DeltaCN). The search results were grouped by charge state ($^{+}$2, $^{+}$3, and greater than $^{+}$3) and tryptic status (fully tryptic, half-tryptic, and nontryptic), resulting in 12 distinct subgroups. In each of these subgroups, the distribution of Xcorr, DeltaCN, and DeltaMass values for (a) direct and (b) decoy database PSMs was obtained; then the direct and decoy subsets were separated by discriminant analysis. Full separation of the direct and decoy PSM subsets is not generally possible; therefore, peptide match probabilities were calculated based on a nonparametric fit of the direct and decoy score distributions. A peptide confidence of 0.95 was set as the minimum threshold. The FDR was

calculated as the percentage of reverse decoy PSMs among all the PSMs that passed the confidence threshold. Each protein identified was required to have a minimum of one peptide; however, this peptide had to be an excellent match with an FDR less than 0.001 and at least one excellent peptide match. After this last filtering step, we estimate that both the protein FDRs were below 1% for each sample analysis. Each dataset was searched twice, once against light and then against heavy protein databases. After the results from SEQUEST were filtered using DTASelect2, ion chromatograms were generated using an updated version of Census software (Yates laboratory). Census calculates peptide ion intensity ratios for each pair of extracted ion chromatograms and filters peptide ratio measurements based on a correlation threshold; the correlation coefficient (values between zero and one) represents the quality of the correlation between the unlabeled and labeled chromatograms and can be used to filter out poor-quality measurements. In addition, Census provides an automated method for detecting and removing statistical outliers. The Grubbs test (P = 0.01) then is applied to remove outlier peptides. Final protein ratios were generated with QuantCompare, which uses Log fold change and TTest P value to identify regulated significant proteins. For a protein to be considered in our screen, it had to be "plotted" on our volcano scatter plot. Proteins with peptide counts present in at least three samples, p 0.05, and an average ratio of treatment over control greater 1.3 or below -1.3 were considered for analysis. The y-axis of these volcano plots is the P value, which requires each protein to be quantified in at least two of the biological replicates. Differentially expressed proteins were analyzed using The Database for Annotation, Visualization, and Integrated Discovery (DAVID) to identify Gene

Ontology (GO) Biological Function categories that were enriched in each of the drug-treated conditions [85,86].

Immunofluorescence analysis

$CD8^+$ T cells were pre-treated with either DMSO or proteasome activator (cyclosporine) followed by drug washout, then activated for 10 minutes using 10 µg/ml platebound anti-CD3 and CD28, in the presence ('continuous cyclosporine condition') or absence of additional cyclosporine ('cyclosporine pre-treatment and drug washout condition'). Immunofluorescence analysis was performed as previously described [14]. The primary antibody used was anti-NFAT1 (D43B1, Cell Signaling). The secondary antibody used was anti-rabbit Alexa Fluor 555 (Life Technologies). DAPI was used to stain DNA (Life Technologies). Images were acquired using a FV1000 laser-scanning confocal microscope (Olympus). Nuclei were distinguished using DAPI staining. The ratio of pixel intensity of nuclear NFAT and total NFAT was quantified in each individual cell using NIH ImageJ software.

Cellular metabolism analysis

$CD8^+$ T cells were treated with vehicle, proteasome inhibitor, or proteasome activator for 4 hours, washed, then cultured with immobilized anti-CD3 and anti-CD28 antibodies and IL-2 for 2 days. 2×10^5 $CD8^+CD44^+$ cells were plated in triplicate and analyzed for extracellular acidification rate (ECAR) and oxygen consumption rate

(OCR) on a Seahorse XF96 (Seahorse Bioscience) according to the manufacturer's instructions. Glycolytic and mitochondrial stress tests were performed according to the manufacturer's instructions.

Statistics

Comparison between groups was done using a two-tailed Student's t-test or one-way ANOVA. P-values < 0.05 were considered significant.

Accession codes

GEO: Single-cell RNA-seq data, GSE89405; proteasome gene expression array data, GSE78750. MassIVE: proteomic data, MSV000079611.

APPENDIX B: SUPPLEMENTARY TABLES

Supplementary Table 1: Gene lists used for Gene Set Enrichment Analysis. Gene lists were taken from previously published microarray data to represent genes enriched in effector, naïve, and memory $CD8^+$ T cell populations.

	MSigDB lists
Genes with increased expression in effector $CD8^+$ T cells compared to naïve and memory	GSE1000002_1582_200_UP, GSE1000002_1580_200_DN
Genes with increased expression in naïve $CD8^+$ T cells compared to effector and memory	GSE1000002_1580_200_UP, GSE1000002_1581_200_UP
Genes with increased expression in memory $CD8^+$ T cells compared to effector and naive	GSE1000002_1581_200_DN, GSE1000002_1582_200_DN

Supplementary Table 2: Quantitative real-time PCR primers. Primers used in quantitative real-time PCR experiments in order to measure gene expression.

	F primer, 5’ to 3’	R primer, 5’ to 3’
Tbx21	AGCAAGGACGGCGAATGTT	GTGGACATATAAGCGGTTCCC
Gzmb	CCACTCTCGACCCTACATGG	GGCCCCCAAAGTGACATTTATT
Il7r	AGTCCTCCTATGTGAGTCCT	ACCCATCTTCTTTGTGTTTCTG
Tcf7	AGCTTTCTCCACTCTACGAACA	AATCCAGAGAGATCGGGGGTC
Ifng	GAGCCAGATTATCTCTTTCTACC	GTTGTTGACCTCAAACTTGG
Il2	AGCAGCTGTTGATGGACCTA	CGCAGAGGTCCAAGTTCAT
Eomes	TGAATGAACCTTCCAAGACTCAGA	GGCTTGAGGCAAAGTGTTGACA
Bcl2	TCGCAGAGATGTCCAGTCAG	CCTGAAGAGTTCCTCCACCA
IIl2rb	CCTTTGACAACCTTCGCCTG	TCTGCTTGAGGCTTAATACGGAT
Cd27	CAGCTTCCCAACTCGACTGTC	GCACCCAGGACGAAGATAAGAA
Glut1	CAGTTCGGCTATAACACTGGTG	GCCCCCGACAGAGAAGATG
Hk2	TGATCGCCTGCTTATTCACGG	TGATCGCCTGCTTATTCACGG
Eno1	GGAAAGGAAGACAGAGTGGGAGGC	CAGATCGACCTCAACAGTGGGATTC
Ldha	AAACCGAGTAATTGGAAGTGGTTG	TCTGGGTTAAGAGACTTCAGGGAG

Supplementary Table 2: Quantitative real-time PCR primers. Continued.

Pfkp	GGTACAGATTCAGCCCTGCACC	GTCGGCACCGCAAGTCAAGG
Prodh	GCACCACGAGCAGTTGTTC	CTTTGTTGTGCCGGATCAGAG
Oat	GGAGTCCACACCTCAGTCG	CCACATCCCACATATAAATGCCT
Gls	GTGAATCAGCAAGTGTGATGGC	CCCCCAGCAACTCCAGATTTTG
Rpl13	AGGGCAGGTTCTGGTATTGGAT	AGGCTCGGAAATGGTAGGGG
18S rRNA	GTAACCCGTTGAACCCCATT	CCATCCAATCGGTAGTAGCG

REFERENCES

1 Joshi, N. S., Cui, W., Chandele, A., Lee, H. K., Urso, D. R., Hagman, J., Gapin, L. & Kaech, S. M. Inflammation directs memory precursor and short-lived effector CD8(+) T cell fates via the graded expression of T-bet transcription factor. *Immunity* **27**, 281-295, doi:10.1016/j.immuni.2007.07.010 (2007).

2 Sallusto, F., Lenig, D., Forster, R., Lipp, M. & Lanzavecchia, A. Two subsets of memory T lymphocytes with distinct homing potentials and effector functions. *Nature* **401**, 708-712, doi:10.1038/44385 (1999).

3 Chang, J. T., Wherry, E. J. & Goldrath, A. W. Molecular regulation of effector and memory T cell differentiation. *Nature immunology* **15**, 1104-1115, doi:10.1038/ni.3031 (2014).

4 Kaech, S. M. & Cui, W. Transcriptional control of effector and memory CD8+ T cell differentiation. *Nature reviews. Immunology* **12**, 749-761, doi:10.1038/nri3307 (2012).

5 Kaech, S. M. & Wherry, E. J. Heterogeneity and cell-fate decisions in effector and memory CD8+ T cell differentiation during viral infection. *Immunity* **27**, 393-405, doi:10.1016/j.immuni.2007.08.007 (2007).

6 Williams, M. A. & Bevan, M. J. Effector and memory CTL differentiation. *Annual review of immunology* **25**, 171-192, doi:10.1146/annurev.immunol.25.022106.141548 (2007).

7 Huber, M. & Lohoff, M. IRF4 at the crossroads of effector T-cell fate decision. *European journal of immunology* **44**, 1886-1895, doi:10.1002/eji.201344279 (2014).

8 Nayar, R., Schutten, E., Jangalwe, S., Durost, P. A., Kenney, L. L., Conley, J. M., Daniels, K., Brehm, M. A., Welsh, R. M. & Berg, L. J. IRF4 Regulates the Ratio of T-Bet to Eomesodermin in CD8+ T Cells Responding to Persistent LCMV Infection. *PloS one* **10**, e0144826, doi:10.1371/journal.pone.0144826 (2015).

9 Banerjee, A., Gordon, S. M., Intlekofer, A. M., Paley, M. A., Mooney, E. C., Lindsten, T., Wherry, E. J. & Reiner, S. L. Cutting edge: The transcription factor eomesodermin enables CD8+ T cells to compete for the memory cell niche. *Journal of immunology* **185**, 4988-4992, doi:10.4049/jimmunol.1002042 (2010).

10 Stemberger, C., Huster, K. M., Koffler, M., Anderl, F., Schiemann, M., Wagner, H. & Busch, D. H. A single naive CD8+ T cell precursor can develop

into diverse effector and memory subsets. *Immunity* **27**, 985-997, doi:10.1016/j.immuni.2007.10.012 (2007).

11 Gerlach, C., van Heijst, J. W., Swart, E., Sie, D., Armstrong, N., Kerkhoven, R. M., Zehn, D., Bevan, M. J., Schepers, K. & Schumacher, T. N. One naive T cell, multiple fates in CD8+ T cell differentiation. *The Journal of experimental medicine* **207**, 1235-1246, doi:10.1084/jem.20091175 (2010).

12 Plumlee, C. R., Sheridan, B. S., Cicek, B. B. & Lefrancois, L. Environmental cues dictate the fate of individual CD8+ T cells responding to infection. *Immunity* **39**, 347-356, doi:10.1016/j.immuni.2013.07.014 (2013).

13 Betschinger, J. & Knoblich, J. A. Dare to be different: asymmetric cell division in Drosophila, C. elegans and vertebrates. *Current biology : CB* **14**, R674-685, doi:10.1016/j.cub.2004.08.017 (2004).

14 Chang, J. T., Palanivel, V. R., Kinjyo, I., Schambach, F., Intlekofer, A. M., Banerjee, A., Longworth, S. A., Vinup, K. E., Mrass, P., Oliaro, J., Killeen, N., Orange, J. S., Russell, S. M., Weninger, W. & Reiner, S. L. Asymmetric T lymphocyte division in the initiation of adaptive immune responses. *Science (New York, N.Y.)* **315**, 1687-1691, doi:10.1126/science.1139393 (2007).

15 Metz, P. J., Arsenio, J., Kakaradov, B., Kim, S. H., Remedios, K. A., Oakley, K., Akimoto, K., Ohno, S., Yeo, G. W. & Chang, J. T. Regulation of asymmetric division and CD8+ T lymphocyte fate specification by protein kinase Czeta and protein kinase Clambda/iota. *Journal of immunology* **194**, 2249-2259, doi:10.4049/jimmunol.1401652 (2015).

16 Arsenio, J., Kakaradov, B., Metz, P. J., Kim, S. H., Yeo, G. W. & Chang, J. T. Early specification of CD8+ T lymphocyte fates during adaptive immunity revealed by single-cell gene-expression analyses. *Nature immunology* **15**, 365-372, doi:10.1038/ni.2842 (2014).

17 Chang, J. T., Ciocca, M. L., Kinjyo, I., Palanivel, V. R., McClurkin, C. E., Dejong, C. S., Mooney, E. C., Kim, J. S., Steinel, N. C., Oliaro, J., Yin, C. C., Florea, B. I., Overkleeft, H. S., Berg, L. J., Russell, S. M., Koretzky, G. A., Jordan, M. S. & Reiner, S. L. Asymmetric proteasome segregation as a mechanism for unequal partitioning of the transcription factor T-bet during T lymphocyte division. *Immunity* **34**, 492-504, doi:10.1016/j.immuni.2011.03.017 (2011).

18 Kisselev, A. F. & Goldberg, A. L. Monitoring activity and inhibition of 26S proteasomes with fluorogenic peptide substrates. *Methods in enzymology* **398**, 364-378, doi:10.1016/s0076-6879(05)98030-0 (2005).

19 Kohler, A., Cascio, P., Leggett, D. S., Woo, K. M., Goldberg, A. L. & Finley, D. The axial channel of the proteasome core particle is gated by the Rpt2 ATPase and controls both substrate entry and product release. *Molecular cell* **7**, 1143-1152 (2001).

20 Kincaid, E. Z., Che, J. W., York, I., Escobar, H., Reyes-Vargas, E., Delgado, J. C., Welsh, R. M., Karow, M. L., Murphy, A. J., Valenzuela, D. M., Yancopoulos, G. D. & Rock, K. L. Mice completely lacking immunoproteasomes show major changes in antigen presentation. *Nature immunology* **13**, 129-135, doi:10.1038/ni.2203 (2012).

21 Zanker, D., Waithman, J., Yewdell, J. W. & Chen, W. Mixed proteasomes function to increase viral peptide diversity and broaden antiviral CD8+ T cell responses. *Journal of immunology (Baltimore, Md. : 1950)* **191**, 52-59, doi:10.4049/jimmunol.1300802 (2013).

22 Glickman, M. H. & Ciechanover, A. The ubiquitin-proteasome proteolytic pathway: destruction for the sake of construction. *Physiological reviews* **82**, 373-428, doi:10.1152/physrev.00027.2001 (2002).

23 Finley, D. Recognition and processing of ubiquitin-protein conjugates by the proteasome. *Annual review of biochemistry* **78**, 477-513, doi:10.1146/annurev.biochem.78.081507.101607 (2009).

24 Vilchez, D., Boyer, L., Morantte, I., Lutz, M., Merkwirth, C., Joyce, D., Spencer, B., Page, L., Masliah, E., Berggren, W. T., Gage, F. H. & Dillin, A. Increased proteasome activity in human embryonic stem cells is regulated by PSMD11. *Nature* **489**, 304-308, doi:10.1038/nature11468 (2012).

25 Jang, J., Wang, Y., Kim, H. S., Lalli, M. A. & Kosik, K. S. Nrf2, a regulator of the proteasome, controls self-renewal and pluripotency in human embryonic stem cells. *Stem cells (Dayton, Ohio)* **32**, 2616-2625, doi:10.1002/stem.1764 (2014).

26 Gibson, H. M., Mishra, A., Chan, D. V., Hake, T. S., Porcu, P. & Wong, H. K. Impaired proteasome function activates GATA3 in T cells and upregulates CTLA-4: relevance for Sezary syndrome. *The Journal of investigative dermatology* **133**, 249-257, doi:10.1038/jid.2012.265 (2013).

27 Muchamuel, T., Basler, M., Aujay, M. A., Suzuki, E., Kalim, K. W., Lauer, C., Sylvain, C., Ring, E. R., Shields, J., Jiang, J., Shwonek, P., Parlati, F., Demo, S. D., Bennett, M. K., Kirk, C. J. & Groettrup, M. A selective inhibitor of the immunoproteasome subunit LMP7 blocks cytokine production and attenuates progression of experimental arthritis. *Nature medicine* **15**, 781-787, doi:10.1038/nm.1978 (2009).

28 Kalim, K. W., Basler, M., Kirk, C. J. & Groettrup, M. Immunoproteasome subunit LMP7 deficiency and inhibition suppresses Th1 and Th17 but enhances regulatory T cell differentiation. *Journal of immunology (Baltimore, Md. : 1950)* **189**, 4182-4193, doi:10.4049/jimmunol.1201183 (2012).

29 Basler, M., Dajee, M., Moll, C., Groettrup, M. & Kirk, C. J. Prevention of experimental colitis by a selective inhibitor of the immunoproteasome. *Journal of immunology (Baltimore, Md. : 1950)* **185**, 634-641, doi:10.4049/jimmunol.0903182 (2010).

30 Rasid, O., Meulenbroeks, C., Grone, A., Zaiss, D. & Sijts, A. Enhanced inflammatory potential of CD4+ T-cells that lack proteasome immunosubunit expression, in a T-cell transfer-based colitis model. *PloS one* **9**, e95378, doi:10.1371/journal.pone.0095378 (2014).

31 Best, J. A., Blair, D. A., Knell, J., Yang, E., Mayya, V., Doedens, A., Dustin, M. L., Goldrath, A. W. & Immunological Genome Project, C. Transcriptional insights into the CD8(+) T cell response to infection and memory T cell formation. *Nature immunology* **14**, 404-412, doi:10.1038/ni.2536 (2013).

32 Kaech, S. M., Hemby, S., Kersh, E. & Ahmed, R. Molecular and functional profiling of memory CD8 T cell differentiation. *Cell* **111**, 837-851 (2002).

33 Ramskold, D., Luo, S., Wang, Y. C., Li, R., Deng, Q., Faridani, O. R., Daniels, G. A., Khrebtukova, I., Loring, J. F., Laurent, L. C., Schroth, G. P. & Sandberg, R. Full-length mRNA-Seq from single-cell levels of RNA and individual circulating tumor cells. *Nature biotechnology* **30**, 777-782, doi:10.1038/nbt.2282 (2012).

34 Banno, A., Garcia, D. A., van Baarsel, E. D., Metz, P. J., Fisch, K., Widjaja, C. E., Kim, S. H., Lopez, J., Chang, A. N., Geurink, P. P., Florea, B. I., Overkleeft, H. S., Ovaa, H., Bui, J. D., Yang, J. & Chang, J. T. Downregulation of 26S proteasome catalytic activity promotes epithelial-mesenchymal transition. *Oncotarget*, doi:10.18632/oncotarget.7596 (2016).

35 Berkers, C. R., van Leeuwen, F. W., Groothuis, T. A., Peperzak, V., van Tilburg, E. W., Borst, J., Neefjes, J. J. & Ovaa, H. Profiling proteasome activity in tissue with fluorescent probes. *Molecular pharmaceutics* **4**, 739-748, doi:10.1021/mp0700256 (2007).

36 Florea, B. I., Verdoes, M., Li, N., van der Linden, W. A., Geurink, P. P., van den Elst, H., Hofmann, T., de Ru, A., van Veelen, P. A., Tanaka, K., Sasaki, K., Murata, S., den Dulk, H., Brouwer, J., Ossendorp, F. A., Kisselev, A. F. & Overkleeft, H. S. Activity-based profiling reveals reactivity of the murine thymoproteasome-specific subunit beta5t. *Chemistry & biology* **17**, 795-801, doi:10.1016/j.chembiol.2010.05.027 (2010).

37 Lee, B. H., Lee, M. J., Park, S., Oh, D. C., Elsasser, S., Chen, P. C., Gartner, C., Dimova, N., Hanna, J., Gygi, S. P., Wilson, S. M., King, R. W. & Finley, D. Enhancement of proteasome activity by a small-molecule inhibitor of USP14. *Nature* **467**, 179-184, doi:10.1038/nature09299 (2010).

38 Manjunath, N., Shankar, P., Wan, J., Weninger, W., Crowley, M. A., Hieshima, K., Springer, T. A., Fan, X., Shen, H., Lieberman, J. & von Andrian, U. H. Effector differentiation is not prerequisite for generation of memory cytotoxic T lymphocytes. *The Journal of clinical investigation* **108**, 871-878, doi:10.1172/jci13296 (2001).

39 Borel, J. F., Feurer, C., Gubler, H. U. & Stahelin, H. Biological effects of cyclosporin A: a new antilymphocytic agent. *Agents and actions* **6**, 468-475 (1976).

40 Clipstone, N. A. & Crabtree, G. R. Identification of calcineurin as a key signalling enzyme in T-lymphocyte activation. *Nature* **357**, 695-697, doi:10.1038/357695a0 (1992).

41 Liu, J., Farmer, J. D., Jr., Lane, W. S., Friedman, J., Weissman, I. & Schreiber, S. L. Calcineurin is a common target of cyclophilin-cyclosporin A and FKBP-FK506 complexes. *Cell* **66**, 807-815 (1991).

42 Hendriks, J., Gravestein, L. A., Tesselaar, K., van Lier, R. A., Schumacher, T. N. & Borst, J. CD27 is required for generation and long-term maintenance of T cell immunity. *Nature immunology* **1**, 433-440, doi:10.1038/80877 (2000).

43 Grayson, J. M., Zajac, A. J., Altman, J. D. & Ahmed, R. Cutting edge: increased expression of Bcl-2 in antigen-specific memory CD8+ T cells. *Journal of immunology (Baltimore, Md. : 1950)* **164**, 3950-3954 (2000).

44 Pearce, E. L., Walsh, M. C., Cejas, P. J., Harms, G. M., Shen, H., Wang, L. S., Jones, R. G. & Choi, Y. Enhancing CD8 T-cell memory by modulating fatty acid metabolism. *Nature* **460**, 103-107, doi:10.1038/nature08097 (2009).

45 van der Windt, G. J. & Pearce, E. L. Metabolic switching and fuel choice during T-cell differentiation and memory development. *Immunological reviews* **249**, 27-42, doi:10.1111/j.1600-065X.2012.01150.x (2012).

46 Wang, R., Dillon, C. P., Shi, L. Z., Milasta, S., Carter, R., Finkelstein, D., McCormick, L. L., Fitzgerald, P., Chi, H., Munger, J. & Green, D. R. The transcription factor Myc controls metabolic reprogramming upon T lymphocyte activation. *Immunity* **35**, 871-882, doi:10.1016/j.immuni.2011.09.021 (2011).

47 Michalek, R. D., Gerriets, V. A., Nichols, A. G., Inoue, M., Kazmin, D., Chang, C. Y., Dwyer, M. A., Nelson, E. R., Pollizzi, K. N., Ilkayeva, O., Giguere, V., Zuercher, W. J., Powell, J. D., Shinohara, M. L., McDonnell, D. P. & Rathmell, J. C. Estrogen-related receptor-alpha is a metabolic regulator of effector T-cell activation and differentiation. *Proceedings of the National Academy of Sciences of the United States of America* **108**, 18348-18353, doi:10.1073/pnas.1108856108 (2011).

48 Doedens, A. L., Phan, A. T., Stradner, M. H., Fujimoto, J. K., Nguyen, J. V., Yang, E., Johnson, R. S. & Goldrath, A. W. Hypoxia-inducible factors enhance the effector responses of CD8(+) T cells to persistent antigen. *Nature immunology* **14**, 1173-1182, doi:10.1038/ni.2714 (2013).

49 Oestreich, K. J., Read, K. A., Gilbertson, S. E., Hough, K. P., McDonald, P. W., Krishnamoorthy, V. & Weinmann, A. S. Bcl-6 directly represses the gene program of the glycolysis pathway. *Nature immunology* **15**, 957-964, doi:10.1038/ni.2985 (2014).

50 Tejera, M. M., Kim, E. H., Sullivan, J. A., Plisch, E. H. & Suresh, M. FoxO1 controls effector-to-memory transition and maintenance of functional CD8 T cell memory. *Journal of immunology (Baltimore, Md. : 1950)* **191**, 187-199, doi:10.4049/jimmunol.1300331 (2013).

51 Chang, C. H., Curtis, J. D., Maggi, L. B., Jr., Faubert, B., Villarino, A. V., O'Sullivan, D., Huang, S. C., van der Windt, G. J., Blagih, J., Qiu, J., Weber, J. D., Pearce, E. J., Jones, R. G. & Pearce, E. L. Posttranscriptional control of T cell effector function by aerobic glycolysis. *Cell* **153**, 1239-1251, doi:10.1016/j.cell.2013.05.016 (2013).

52 Verbist, K. C., Guy, C. S., Milasta, S., Liedmann, S., Kaminski, M. M., Wang, R. & Green, D. R. Metabolic maintenance of cell asymmetry following division in activated T lymphocytes. *Nature* **532**, 389-393, doi:10.1038/nature17442 (2016).

53 Lin, W. H., Adams, W. C., Nish, S. A., Chen, Y. H., Yen, B., Rothman, N. J., Kratchmarov, R., Okada, T., Klein, U. & Reiner, S. L. Asymmetric PI3K Signaling Driving Developmental and Regenerative Cell Fate Bifurcation. *Cell reports* **13**, 2203-2218, doi:10.1016/j.celrep.2015.10.072 (2015).

54 Pollizzi, K. N., Sun, I. H., Patel, C. H., Lo, Y. C., Oh, M. H., Waickman, A. T., Tam, A. J., Blosser, R. L., Wen, J., Delgoffe, G. M. & Powell, J. D. Asymmetric inheritance of mTORC1 kinase activity during division dictates CD8(+) T cell differentiation. *Nature immunology* **17**, 704-711, doi:10.1038/ni.3438 (2016).

55 Pan, J., Zhang, Q., Wang, Y. & You, M. 26S proteasome activity is down-regulated in lung cancer stem-like cells propagated in vitro. *PloS one* **5**, e13298, doi:10.1371/journal.pone.0013298 (2010).

56 Chen, Z., Barbi, J., Bu, S., Yang, H. Y., Li, Z., Gao, Y., Jinasena, D., Fu, J., Lin, F., Chen, C., Zhang, J., Yu, N., Li, X., Shan, Z., Nie, J., Gao, Z., Tian, H., Li, Y., Yao, Z., Zheng, Y., Park, B. V., Pan, Z., Zhang, J., Dang, E., Li, Z., Wang, H., Luo, W., Li, L., Semenza, G. L., Zheng, S. G., Loser, K., Tsun, A., Greene, M. I., Pardoll, D. M., Pan, F. & Li, B. The ubiquitin ligase Stub1 negatively modulates regulatory T cell suppressive activity by promoting degradation of the transcription factor Foxp3. *Immunity* **39**, 272-285, doi:10.1016/j.immuni.2013.08.006 (2013).

57 van Loosdregt, J., Fleskens, V., Fu, J., Brenkman, A. B., Bekker, C. P., Pals, C. E., Meerding, J., Berkers, C. R., Barbi, J., Grone, A., Sijts, A. J., Maurice, M. M., Kalkhoven, E., Prakken, B. J., Ovaa, H., Pan, F., Zaiss, D. M. & Coffer, P. J. Stabilization of the transcription factor Foxp3 by the deubiquitinase USP7 increases Treg-cell-suppressive capacity. *Immunity* **39**, 259-271, doi:10.1016/j.immuni.2013.05.018 (2013).

58 Araki, K., Turner, A. P., Shaffer, V. O., Gangappa, S., Keller, S. A., Bachmann, M. F., Larsen, C. P. & Ahmed, R. mTOR regulates memory CD8 T-cell differentiation. *Nature* **460**, 108-112, doi:10.1038/nature08155 (2009).

59 Sukumar, M., Liu, J., Ji, Y., Subramanian, M., Crompton, J. G., Yu, Z., Roychoudhuri, R., Palmer, D. C., Muranski, P., Karoly, E. D., Mohney, R. P., Klebanoff, C. A., Lal, A., Finkel, T., Restifo, N. P. & Gattinoni, L. Inhibiting glycolytic metabolism enhances CD8+ T cell memory and antitumor function. *The Journal of clinical investigation* **123**, 4479-4488, doi:10.1172/jci69589 (2013).

60 Dobin, A., Davis, C. A., Schlesinger, F., Drenkow, J., Zaleski, C., Jha, S., Batut, P., Chaisson, M. & Gingeras, T. R. STAR: ultrafast universal RNA-seq aligner. *Bioinformatics* **29**, 15-21, doi:10.1093/bioinformatics/bts635 (2013).

61 Mouse Genome Sequencing, C., Waterston, R. H., Lindblad-Toh, K., Birney, E., Rogers, J., Abril, J. F., Agarwal, P., Agarwala, R., Ainscough, R., Alexandersson, M., An, P., Antonarakis, S. E., Attwood, J., Baertsch, R., Bailey, J., Barlow, K., Beck, S., Berry, E., Birren, B., Bloom, T., Bork, P., Botcherby, M., Bray, N., Brent, M. R., Brown, D. G., Brown, S. D., Bult, C., Burton, J., Butler, J., Campbell, R. D., Carninci, P., Cawley, S., Chiaromonte, F., Chinwalla, A. T., Church, D. M., Clamp, M., Clee, C., Collins, F. S., Cook, L. L., Copley, R. R., Coulson, A., Couronne, O., Cuff, J., Curwen, V., Cutts, T., Daly, M., David, R., Davies, J., Delehaunty, K. D., Deri, J., Dermitzakis, E. T., Dewey, C., Dickens, N. J., Diekhans, M., Dodge, S., Dubchak, I., Dunn, D. M., Eddy, S. R., Elnitski, L., Emes, R. D., Eswara, P., Eyras, E., Felsenfeld,

A., Fewell, G. A., Flicek, P., Foley, K., Frankel, W. N., Fulton, L. A., Fulton, R. S., Furey, T. S., Gage, D., Gibbs, R. A., Glusman, G., Gnerre, S., Goldman, N., Goodstadt, L., Grafham, D., Graves, T. A., Green, E. D., Gregory, S., Guigo, R., Guyer, M., Hardison, R. C., Haussler, D., Hayashizaki, Y., Hillier, L. W., Hinrichs, A., Hlavina, W., Holzer, T., Hsu, F., Hua, A., Hubbard, T., Hunt, A., Jackson, I., Jaffe, D. B., Johnson, L. S., Jones, M., Jones, T. A., Joy, A., Kamal, M., Karlsson, E. K., Karolchik, D., Kasprzyk, A., Kawai, J., Keibler, E., Kells, C., Kent, W. J., Kirby, A., Kolbe, D. L., Korf, I., Kucherlapati, R. S., Kulbokas, E. J., Kulp, D., Landers, T., Leger, J. P., Leonard, S., Letunic, I., Levine, R., Li, J., Li, M., Lloyd, C., Lucas, S., Ma, B., Maglott, D. R., Mardis, E. R., Matthews, L., Mauceli, E., Mayer, J. H., McCarthy, M., McCombie, W. R., McLaren, S., McLay, K., McPherson, J. D., Meldrim, J., Meredith, B., Mesirov, J. P., Miller, W., Miner, T. L., Mongin, E., Montgomery, K. T., Morgan, M., Mott, R., Mullikin, J. C., Muzny, D. M., Nash, W. E., Nelson, J. O., Nhan, M. N., Nicol, R., Ning, Z., Nusbaum, C., O'Connor, M. J., Okazaki, Y., Oliver, K., Overton-Larty, E., Pachter, L., Parra, G., Pepin, K. H., Peterson, J., Pevzner, P., Plumb, R., Pohl, C. S., Poliakov, A., Ponce, T. C., Ponting, C. P., Potter, S., Quail, M., Reymond, A., Roe, B. A., Roskin, K. M., Rubin, E. M., Rust, A. G., Santos, R., Sapojnikov, V., Schultz, B., Schultz, J., Schwartz, M. S., Schwartz, S., Scott, C., Seaman, S., Searle, S., Sharpe, T., Sheridan, A., Shownkeen, R., Sims, S., Singer, J. B., Slater, G., Smit, A., Smith, D. R., Spencer, B., Stabenau, A., Stange-Thomann, N., Sugnet, C., Suyama, M., Tesler, G., Thompson, J., Torrents, D., Trevaskis, E., Tromp, J., Ucla, C., Ureta-Vidal, A., Vinson, J. P., Von Niederhausern, A. C., Wade, C. M., Wall, M., Weber, R. J., Weiss, R. B., Wendl, M. C., West, A. P., Wetterstrand, K., Wheeler, R., Whelan, S., Wierzbowski, J., Willey, D., Williams, S., Wilson, R. K., Winter, E., Worley, K. C., Wyman, D., Yang, S., Yang, S. P., Zdobnov, E. M., Zody, M. C. & Lander, E. S. Initial sequencing and comparative analysis of the mouse genome. *Nature* **420**, 520-562, doi:10.1038/nature01262 (2002).

62 Maaten, L. H., G.E. Visualizing High-Dimensional Data Using t-SNE. *Journal of Machine Learning Research* **9**, 2579-2605 (2008).

63 Maaten, L. Barnes-Hut-SNE. *arXIv* **1301** (2013).

64 Amir el, A. D., Davis, K. L., Tadmor, M. D., Simonds, E. F., Levine, J. H., Bendall, S. C., Shenfeld, D. K., Krishnaswamy, S., Nolan, G. P. & Pe'er, D. viSNE enables visualization of high dimensional single-cell data and reveals phenotypic heterogeneity of leukemia. *Nature biotechnology* **31**, 545-552, doi:10.1038/nbt.2594 (2013).

65 Bendall, S. C., Simonds, E. F., Qiu, P., Amir el, A. D., Krutzik, P. O., Finck, R., Bruggner, R. V., Melamed, R., Trejo, A., Ornatsky, O. I., Balderas, R. S., Plevritis, S. K., Sachs, K., Pe'er, D., Tanner, S. D. & Nolan, G. P. Single-cell mass cytometry of differential immune and drug responses across a human

hematopoietic continuum. *Science* **332**, 687-696, doi:10.1126/science.1198704 (2011).

66 Cheng, Y., Wong, M. T., van der Maaten, L. & Newell, E. W. Categorical Analysis of Human T Cell Heterogeneity with One-Dimensional Soli-Expression by Nonlinear Stochastic Embedding. *Journal of immunology* **196**, 924-932, doi:10.4049/jimmunol.1501928 (2016).

67 Love, M. I., Huber, W. & Anders, S. Moderated estimation of fold change and dispersion for RNA-seq data with DESeq2. *Genome biology* **15**, 550, doi:10.1186/s13059-014-0550-8 (2014).

68 Robinson, M. D., McCarthy, D. J. & Smyth, G. K. edgeR: a Bioconductor package for differential expression analysis of digital gene expression data. *Bioinformatics* **26**, 139-140, doi:10.1093/bioinformatics/btp616 (2010).

69 Fan, J., Salathia, N., Liu, R., Kaeser, G. E., Yung, Y. C., Herman, J. L., Kaper, F., Fan, J. B., Zhang, K., Chun, J. & Kharchenko, P. V. Characterizing transcriptional heterogeneity through pathway and gene set overdispersion analysis. *Nature methods* **13**, 241-244, doi:10.1038/nmeth.3734 (2016).

70 Li, J. & Tibshirani, R. Finding consistent patterns: a nonparametric approach for identifying differential expression in RNA-Seq data. *Statistical methods in medical research* **22**, 519-536, doi:10.1177/0962280211428386 (2013).

71 Stephens, M. A. EDF Statistics for Goodness of Fit and Some Comparisons. *Journal of the American Statistical Association* **69**, 730-737, doi:DOI:10.2307/2286009 (1974).

72 Geurts, P. E., D.; Wehenkel, L. Extremely Randomized Trees. *Machine Learning* **62**, 3-42, doi:10.1007/s10994-006-6226-1 (2006).

73 Pedregosa, F. V., G; Gramfor, A. Scikit-learn: Machine Learning in Python. *Journal of Machine Learning Research* **12**, 2825-2830 (2011).

74 Heinz, S., Benner, C., Spann, N., Bertolino, E., Lin, Y. C., Laslo, P., Cheng, J. X., Murre, C., Singh, H. & Glass, C. K. Simple combinations of lineage-determining transcription factors prime cis-regulatory elements required for macrophage and B cell identities. *Molecular cell* **38**, 576-589, doi:10.1016/j.molcel.2010.05.004 (2010).

75 Chen, J., Bardes, E. E., Aronow, B. J. & Jegga, A. G. ToppGene Suite for gene list enrichment analysis and candidate gene prioritization. *Nucleic acids research* **37**, W305-311, doi:10.1093/nar/gkp427 (2009).

76 Wang, J., Duncan, D., Shi, Z. & Zhang, B. WEB-based GEne SeT AnaLysis Toolkit (WebGestalt): update 2013. *Nucleic acids research* **41**, W77-83, doi:10.1093/nar/gkt439 (2013).

77 Mootha, V. K., Lindgren, C. M., Eriksson, K. F., Subramanian, A., Sihag, S., Lehar, J., Puigserver, P., Carlsson, E., Ridderstrale, M., Laurila, E., Houstis, N., Daly, M. J., Patterson, N., Mesirov, J. P., Golub, T. R., Tamayo, P., Spiegelman, B., Lander, E. S., Hirschhorn, J. N., Altshuler, D. & Groop, L. C. PGC-1alpha-responsive genes involved in oxidative phosphorylation are coordinately downregulated in human diabetes. *Nature genetics* **34**, 267-273, doi:10.1038/ng1180 (2003).

78 Subramanian, A., Tamayo, P., Mootha, V. K., Mukherjee, S., Ebert, B. L., Gillette, M. A., Paulovich, A., Pomeroy, S. L., Golub, T. R., Lander, E. S. & Mesirov, J. P. Gene set enrichment analysis: a knowledge-based approach for interpreting genome-wide expression profiles. *Proceedings of the National Academy of Sciences of the United States of America* **102**, 15545-15550, doi:10.1073/pnas.0506580102 (2005).

79 Luckey, C. J., Bhattacharya, D., Goldrath, A. W., Weissman, I. L., Benoist, C. & Mathis, D. Memory T and memory B cells share a transcriptional program of self-renewal with long-term hematopoietic stem cells. *Proceedings of the National Academy of Sciences of the United States of America* **103**, 3304-3309, doi:10.1073/pnas.0511137103 (2006).

80 Ong, S. E., Blagoev, B., Kratchmarova, I., Kristensen, D. B., Steen, H., Pandey, A. & Mann, M. Stable isotope labeling by amino acids in cell culture, SILAC, as a simple and accurate approach to expression proteomics. *Molecular & cellular proteomics : MCP* **1**, 376-386 (2002).

81 Washburn, M. P., Wolters, D. & Yates, J. R., 3rd. Large-scale analysis of the yeast proteome by multidimensional protein identification technology. *Nature biotechnology* **19**, 242-247, doi:10.1038/85686 (2001).

82 Park, S. K., Venable, J. D., Xu, T. & Yates, J. R., 3rd. A quantitative analysis software tool for mass spectrometry-based proteomics. *Nature methods* **5**, 319-322, doi:10.1038/nmeth.1195 (2008).

83 Tabb, D. L., McDonald, W. H. & Yates, J. R., 3rd. DTASelect and Contrast: tools for assembling and comparing protein identifications from shotgun proteomics. *Journal of proteome research* **1**, 21-26 (2002).

84 McDonald, W. H., Tabb, D. L., Sadygov, R. G., MacCoss, M. J., Venable, J., Graumann, J., Johnson, J. R., Cociorva, D. & Yates, J. R., 3rd. MS1, MS2, and SQT-three unified, compact, and easily parsed file formats for the storage of

shotgun proteomic spectra and identifications. *Rapid communications in mass spectrometry : RCM* **18**, 2162-2168, doi:10.1002/rcm.1603 (2004).

85 Huang da, W., Sherman, B. T. & Lempicki, R. A. Systematic and integrative analysis of large gene lists using DAVID bioinformatics resources. *Nature protocols* **4**, 44-57, doi:10.1038/nprot.2008.211 (2009).

86 Huang da, W., Sherman, B. T. & Lempicki, R. A. Bioinformatics enrichment tools: paths toward the comprehensive functional analysis of large gene lists. *Nucleic acids research* **37**, 1-13, doi:10.1093/nar/gkn923 (2009).